Non-Linear Effects on Stopping of Fast Moving Molecular Ions Through Solids

by

Tyler L. Wilson

A thesis
presented to the University of Waterloo
in fulfilment of the
thesis requirement for the degree of
Master of Mathematics
in
Applied Mathematics

Waterloo, Ontario, Canada, 2007

I hereby declare that I am the sole author of this thesis. This is a true copy of the thesis, including any required final revisions, as accepted by my examiners.

I understand that my thesis may be made electronically available to the public.

Abstract

This thesis studies the non-linear (Barkas) effects on stopping of fast moving molecular ions through solids. We model the solid target by a rigid lattice of positive ion cores surrounded by a gas of electrons. To model the electron gas we use a hydrodynamic model with a Thomas-Fermi-von Weizsäcker expression for the internal energy. The disturbance to the charge density and velocity profile of the gas due to the intruder is assumed small and a perturbation expansion is used. The gas is assumed to be initially at rest.

A derivation for the first and second order stopping force on an projectile due to the induced charge density of the target is given. Structure factors are introduced to capture the physics relating to the structure of the projectile and to allow maximum flexibility and generalization.

The second order stopping force is calculated using a novel "holepunch" integration method and is compared to other available methods.

Results are obtained for the case of a dicluster of protons which are colinear with their direction of motion as well as for a dicluster of protons which are randomly oriented incident on an aluminum target and compared to the single proton case.

Acknowledgements

I thank my supervisor Dr. Miskovic for his help before and during my graduate studies. I also thank Dr. Frank Goodman and Dr. Francis Poulin for their valuable insight. As well, I thank Duncan Mowbray for all his helpful suggestions, discussions and advice. Finally, I thank Maria Khomenko for all her help last summer.

Last, but not least, I thank my parents whose support has not only made this work possible, but every other success in my life.

Dedication

To my parents, this is yours as much as it is mine.

To my friends, despite your best efforts, I am proud to say I finished. I am even more proud to call you my friends.

Contents

List of Figures

List of Tables

Chapter 1

Introduction

1.1 Motivation

Since the beginning of the 20th century, the study of the interaction between atomic projectiles and various target media has been studied extensively. Beginning with the famous studies conducted by Rutherford at the turn of the century, experimental and theoretical methods have dramatically increased in sophistication and precision. The interest in these projectile-target interactions goes far beyond probing fundamental physical processes. The field has also been fueled by ongoing fusion research as well as materials modification.

One method of controlled fusion is to implode an inertial confinement fusion pellet by bombardment from a beam of light ions [1]. However, to properly design the target for optimal performance one requires a description of deposition of energy into the pellet. Ideally, this deposition model should be flexible enough to describe results for a wide range of target materials as well as projectile ions. Furthermore, fairly recently, the potential of initiating fusion reaction in solids has been suggested and discussed [2, 3]. In these studies, rather than using a beam of light ions as projectiles, clusters of molecules are used. Again however, a firm theoretical understanding of the underlying processes would be of great use and benefit for further exploration of fusion methods.

On the other hand, the use of bombardment of solid targets by ion beams has long been studied for their ability to leave ion tracks [4] through the solid. This idea may be extended to high energy beams of clusters, for example in [5]. This area has received a great deal of attention

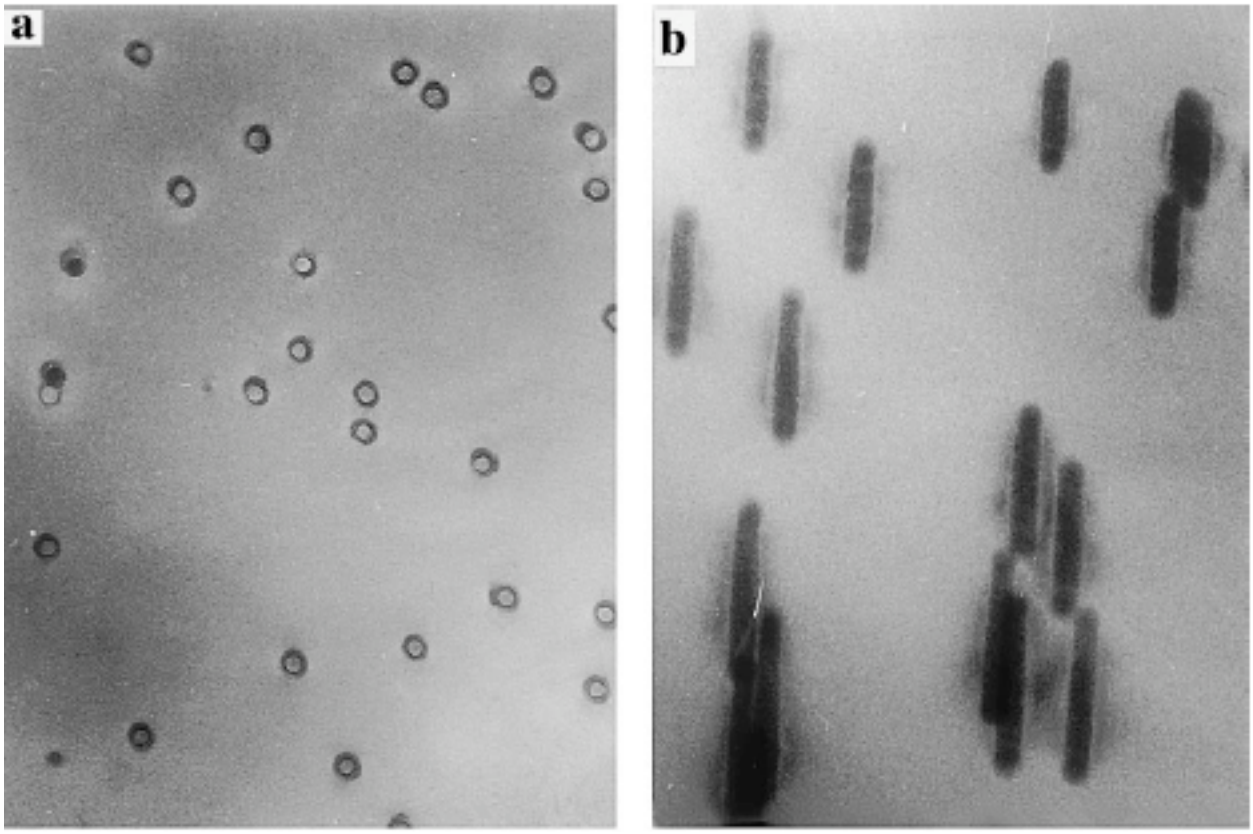

Figure 1.1: Ion Tracks

recently due to its applicability to the creation of carbon nanotubes [6]. Once again, the key issue is to understand how energy is deposited as the ion (or cluster) traverses the solid target.

What is more is that when a beam of ions is used to bombard a target, the distances between consecutive ions are so large that the excitations which occur in the target have sufficient time to relax before the following ion. This is not so for clusters of ions where the intermolecular distance of the projectile does not allow the medium to relax before being excited again by another ion. This effect was shown by Brandt, Ratkowski and Ritchie ([7]) who showed that H_2^+ and H_3^+ lost more energy per proton than isolated protons.

These physical applications are examples of why energy deposition is of interest, specifically in recent years. One particular aspect of this issue is the consideration of how much energy is lost by the projectile per unit distance of travel through the target. This quantity is called the

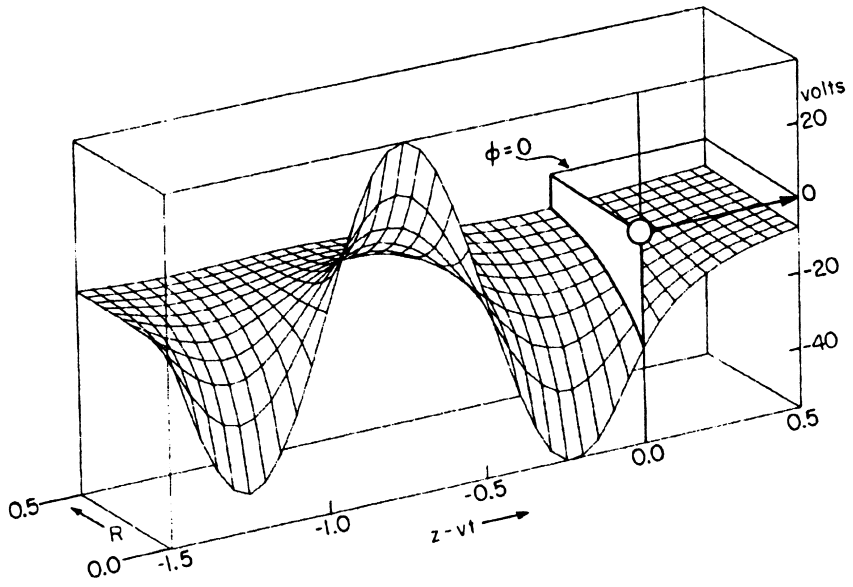

Figure 1.2: Potential distribution from a 400 keV proton traversing carbon ($\hbar\omega_p = 25.0$eV). Distances are shown in units of $\lambda = 14.5\mathring{A}$ [9].

stopping force and in some works the *stopping power*. The stopping force is what we consider in this work.

The full dynamical picture of a projectile's interaction with the electron 'sea' may be replaced by a simplified picture of a swift moving projectile through an electron gas. As this projectile travels through the gas it induces an electron density 'wake' behind it [8], much like a boat on the surface of a lake (Figure 1.2). This wake will then alter the electric field acting on the projectile, effectively slowing it down. This is clear from Figure 1.2 where the slope of the plot is directly related to the stopping force which would be experienced by an ion behind the leading ion. Even for single ion projectiles this interaction may be quite complex. Most work considers only the linear wake (proportional to the charge on the projectile). What's more is that for a cluster of ions transversing the electron gas, the wakes may constructively and destructively interfere. Many different attempts have been made to give a description of this system in a rigorous fashion.

Within the area of stopping force, there are many sub-areas and methods to understanding the problem. One method in particular is to use a perturbative approach by assuming the projectile causes only a small disturbance in the overall charge density profile of the target. This

small disturbance causes only a small change in the equilibrium electric potential throughout the system.

This approach can be a very helpful simplification in an attempt to solve the system. However, the system can still be very complex for general projectiles and targets. Work has been done previously to calculate the stopping force by a *single* ion as a projectile to first order in the perturbation expansion. This work was furthered by studying the second order correction to stopping force of a single ion [10, 11]. This second order correction is called the *Barkas* effect, which was named after W.H. Barkas who first experimentally discovered the charge-sign dependence on the stopping force of an ion [12, 13, 14]. The first order approximation provides no such dependance since results in this regime are quadratically dependent on the charge of the projectile.

As shown in Figure 1.3 there is clearly a non-linear effect on the potential that the projectile induces in the medium. The first-order approximation, $g^{(1)}$ is defined through,

$$\Phi^{(1)}_{ind}(\mathbf{R}) = \frac{e_1\omega_p}{v} g^{(1)}(\mathbf{R})\,, \tag{1.1}$$

with $\mathbf{R} = \mathbf{r} - \mathbf{v}t$, v as the projectile speed, e_1 as the charge on projectile. Similarly, for the second order correction,

$$\Phi^{(2)}_{ind}(\mathbf{R}) = \frac{e_1\omega_p}{v}\frac{\pi e_1 e\omega_p}{mv^3} g^{(2)}(\mathbf{R})\,, \tag{1.2}$$

with m as the mass of the electron, e as the charge on an electron and ω_p is the plasma frequency.

We see in Figure (1.3) the difference between the first order induced potential and the second order induced potential. It is the purpose of this work to explore how the stopping force is effected by these differences in linear (first order) and non-linear (second order) induced potentials.

While non-linear effects in stopping of single ions have been studied over the years, only a few studies appeared on such effects on stopping of clusters and all the studies were all limited to slow diclusters [15, 16, 17]. The stopping of fast clusters was always treated in the literature by linear theories [18, 19, 20]. Part of the motivation of the present work is to remedy this situation and analyze the non-linear effects in the stopping of fast clusters in solids.

1.2 Physical Model

The purpose of this work is to expand upon previous work carried out in the single ion case, particularily in the medium to high speed regime. Our work specifically deals with ion clusters

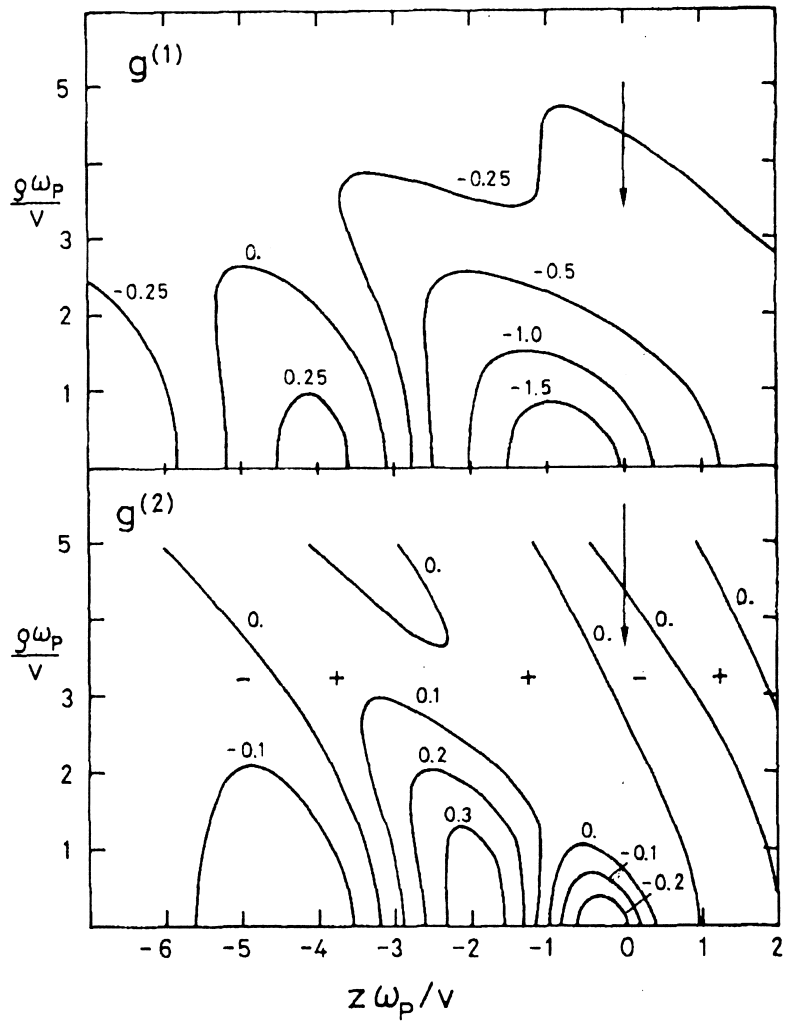

Figure 1.3: Contour plot of the reduced first and second order induced potentials for a static electron gas with $(2\pi v^2/\hbar\omega_p) = 4$. The z direction points in the direction of projectile velocity and the ρ direction is perpendicular to it. The projectile is located at $(z, \rho) = (0, 0)$. The coordinates are given in units of the adiabatic distance $(\frac{v}{\omega_p})$[10].

of at most two ions, and these may be treated as small perturbations when compared to the charge density profile of the target.

As a fast cluster (having a speed in excess of the Bohr speed) travels through a solid it is

subject to many complex interactions with the target medium. As it passes through the first few layers of atoms in the target the projectile loses all of its valence shell electrons. This usually happens on the time scale of about 1 fs. Despite this striping, the charge state of the constituent ions is quickly ($\approx$1fs) equilibrated [21]. As the projectile penetrates further into the target the electronic excitations in the target exhibit strong interference effects due to the close proximity of constituent ions. This is called the *vicinage effect* [22] and it is the constructive interference that comes from the vicinage effect which gives rise to the enhanced energy loses. If the projectile continues to penetrate the target then the dynamically screened inter-ionic forces and elastic scattering of constituent ions off the target ions will cause the projectile's ions to spatially disperse. This effect is called the Coulomb explosion [7]. These competing mechanisms give rise to increasing inter-ionic distances ([18, 19]) which develop over a time scale of about 10 fs. As the inter-ionic distance grows, the effect on the stopping force due to the vicinage effect diminishes and becomes quite small after several 10 fs [20]. On the time scales under consideration, it is reasonable to treat the target as a lattice of rigid positive atomic cores surrounded by a 'sea' of electrons. Since the atomic cores are much heavier than their valence electron counterparts, the overwhelming dynamical response of the medium due to the intruder is from the valence electrons. It is also reasonable to neglect the effect of the Coulomb explosion in sufficiently thin targets and treat the clusters of as rigid over the entire region.

Regarding the microscopic description of the dynamical response of the electron gas in the target, some earlier models which have been considered include the hydrodynamic model [23], many body perturbation methods using the random phase approximation (RPA) [24, 25], an extension of Lindhard's method for an electron gas [10] and a time dependent Hartree self-consistent-field method [11]. As pointed out in [11], all of the aforementioned models have self-consistent fields and obey conservation laws up to second order in the magnitude of the charge of the projectile. Further, it is shown that for single ions with medium to large speeds, the hydrodynamic model (with suitable choices for the internal energy and in the case of a static electron gas) reproduces the results other models, as shown in Figures 1.4 and 1.5 for the first- and second- order stopping forces. Since this is precisely the regime targeted by this work and since the hydrodynamic model is computationally the most straightforward, it offers the best opportunity to extend the exploration of stopping force of ion clusters.

Of course a classical fluid approach to the case of an electron gas would not be reasonable

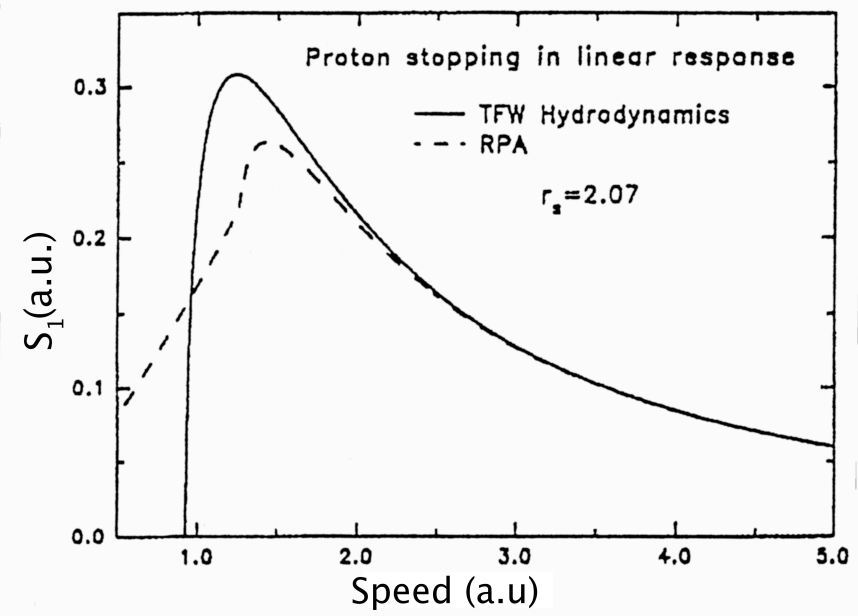

Figure 1.4: Comparison of proton stopping forces through a solid with Wigner-Seitz radius (r_s) of 2.07 a.u. The solid line (——) is calculated using the TFW hydrodynamic model. The dashed line (- - -) is calculated using the random phase approximation [11].

since the electrons are clearly outside the domain of classical physics. The quantum nature of the system enters through the expression for the internal energy, $E_{int}[n]$,

$$E_{int}[n] = U[n] + G[n]\,, \tag{1.3}$$

where n is the electron number density of the gas, U is the classical coulomb energy, and G is the rest. It is the choice of G which specifies the quantum nature of the gas. In many studies G is defined as the sum of the kinetic energy per particle of a degenerate Fermi gas and a correction term due to von Weizsäcker. Thus,

$$G[n] = T_{TF}[n] + T_W[n]\,. \tag{1.4}$$

This approximation for the energy G is called the Thomas-Fermi-Weizsäcker model and is discussed in appendix B.

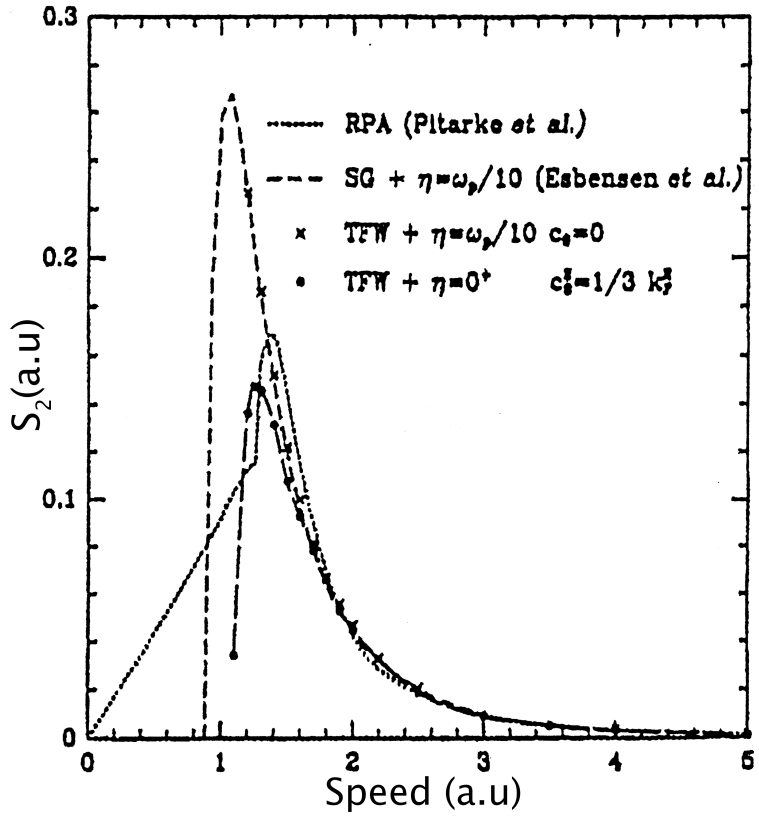

Figure 1.5: Coefficient of the Barkas correction term at medium to high speeds for a proton through an electron gas with Wigner-Seitz radius (r_s) of 2.07 a.u.. The dotted line ($\cdots$) is calculated using the random phase approximation [26]. The dashed line ($\cdots$) is calculated using the TFW hydrodynamic model with a static electron gas [10]. The x's denote the calculations carried out using the TFW model with $c_0 = 0$ (or in this work $\alpha = 0$) and $\eta = \omega_p/10$. $\cdot$ indicates calculations done with $\eta = 0^+$ and $c_0^2 = 1/3k_F^2$ [11].

1.3 Outline

The work contained here focuses on two specific cases of ion cluster interaction with an electron gas. The first is the case of a colinear di-cluster consisting of two protons aligned in the direction of the cluster's velocity. The second case is a randomly oriented cluster of two protons.

Chapter 2 deals exclusively with the derivation of stopping force using the hydrodynamic

model. We shall see how expressions for the first order and second order stopping forces come about naturally from a perturbation expansion. The important thing will be to notice how the second order correction to the stopping force will indeed have a dependency on Z^3, and thus will inherently depend on the sign of the charge. This is the aforementioned Barkas effect.

In the third chapter we shall discuss the methods used to calculate the first and second order stopping force for both the colinear cluster and randomly oriented di-cluster. These will include discussion about the numerical integration methods. Due to the appearance of singularities in the integrand, special care needs to be taken when integrating over certain regions. What's more is that, in the case of the second order correction, regular numerical integration methods prove to be completely unreliable. This section will discuss a novel approach to circumventing these issues and obtaining accurate, reliable results.

Chapter 4 will provide justification and verification of the methods we used which were described in chapter 3.

Chapter 5 will be dedicated to presenting and discussing the results and how they compare to previous results. Although the complexity of the calculations and unavailability of experimental data limit somewhat the ability to independently check the results, this section will discuss the clever way one can argue that the results are indeed a reliable description of the physical process.

Finally a short conclusion will be given, outlining the work done, its place amongst the work done by others and possibilities for future work.

Throughout the work we shall use atomic units and Gauss' electrostatic units, ie: $m = \hbar = e = 1$ and $4\pi\epsilon_0 = 1$, where e is the proton charge.

Chapter 2

Stopping Force

In this chapter we describe the general formalism of stopping force. We begin by describing the derivation of the expression for the stopping force, and then move on to outlining the hydrodynamic model of a static electron gas and how it can be used to calculate the stopping force of a charged projectile moving through a static electron gas.

2.1 Stopping Force

Consider a charged projectile moving through a static electron gas with a velocity $\mathbf{v}(\mathbf{r}, t)$. As the projectile moves through the gas it experiences forces due to the interaction of the projectile's charges with the electrons in the gas. The stopping force is defined to be the force that the projectile experiences in the direction of motion. Thus,

$$S = -\hat{\mathbf{v}} \cdot \mathbf{F}\,, \tag{2.1}$$

where $\mathbf{F}$ is the force experienced by the projectile due to the polarization of the electron gas and $\hat{\mathbf{v}} = \mathbf{v}/\|\mathbf{v}\|$.

We describe the projectile by a charge density $\rho_{ext}(\mathbf{r}, t)$ where $\mathbf{r}$ is the position vector in the laboratory coordinate system. Again, we assume that the cluster is rigid and doesn't experience Coulomb explosion or any other deformation during its travel through the gas. As pointed out, this is an acceptable assumption provided that the time scale of transversal of the gas is small relative to the time scale of the deformation. Thus, the charge density of the projectile remains

constant and has no explicit time dependence. The electric force experienced by the projectile over a differential volume element $d^3\mathbf{r}$ at position $\mathbf{r}$ is,

$$d\mathbf{F} = -\rho_{ext}(\mathbf{r},t)\vec{\nabla}\Phi_{ind}(\mathbf{r},t)d^3\mathbf{r}\,, \tag{2.2}$$

where Φ_{ind} is the electrostatic potential induced by the polarization of the medium due to the presence of the external charge $\rho_{ext}(\mathbf{r},t)$ at $\mathbf{r}$ and time t. It is important to realize that this electrostatic potential is due to contributions from the background positive ion cores and from the electron gas. By integrating over all $\mathbf{r}$ space we can find the total stopping force,

$$S = \frac{1}{\|\mathbf{v}\|}\int d^3\mathbf{r}\,\rho_{ext}(\mathbf{r},t)\,\mathbf{v}\cdot\vec{\nabla}\Phi_{ind}(\mathbf{r},t)\,. \tag{2.3}$$

The task now is to describe $\Phi_{ind}(\mathbf{r},t)$ in a self consistent manner. To this end, we use the hydrodynamic model.

2.2 Hydrodynamic Model

In this section we derive the hydrodynamic equations for an inhomogenous electron gas using variational principles.

We begin by characterizing the gas by the electron number density $n(\mathbf{r},t)$ and the hydrodynamical velocity, $\mathbf{u}(\mathbf{r},t)$. Further, we assume the flow to be irrotational, and hence may introduce a velocity potential, $\psi(\mathbf{r},t)$, such that

$$\mathbf{u}(\mathbf{r},t) = -\vec{\nabla}\psi(\mathbf{r},t)\,. \tag{2.4}$$

We can write the Hamiltonian for this system as,

$$H[n(\mathbf{r},t),\psi(\mathbf{r},t)] = H_{kinetic} + H_{int} + H_{Coul} + H_{ext} + H_{+}\,, \tag{2.5}$$

where the $H_{kinetic}\,, H_{int}\,, H_{Coul}\,, H_{ext}\,, H_{+}$ are the contributions to the total energy made by the macroscopic motion of the electrons, the energy due to the internal kinetic energy of the gas, the Coulomb energy from electron-electron interactions, the energy due to external forces and the energy due to the positive ion cores respectively.

From considering 2.4 we can write the macroscopic motion contribution as,

$$H_{kinetic} = \int d^3\mathbf{r}\, \frac{1}{2} |\overrightarrow{\nabla}\psi|^2\, n(\mathbf{r},t)\,, \tag{2.6}$$

the internal energy as,

$$H_{int}[n(\mathbf{r},t)] = G[n(\mathbf{r},t)]\,, \tag{2.7}$$

the Coulomb term,

$$H_{Coul} = \frac{1}{2}\int d^3\mathbf{r} \int d\mathbf{r}'\, \frac{n(\mathbf{r},t)n(\mathbf{r}',t)}{|\mathbf{r}-\mathbf{r}'|}\,, \tag{2.8}$$

and the external contribution as,

$$H_{ext} = -\int d^3\mathbf{r}\, n(\mathbf{r},t)\phi_{ext}(\mathbf{r},t)\,, \tag{2.9}$$

where $\phi_{ext}(\mathbf{r},t)$ is the potential due to the external projectile moving through the gas,

$$\phi_{ext}(\mathbf{r},t) = \int d^3\mathbf{r}'\, \frac{\rho_{ext}(\mathbf{r},t)}{|\mathbf{r}-\mathbf{r}'|}\,, \tag{2.10}$$

and G is a functional to be described in a subsequent section. The contribution due to the positive ion cores, H_+, is given by,

$$H_+ = -\int d^3\mathbf{r}\, n(\mathbf{r},t) V_+(\mathbf{r})\,. \tag{2.11}$$

Thus, the total energy of the system is then given by,

$$\begin{aligned} H[n(\mathbf{r},t),\psi(\mathbf{r},t)] \;=\; & \int d^3\mathbf{r}\, \frac{1}{2}|\overrightarrow{\nabla}\psi|^2 n(\mathbf{r},t) + G[n(\mathbf{r},t)] \\ & + \frac{1}{2}\int d^3\mathbf{r} \int d^3\mathbf{r}'\, \frac{n(\mathbf{r},t)n(\mathbf{r}',t)}{|\mathbf{r}-\mathbf{r}'|} - \int d^3\mathbf{r}\, n(\mathbf{r},t)\phi_{ext}(\mathbf{r},t) \\ & - \int d^3\mathbf{r}\, n(\mathbf{r},t) V_+(\mathbf{r})\,. \end{aligned} \tag{2.12}$$

where V_+ is the electrostatic potential produced by the positive ion cores.

Now, by treating ψ and n as conjugate variables, we can appeal to the variational principle,

$$\delta \int_{t_1}^{t_2} L\, dt = 0\,, \tag{2.13}$$

to obtain the equations of motion. The Lagrangian, L, in 2.13 is given by,

$$L = \int d^3\mathbf{r}\, n(\mathbf{r},t)\frac{d\psi(\mathbf{r},t)}{dt} - H[n(\mathbf{r},t),\psi(\mathbf{r},t)]\,, \tag{2.14}$$

with normalization constraint,

$$\int d^3\mathbf{r}\, n(\mathbf{r},t) = N\,, \tag{2.15}$$

where N is the total number of electrons.

By using the Euler-Lagrange equations,

$$\frac{\partial}{\partial t}\frac{\partial L}{\partial \psi'} - \frac{\partial L}{\partial \psi} = 0\,, \tag{2.16}$$

$$\frac{\partial}{\partial t}\frac{\partial L}{\partial n'} - \frac{\partial L}{\partial n} = 0\,, \tag{2.17}$$

where $\psi' = \frac{\partial \psi}{\partial t}$ and $n' = \frac{\partial n}{\partial t}$, we can obtain partial differential equations describing the evolution of n and ψ.

From 2.14 and 2.12 we obtain,

$$\frac{\partial L}{\partial \psi'} = n\,, \tag{2.18}$$

$$\frac{\partial L}{\partial \psi} = \overrightarrow{\nabla}\cdot(n\overrightarrow{\nabla}\psi)\,, \tag{2.19}$$

$$\frac{\partial L}{\partial n'} = 0\,, \tag{2.20}$$

$$\frac{\partial L}{\partial n} = \frac{\partial \psi}{\partial t} - \frac{\delta G}{\delta n} - \frac{1}{2}|\overrightarrow{\nabla}\psi|^2 + \Phi(\mathbf{r},t)\,. \tag{2.21}$$

We immediately can see that G is the term which brings in the quantum effects as the rest of the terms are purely of classical nature.

We have also defined $\Phi(\mathbf{r},t)$ in 2.21 to encapsulate the total electrostatic potential,

$$\Phi(\mathbf{r},t) = -\int d^3\mathbf{r}'\frac{n(\mathbf{r}',t)}{|\mathbf{r}-\mathbf{r}'|} + \phi_{ext}(\mathbf{r},t) + V_+(\mathbf{r})\,, \tag{2.22}$$

which one can see obeys the Poisson equation for the total charge,

$$\nabla^2\Phi(\mathbf{r},t) = -4\pi[\rho_{ext}(\mathbf{r},t) + n_+ - n(\mathbf{r},t)]\,, \tag{2.23}$$

where n_+ is the number density of the positive ion cores.

Thus, upon substitution back into the Euler-Lagrange equations we obtain,

$$\frac{\partial n}{\partial t} = \overrightarrow{\nabla} \cdot (n \overrightarrow{\nabla} \psi) \,, \tag{2.24}$$

$$\frac{\partial \psi}{\partial t} + \eta\psi = \frac{\delta G}{\delta n} + \frac{1}{2} |\overrightarrow{\nabla}\psi|^2 - \Phi(\mathbf{r}, t) \,, \tag{2.25}$$

where the term $\eta\psi$ was added by hand to introduce friction into the system.

We easily identify 2.24 as the continuity equation for a classical fluid and 2.25 as the Bernoulli equation. If we set $G = 0$ this set of equations becomes just the evolution equations for a classical fluid. It is in this light that we can see that the quantum nature of the system enters through G exclusively, as will be mentioned in Appendix A.

Our method of approach is to assume that the charge density of our projectile will be small compared to the charge density of the electron gas. This allows us to perturbatively expand the charge density about the equilibrium charge density, n_0. Note that when in equilibrium, $n_0 = n_+$. Expanding about n_0,

$$n(\mathbf{r}, t) = n_0 + \lambda n_1(\mathbf{r}, t) + \lambda^2 n_2(\mathbf{r}, t) + \dots \,. \tag{2.26}$$

Since we are assuming our charged projectile will induce only a small change in the charge density of the electron gas, we can assume that the velocity field of the gas may also be expanded about its equilibrium value $\mathbf{u}_0$,

$$\mathbf{u}(\mathbf{r}, t) = \mathbf{u}_0 + \lambda \mathbf{u}_1(\mathbf{r}, t) + \lambda^2 \mathbf{u}_2(\mathbf{r}, t) + \dots \,. \tag{2.27}$$

We shall consider only the case of a static gas, and thus it's at rest in equilibrium, ie, $\mathbf{u}_0 = 0$. Thus,

$$\mathbf{u}(\mathbf{r}, t) = \lambda \mathbf{u}_1(\mathbf{r}, t) + \lambda^2 \mathbf{u}_2(\mathbf{r}, t) + \dots \,, \tag{2.28}$$

which, in its potential form is,

$$\psi(\mathbf{r}, t) = \lambda \psi_1(\mathbf{r}, t) + \lambda^2 \psi_2(\mathbf{r}, t) + \dots \,. \tag{2.29}$$

Thus,

$$\mathbf{u}(\mathbf{r}, t) = -\vec{\nabla}(\lambda \psi_1(\mathbf{r}, t) + \lambda^2 \psi_2(\mathbf{r}, t) + \dots) \,. \tag{2.30}$$

Likewise we shall see that we may write,

$$\frac{\delta G}{\delta n} = \left(\frac{\delta G}{\delta n}\right)_0 + \lambda \left(\frac{\delta G}{\delta n}\right)_1 + \lambda^2 \left(\frac{\delta G}{\delta n}\right)_2 + \dots . \tag{2.31}$$

We can use these expansions in the continuity equations and the momentum (Bernoulli) equation.

2.2.1 Continuity Equation

From the continuity equation (2.24) we have that,

$$\frac{\partial n}{\partial t} + \vec{\nabla} \cdot (n\mathbf{u}) = 0\,, \tag{2.32}$$

Substituting in our perturbation expansions 2.26 and 2.30,

$$\frac{\partial}{\partial t}\left(n_0 + \lambda n_1 + \lambda^2 n_2\right) + \vec{\nabla} \cdot \Big((n_0 + \lambda n_1 + \lambda^2 n_2)(-\vec{\nabla}(\lambda\psi_1 + \lambda^2\psi_2))\Big) = 0 \tag{2.33}$$

which, when we collect like powers of λ gives,

$$\lambda\left(\frac{\partial n_1}{\partial t} - n_0\nabla^2\psi_1\right) + \lambda^2\left(\frac{\partial n_2}{\partial t} - n_0\nabla^2\psi_2 - \vec{\nabla}\cdot(n_1\vec{\nabla}\psi_1)\right) = 0\,. \tag{2.34}$$

Thus, our expressions for the first and second order continuity equation is,

$$\text{First Order:} \quad \tfrac{\partial n_1}{\partial t} - n_0\nabla^2\psi_1 = 0 \tag{2.35}$$

$$\text{Second Order:} \quad \tfrac{\partial n_2}{\partial t} - n_0\nabla^2\psi_2 - \vec{\nabla}\cdot(n_1\vec{\nabla}\psi_1) = 0\,. \tag{2.36}$$

We now turn our attention to the momentum equation.

2.2.2 Momentum Equation

As outlined in the previous section, we use the perturbation expansions 2.26 and 2.30 in the momentum equation, 2.25. However, first we take the gradient of both sides of 2.25,

$$\vec{\nabla}\left(\frac{\partial\psi}{\partial t} + \eta\psi\right) = \vec{\nabla}\left(\frac{\delta G}{\delta n} + \frac{1}{2}|\vec{\nabla}\psi|^2 - \Phi(\mathbf{r},t)\right)\,, \tag{2.37}$$

which gives,

$$\frac{\partial \mathbf{u}}{\partial t} + \mathbf{u} \cdot \vec{\nabla}\mathbf{u} = -\vec{\nabla}\Phi - \vec{\nabla}\left(\frac{\delta G}{\delta n}\right) - \eta \mathbf{u}\,. \tag{2.38}$$

As in the previous section we substitute our expansion 2.30 into 2.38,

$$\begin{aligned}\frac{\partial}{\partial t}\left(\vec{\nabla}(\lambda\psi_1 + \lambda^2\psi_2 + \ldots)\right) - \quad & \vec{\nabla}(\lambda\psi_1 + \lambda^2\psi_2 + \ldots) \cdot \vec{\nabla}(\vec{\nabla}\lambda\psi_1 + \lambda^2\vec{\nabla}\psi_2 + \ldots) \\ = \quad & \vec{\nabla}\Phi + \vec{\nabla}\left(\tfrac{\delta G}{\delta n}\right) - \eta\vec{\nabla}(\lambda\psi_1 + \lambda^2\psi_2 + \ldots)\,. \end{aligned} \tag{2.39}$$

Taking the divergence of both sides,

$$\begin{aligned}\vec{\nabla} \cdot \left[\frac{\partial}{\partial t}\left(\vec{\nabla}(\lambda\psi_1 + \lambda^2\psi_2 + \ldots)\right) - \vec{\nabla}(\lambda\psi_1 + \lambda^2\psi_2 + \ldots) \cdot \vec{\nabla}(\vec{\nabla}\lambda\psi_1 + \lambda^2\vec{\nabla}\psi_2 + \ldots)\right] \\ = \nabla^2\Phi + \vec{\nabla} \cdot \left[\vec{\nabla}\left(\frac{\delta G}{\delta n}\right) - \eta\vec{\nabla}(\lambda\psi_1 + \lambda^2\psi_2 + \ldots)\right]\,. \end{aligned} \tag{2.40}$$

Using our knowledge from Poisson's equation 2.23 and our expansion 2.26 for n we obtain,

$$\begin{aligned}&\vec{\nabla} \cdot \left[\frac{\partial}{\partial t}\left(\vec{\nabla}(\lambda\psi_1 + \lambda^2\psi_2 + \ldots)\right) - \vec{\nabla}(\lambda\psi_1 + \lambda^2\psi_2 + \ldots) \cdot \vec{\nabla}(\vec{\nabla}\lambda\psi_1 + \lambda^2\vec{\nabla}\psi_2 + \ldots)\right] \\ &= -4\pi[\rho_{ext}(\mathbf{r},t) - \lambda n_1(\mathbf{r},t) - \lambda^2 n_2(\mathbf{r},t) + \ldots] + \vec{\nabla} \cdot \left[\vec{\nabla}\left(\frac{\delta G}{\delta n}\right) - \eta\vec{\nabla}(\lambda\psi_1 + \lambda^2\psi_2 + \ldots)\right] \end{aligned} \tag{2.41}$$

where we have used the fact that at equilibrium, $n_+ = n_0$.

Once again, as in the previous section, we collect like terms of λ and neglect terms which are higher than second order. This gives,

$$\text{First Order:} \quad -\tfrac{\partial}{\partial t}\nabla^2\psi_1 = -4\pi\left(\rho_{ext} - n_1\right) - \nabla^2\left(\tfrac{\delta G}{\delta n}\right)_1 + n\nabla^2\psi_1 \tag{2.42}$$

$$\text{Second Order:} \quad -\tfrac{\partial}{\partial t}\nabla^2\psi_2 + \tfrac{1}{2}\nabla^2(\vec{\nabla}\psi_1)^2 = 4\pi n_2 - \nabla^2\left(\tfrac{\delta G}{\delta n}\right)_2 \tag{2.43}$$

It is worth pointing out here that, if we return to 2.38 and define the *total material derivative* of the velocity of a fluid flow to be,

$$\frac{\mathcal{D}\mathbf{u}}{\mathcal{D}t} = \frac{\partial \mathbf{u}}{\partial t} + \mathbf{u} \cdot \vec{\nabla}\mathbf{u}\,. \tag{2.44}$$

Then by multiplying 2.38 by n on both sides we obtain,

$$n\left(\frac{\partial \mathbf{u}}{\partial t} + \mathbf{u} \cdot \vec{\nabla}\mathbf{u}\right) = -n\mathbf{E} - \vec{\nabla}\left(\frac{\delta G}{\delta n}\right) - \eta n\mathbf{u}\,, \tag{2.45}$$

And thus,

$$\frac{\mathcal{D}\mathbf{p}}{\mathcal{D}t} = \mathbf{F} = \mathbf{F}_e + \mathbf{F}_f + \mathbf{F}_{int} \tag{2.46}$$

where we have identified $\mathbf{F}_e = -n\mathbf{E}$ as the electric force per unit volume, $\mathbf{F}_{int} = -\vec{\nabla}\left(\frac{\delta G}{\delta n}\right) n$ as the internal interaction force per unit volume, $\mathbf{F}_f = -\eta m\mathbf{u}$ as the frictional force per unit volume, and $\mathbf{p}$ as the momentum per unit volume of the fluid. This description clearly allows one to see that 2.45 is nothing more than Newton's Second Law.

2.2.3 Internal Energy

In section 2.2 we mentioned the contribution by the internal energy to the total energy of he system. We claimed that the internal energy was a functional of the electron density and called this functional, G. The model we use for G is the so called "Thomas-Fermi-Weizsäcker" model.

The Thomas-Fermi-Weizsäcker model gives the internal energy of an electron gas as,

$$G[n] = \int d^3\mathbf{r}\, n(\mathbf{r},t)\left(\frac{3}{10}\left(3\pi^2 n\right)^{2/3} + \frac{1}{8}\frac{(\vec{\nabla}n)^2}{n^2}\right) \tag{2.47}$$

The first term is the Thomas-Fermi kinetic energy and the second term is the von Weizsäcker correction. The internal energy enters into our expression for stopping force through its functional derivative, $\frac{\delta G}{\delta n}$.

From variational calculus the functional derivative of a functional $F[p] = \int d^3\mathbf{r} f(\mathbf{r}, p, \vec{\nabla}p, \nabla^2 p, \ldots)$ with respect to a function p is defined to be [27],

$$\frac{\delta F[p]}{\delta p} = \frac{\partial f}{\partial p} - \vec{\nabla}\cdot\frac{\partial f}{\partial(\vec{\nabla}p)} + \nabla^2\frac{\partial f}{\partial(\nabla^2 p)} - \ldots . \tag{2.48}$$

In our case we have $G[n] = \int d^3\mathbf{r}\, f(n, \vec{\nabla}n)$ where

$$f(n,\vec{\nabla}) = \frac{3}{10}\left(3\pi^2\right)^{2/3} n^{5/3} + \frac{1}{8}\frac{(\vec{\nabla}n)^2}{n}\,. \tag{2.49}$$

Thus, we have,

$$\frac{\delta G}{\delta n} = \left(\frac{\partial}{\partial n} - \vec{\nabla}\cdot\frac{\partial}{\partial(\vec{\nabla}n)}\right)\left(\frac{3}{10}\left(3\pi^2\right)^{2/3} n^{5/3} + \frac{1}{8}\frac{(\vec{\nabla}n)^2}{n}\right), \tag{2.50}$$

which ultimately yields,

$$\frac{\delta G}{\delta n} = \frac{1}{2}\left(3\pi^2 n\right)^{2/3} + \frac{1}{8}\frac{(\vec{\nabla} n)^2}{n^2} - \frac{1}{4}\frac{\nabla^2 n}{n}\,. \tag{2.51}$$

As indicated from 2.31 we are able to write 2.51 as a perturbation expansion. This occurs naturally when we use our expansion for n (ie: 2.26) in our functional derivative for G. This substitution gives,

$$\begin{aligned} n^{2/3} &= \left(n_0 + \lambda n_1 + \lambda^2 n_2\right)^{2/3} \\ &\approx n_0^{2/3} + \lambda\frac{2}{3}\frac{n_1}{n_0^{1/3}} + \lambda^2 n_0^{2/3}\left(\frac{2}{3}\frac{n_2}{n_0} - \frac{1}{9}\frac{n_1^2}{n_0^2}\right)\,, \end{aligned}$$

$$\begin{aligned} \frac{\| \vec{\nabla} n \|^2}{n^2} &= \frac{\lambda^2 \vec{\nabla} n_1 \cdot \vec{\nabla} n_1}{\left(n_0 + \lambda n_1 + \lambda^2 n_2\right)^2} \\ &\approx \lambda^2 \frac{\vec{\nabla} n_1 \cdot \vec{\nabla} n_1}{n_0^2} \end{aligned}$$

$$\begin{aligned} \frac{\nabla^2 n}{n} &= \frac{\nabla^2\left(n_0 + \lambda n_1 + \lambda^2 n_2\right)}{n_0 + \lambda n_1 + \lambda^2 n_2} \\ &\approx \lambda\frac{\nabla^2 n_1}{n_0} + \lambda^2\left(\frac{\nabla^2 n_2}{n_0} - \frac{n_1 \nabla^2 n_1}{n_0^2}\right) \end{aligned}$$

As done before, we gather the terms together with respect to powers of λ, excluding terms higher than second order. In this way we can write, as desired,

$$\frac{\delta G}{\delta n} = \left(\frac{\delta G}{\delta n}\right)_0 + \lambda\left(\frac{\delta G}{\delta n}\right)_1 + \lambda^2\left(\frac{\delta G}{\delta n}\right)_2 \tag{2.52}$$

where,

$$\left(\frac{\delta G}{\delta n}\right)_0 = \frac{3}{2}\alpha\,, \tag{2.53}$$

$$\left(\frac{\delta G}{\delta n}\right)_1 = \alpha\frac{n_1}{n_0} - \beta\frac{\nabla^2 n_1}{n_0}\,, \tag{2.54}$$

$$\left(\frac{\delta G}{\delta n}\right)_2 = \alpha\left(\frac{n_2}{n_0} - \frac{1}{6}\frac{n_1^2}{n_0^2}\right) + \frac{\beta}{2}\left(\frac{\vec{\nabla} n_1}{n_0}\right)^2 - \beta\frac{\nabla^2 n_2}{n_0} + \beta\frac{n_1 \nabla^2 n_1}{n_0}\,, \tag{2.55}$$

where $\alpha = \frac{1}{3}(3\pi n_0)^{2/3}$ and $\beta = \frac{1}{4}$.

2.3 Stopping Force On A Cluster

Having developed the hydrodynamic equations in first and second order, in this section we further develop our expression for the stopping force. We use a perturbation approach here to enable us to make a connection with the hydrodynamic equations developed above.

From our expression for the stopping force, 2.3, we have,

$$S = \frac{1}{\|\mathbf{v}\|} \int d^3\mathbf{r}\, \rho_{ext}(\mathbf{r})\, \mathbf{v} \cdot \vec{\nabla}\Phi_{ind}(\mathbf{r}, t)\,. \tag{2.56}$$

Now the induced potential is given by the expression,

$$\Phi_{ind}(\mathbf{r}, t) = \int d^3\mathbf{r}' \frac{\rho_{ind}(\mathbf{r}', t)}{|\mathbf{r} - \mathbf{r}'|}\,, \tag{2.57}$$

with ρ_{ind} being the charge density of the electron gas which is induced by the disturbing projectile. Since this disturbance is small, we again expand,

$$\rho_{ind}(\mathbf{r}, t) = \lambda\rho^{(1)}_{ind}(\mathbf{r}, t) + \lambda^2\rho^{(2)}_{ind}(\mathbf{r}, t) + \dots\,. \tag{2.58}$$

Thus,

$$\Phi_{ind}(\mathbf{r}, t) = \int d^3\mathbf{r}' \frac{\lambda\rho^{(1)}_{ind}(\mathbf{r}', t) + \lambda^2\rho^{(2)}_{ind}(\mathbf{r}', t) + \dots}{|\mathbf{r} - \mathbf{r}'|}\,, \tag{2.59}$$

$$= \lambda\Phi^{(1)}_{ind}(\mathbf{r}, t) + \lambda^2\Phi^{(2)}_{ind}(\mathbf{r}, t) + \dots\,. \tag{2.60}$$

We now write the stopping force as its own expansion,

$$S = \lambda S_1 + \lambda^2 S_2 + \dots\,, \tag{2.61}$$

where,

$$S_i = \frac{1}{\|\mathbf{v}\|} \int d^3\mathbf{r}\, \rho_{ext}(\mathbf{r}, t)\, \mathbf{v} \cdot \vec{\nabla}\Phi^{(i)}_{ind}(\mathbf{r}, t)\,, \tag{2.62}$$

and,

$$\Phi^{(i)}_{ind}(\mathbf{r}, t) = \int d^3\mathbf{r}' \frac{\rho^{(i)}_{ind}(\mathbf{r}', t)}{|\mathbf{r} - \mathbf{r}'|}\,. \tag{2.63}$$

Now, in light of the above formulation of the hydrodynamic model, the induced charge density ρ_{ind} is nothing more than the negative variation from equilibrium of the electron charge density, n. Thus,

$$\rho_{ind}^{(i)}(\mathbf{r},t) = -n_i(\mathbf{r},t)\,. \tag{2.64}$$

We will use the Fourier Transform to remove the $\vec{\nabla}$ operator in 2.62 and turn it into an algebraic equation.

The Fourier Transform, $\mathcal{F}$, of a scalar quantity, $A(\mathbf{r},t)$ is defined by,

$$A(\mathbf{r},t) = \int \frac{d^3\mathbf{k}}{(2\pi)^3}\,\frac{d\omega}{2\pi}\,\tilde{A}(\mathbf{k},\omega)e^{\imath\mathbf{k}\cdot\mathbf{r}-\imath\omega t}\,,$$

and its inverse transform,

$$\begin{aligned}\tilde{A}(\mathbf{k},\omega) &= \int d^3\mathbf{r}\,dt\,A(\mathbf{r},t)e^{-\imath\mathbf{k}\cdot\mathbf{r}+\imath\omega t}\,, &(2.65)\\ &= \mathcal{F}\left[A(\mathbf{r},t)\right]\,. &(2.66)\end{aligned}$$

Thus,

$$\Phi_{ind}^{(i)}(\mathbf{r},t) = \int \frac{d^3\mathbf{k}}{(2\pi)^3}\,\frac{d\omega}{2\pi}\,\tilde{\Phi}_{ind}^{(i)}(\mathbf{k},\omega)e^{\imath\mathbf{k}\cdot\mathbf{r}-\imath\omega t}\,, \tag{2.67}$$

and,

$$\vec{\nabla}\Phi_{ind}^{(i)}(\mathbf{r},t) = -\imath\int \frac{d^3\mathbf{k}}{(2\pi)^3}\,\frac{d\omega}{2\pi}\,\mathbf{k}\tilde{\Phi}_{ind}^{(i)}(\mathbf{k},\omega)e^{\imath\mathbf{k}\cdot\mathbf{r}-\imath\omega t}\,. \tag{2.68}$$

Now, from 2.64 and the definition of the Fourier Transform we have that,

$$\begin{aligned}\tilde{\Phi}_{ind}(\mathbf{k},\omega) &= \int d^3\mathbf{r}\,dt\,\Phi_{ind}(\mathbf{r},t)e^{-\imath\mathbf{k}\cdot\mathbf{r}+\imath\omega t}\,, &(2.69)\\ &= \int d^3\mathbf{r}\,dt\int d^3\mathbf{r}'\frac{\rho_{ind}^{(i)}(\mathbf{r}',t)}{|\mathbf{r}-\mathbf{r}'|}e^{-\imath\mathbf{k}\cdot\mathbf{r}+\imath\omega t} &(2.70)\\ &= -\int d^3\mathbf{r}\,dt\int d^3\mathbf{r}'\frac{n_i(\mathbf{r}',t)}{|\mathbf{r}-\mathbf{r}'|}e^{-\imath\mathbf{k}\cdot\mathbf{r}+\imath\omega t} &(2.71)\\ &= -\tfrac{4\pi}{k^2}\tilde{n}_i(\mathbf{k},\omega)\,. &(2.72)\end{aligned}$$

Hence, 2.62 becomes,

$$S_i = -\frac{\imath}{v}\int d^3\mathbf{r}\,\rho_{ext}(\mathbf{r},t)\int \frac{d^3\mathbf{k}}{(2\pi)^3}\frac{d\omega}{2\pi}\frac{4\pi}{k^2}\tilde{n}_i(\mathbf{k},\omega)\,(\mathbf{k}\cdot\mathbf{v})\,e^{\imath\mathbf{k}\cdot\mathbf{r}-\imath\omega t} \tag{2.73}$$

Clearly we can see that the ith order stopping force depends crucially on the Fourier Transform of the ith electron density in our hydrodynamic model, $\tilde{n}_i(\mathbf{k},\omega)$.

2.3.1 Electron Density

In the above sections it was shown that the stopping force depended on $\tilde{n}$ which is the fourier transfrom of the electron density in our hydrodynamic model of the electron gas.

First Order Electron Density

We begin by taking the Fourier Transform of the first order continuity equation, 2.35,

$$\mathcal{F}\left(\frac{\partial n_1}{\partial t}\right) - \mathcal{F}\left(n_0 \nabla^2 \psi_1\right) = 0\,. \tag{2.74}$$

From the definition of the Fourier Transform, we have,

$$\mathcal{F}\left(\frac{\partial n_1}{\partial t}\right) = (-\imath\omega)\tilde{n_1}(\mathbf{k},\omega)\,. \tag{2.75}$$

Likewise,

$$\mathcal{F}\left(n_0 \nabla^2 \psi_1\right) = (-k^2) n_0 \tilde{\psi_1}(\mathbf{k},\omega)\,, \tag{2.76}$$

Thus, in Fourier space, the continuity equation becomes,

$$-\imath\omega\tilde{n}_1(\mathbf{k},\omega) + n_0 k^2 \tilde{\psi_1}(\mathbf{k},\omega) = 0\,. \tag{2.77}$$

From 2.77 can solve for ψ_1,

$$\tilde{\psi_1}(\mathbf{k},\omega) = \frac{\imath\omega\tilde{n}_1}{k^2 n_0}\,. \tag{2.78}$$

Now performing the Fourier Transform of the first order momentum equation, 2.42,

$$\mathcal{F}\left(-\frac{\partial}{\partial t}\nabla^2\psi_1\right) = \mathcal{F}\left(4\pi\left(n_1 - \rho_{ext}\right) - \nabla^2\left(\frac{\delta G}{\delta n}\right)_1\right) + \mathcal{F}\left(-\vec{\nabla}\eta\mathbf{u}\right)\,, \tag{2.79}$$

we obtain,

$$\imath\omega(-k^2)\tilde{\psi_1} = 4\pi\left(\tilde{n}_1 - \tilde{\rho}_{ext}\right) + k^2\left(\alpha\frac{\tilde{n}_1}{n_0} - \beta\frac{-k^2\tilde{n}_1}{n_0}\right) + \eta\left(-k^2\tilde{\psi_1}\right)\,. \tag{2.80}$$

Substituting our value for $\tilde{\psi_1}$ and identifying the plasma frequency, ω_p, as,

$$\omega_p^2 = 4\pi n_0\,, \tag{2.81}$$

we arrive at,

$$\left(-\omega^2 + \omega_p^2 + \alpha k^2 + \beta k^4 - \imath\omega\eta\right)\tilde{n}_1 = \omega_p^2 \tilde{\rho}_{ext}\,. \tag{2.82}$$

We simplify this expression by introducing a new function $N(\mathbf{k},\omega)$ (which is related to the dielectric function)

$$N(\mathbf{k},\omega) = \beta k^4 + \alpha k^2 - \omega^2 + \omega_p^2 - \imath\omega\eta\,, \tag{2.83}$$

which allows us to write the first order electron density as,

$$\tilde{n}_1(\mathbf{k},\omega) = \frac{\omega_p^2}{N(\mathbf{k},\omega)}\tilde{\rho}_{ext}(\mathbf{k},\omega) \tag{2.84}$$

Note that the Fourier Transfrom of the dielectric function of the electron gas in the hydrodynamic model is,

$$\varepsilon(\mathbf{k},\omega) = \left[1 - \frac{\omega_p^2}{N(\mathbf{k},\omega)}\right]^{-1}\,. \tag{2.85}$$

Second Order Electron Desnity

To find the second order electron density we begin by performing the Fourier Transform on the 2nd order continuity equation 2.36,

$$\mathcal{F}\left(\frac{\partial n_2}{\partial t} - n_0\nabla^2\psi_2\right) - \mathcal{F}\left(\vec{\nabla}\cdot(n_1\vec{\nabla}\psi_1)\right) = 0\,, \tag{2.86}$$

which gives,

$$-\imath\omega\tilde{n_2} + n_0 k^2\tilde{\psi}_2 - \imath\mathbf{k}\cdot\mathcal{F}(n_1\vec{\nabla}\psi_1) = 0\,. \tag{2.87}$$

The last term has been considered separately, since one must be careful when applying the Fourier Transform to a product of functions. When taking the Fourier Transform of products of functions we must apply the convolution theorem. Thus,

$$\mathcal{F}(n_1\vec{\nabla}\psi_1) = \imath\int_{-\infty}^{\infty}\tilde{n}_1(\mathbf{k}',\omega')(\mathbf{k}'-\mathbf{k})\tilde{\psi}_1(\mathbf{k}-\mathbf{k}',\omega-\omega')d\mathbf{k}'\,d\omega'\,, \tag{2.88}$$

$$= \mathcal{F}(n_1) * \mathcal{F}(\vec{\nabla}\psi_1)\,. \tag{2.89}$$

Thus, the transformed, second order continuity equation becomes,

$$-\imath\omega\tilde{n_2} + n_0 k^2\tilde{\psi}_2 - \mathcal{F}(n_1) * \mathcal{F}(\vec{\nabla}\psi_1) = 0\,. \tag{2.90}$$

Likewise, we transform the second order momentum equation, 2.43,

$$\mathcal{F}\left(-\frac{\partial}{\partial t}\nabla^2\psi_2\right)+\mathcal{F}\left(\frac{1}{2}\nabla^2(\vec{\nabla}\psi_1)^2\right)=\mathcal{F}\left(4\pi n_2\right)-\mathcal{F}\left(\nabla^2\left(\frac{\delta G}{\delta n}\right)_2\right). \tag{2.91}$$

From which we obtain the following parts,

$$\mathcal{F}\left(-\frac{\partial}{\partial t}\nabla^2\psi_2\right)= -\imath\omega k^2\tilde{\psi_2}\,, \tag{2.92}$$

$$\mathcal{F}\left(\frac{1}{2}\nabla^2(\vec{\nabla}\psi_1)^2\right)= -\tfrac{1}{2}k^2\mathcal{F}(\vec{\nabla}\psi_1)\dot{*}\mathcal{F}(\vec{\nabla}\psi_1)\,, \tag{2.93}$$

$$\mathcal{F}\left(4\pi n_2\right)= 4\pi\tilde{n_2}\,, \tag{2.94}$$

$$\mathcal{F}\left(\nabla^2\left(\frac{\delta G}{\delta n}\right)_2\right)= -k^2\mathcal{F}\left(\tfrac{\delta G}{\delta n}\right)_2\,, \tag{2.95}$$

where the $\dot{*}$ reminds us that we are taking the convolution of transformations of two vector quantities that have been dotted together.

Now, using 2.55 the Fourier Transform of 2.95 is,

$$\mathcal{F}\left(\frac{\delta G}{\delta n}\right)_2 = \mathcal{F}\left[\alpha\left(\frac{n_2}{n_0}-\frac{1}{6}\frac{n_1^2}{n_0^2}\right)+\frac{\beta}{2n_0^2}((\vec{\nabla}n_1)^2-2n_0\nabla^2n_2+2n_1\nabla^2n_1)\right], \tag{2.96}$$

$$\begin{aligned}= {}& \alpha\left(\frac{\tilde{n_2}}{n_0}-\frac{\mathcal{F}(n_1)*\mathcal{F}(n_1)}{6n_0^2}\right)+\frac{\beta}{2n_0^2}\left[\mathcal{F}(\vec{\nabla}n_1)\dot{*}\mathcal{F}(\vec{\nabla}n_1)-2n_0k^2\tilde{n_2}\right.\\ &\left.+2\mathcal{F}(n_1)*\mathcal{F}(\nabla^2n_1)\right].\end{aligned} \tag{2.97}$$

Thus, the two equations we need to solve are,

$$-\imath\omega\tilde{n_2}+n_0k^2\tilde{\psi_2} = \mathcal{F}(n_1)*\mathcal{F}(\vec{\nabla}\psi_1)\,, \tag{2.98}$$

$$\begin{aligned}-\imath\omega k^2\tilde{\psi_2}-\tilde{n_2}\left[4\pi+k^2\left(\frac{\alpha}{n_0}-2n_0k^2\right)\right] = {}& \frac{1}{2}k^2\mathcal{F}(\vec{\nabla}\psi_1)\dot{*}\mathcal{F}(\vec{\nabla}\psi_1)\\ &+k^2\left[\frac{\beta}{2n_0^2}(\mathcal{F}(\vec{\nabla}n_1)\dot{*}\mathcal{F}(\vec{\nabla}n_1)-\alpha\frac{\mathcal{F}(n_1)*\mathcal{F}(n_1)}{6n_0^2}\right.\\ &\left.-2\mathcal{F}(n_1)*\mathcal{F}(\nabla^2n_1))\right].\end{aligned} \tag{2.99}$$

What one should notice about 2.98 and 2.99 is that they are algebraic in the unknown quantities, $\tilde{\psi_2}$ and $\tilde{n_2}$.

To simplify our expression we define the following quantities,

$$\mathbf{k}'' = \mathbf{k} - \mathbf{k}' , \tag{2.100}$$

$$\omega'' = \omega - \omega' , \tag{2.101}$$

and introduce suitable delta functions to make the expressions for the convolutions more symmetric,

$$\mathcal{F}(C) * \mathcal{F}(B) = \int d^3\mathbf{k}' d\omega' \tilde{C}(\mathbf{k} - \mathbf{k}', \omega - \omega') \tilde{B}(\mathbf{k}', \omega') , \tag{2.102}$$

$$= \int d^3\mathbf{k}' d^3\mathbf{k}'' d\omega' d\omega'' \delta(\mathbf{k} - \mathbf{k}' - \mathbf{k}'') \delta(\omega - \omega' - \omega'') \tilde{C}(\mathbf{k}', \omega') \tilde{B}(\mathbf{k}'', \omega'') , \tag{2.103}$$

for arbitrary functions B and C.

Further, we define the quantity, W as,

$$W = \frac{1}{2} \left[-\omega\omega''\mathbf{k}\cdot\mathbf{k}''k'^2 - \omega\omega'\mathbf{k}\cdot\mathbf{k}'k''^2 - \omega'\omega''k^2\mathbf{k}'\cdot\mathbf{k}'' + \beta k^2 k'^2 k''^2 \left(k''^2 + k'^2 + \mathbf{k}'\cdot\mathbf{k}'' \right) \right] , \tag{2.104}$$

as well as,

$$A(\mathbf{k}, \mathbf{k}', \mathbf{k}'', \omega, \omega', \omega'') = W + \frac{\alpha}{6} k^2 k'^2 k''^2 . \tag{2.105}$$

These two definitions make the final expression for $\tilde{n_2}$ much more compact,

$$\tilde{n}_2(\mathbf{k}, \omega) = n_0 \int \frac{d^3\mathbf{k}'}{(2\pi)^4} d^3\mathbf{k}'' \, d\omega' \, d\omega'' \, \delta(\mathbf{k} - \mathbf{k}' - \mathbf{k}'') \delta(\omega - \omega' - \omega'') \frac{\phi_{ext}(\mathbf{k}', \omega') \phi_{ext}(\mathbf{k}'', \omega'') A(\mathbf{k}, \mathbf{k}', \mathbf{k}'', \omega, \omega', \omega'')}{N(\mathbf{k}, \omega) N(\mathbf{k}', \omega') N(\mathbf{k}'', \omega'')} , \tag{2.106}$$

with N defined as in 2.83.

2.3.2 Structure Factor of a Cluster

In the above section we were able to find the first and second order electron densities in Fourier space. Likewise we wish to describe the charge density of the projectile in Fourier space as well. We shall find it convenient when formulating a general formula for the stopping force to define a quantity called the *structure factor* which captures the physics stemming from the geometrical configuration of the projectile.

General First Order Structure Factor, F_2

From the definition of the Fourier Transform we have that the external charge density in Fourier space of a projectile moving at constant velocity $\mathbf{v}$ is given by,

$$\tilde{\rho}_{ext}(\mathbf{k},\omega) = \int d^3\mathbf{r}\, dt\, \rho_{ext}(\mathbf{r},t)\, e^{-\imath\mathbf{k}\cdot\mathbf{r}+\imath\omega t}\,, \tag{2.107}$$

$$= \int d^3\mathbf{r}\, dt\, \rho_{proj}(\mathbf{r}-\mathbf{v}t)\, e^{-\imath\mathbf{k}\cdot\mathbf{r}+\imath\omega t}\,, \tag{2.108}$$

where ρ_{proj} is the charge density of the projectile in the projectile's frame of reference. Note that in the projectile's frame of reference, Φ_{ind} does not change in time.

If we define an auxillary variable, $\mathbf{x} = \mathbf{r} - \mathbf{v}t$ then 2.108 becomes,

$$\tilde{\rho}_{ext}(\mathbf{k},\omega) = \int d^3\mathbf{x}\, dt\, \rho_{proj}(\mathbf{x})\, e^{-\imath\mathbf{k}\cdot(\mathbf{x}+\mathbf{v}t)+\imath\omega t}\,, \tag{2.109}$$

$$= \int dt\, e^{\imath(\omega-\mathbf{k}\cdot\mathbf{v})t} \int d^3\mathbf{x}\, \rho_{proj}(\mathbf{x}) e^{-\imath\mathbf{k}\cdot\mathbf{x}} \tag{2.110}$$

$$= 2\pi\delta(\omega-\mathbf{k}\cdot\mathbf{v})\tilde{\rho}_{proj}(\mathbf{k})\,. \tag{2.111}$$

Returning now to our expression for the stopping force, for the first order calculation we have,

$$S_1 = -\frac{\imath}{v}\int d^3\mathbf{r}\, \rho_{ext}(\mathbf{r},t) \int \frac{d^3\mathbf{k}}{(2\pi)^3}\frac{d\omega}{2\pi}\frac{4\pi}{k^2}\tilde{n}_1(\mathbf{k},\omega)\,(\mathbf{k}\cdot\mathbf{v})\, e^{\imath\mathbf{k}\cdot\mathbf{r}-\imath\omega t}\,, \tag{2.112}$$

and from the first order electron density calculation 2.84, we then have,

$$S_1 = -\frac{\imath}{v}\int d^3\mathbf{r}\, \rho_{ext}(\mathbf{r},t) \int \frac{d^3\mathbf{k}}{(2\pi)^3}\frac{d\omega}{2\pi}\frac{4\pi}{k^2}\frac{\omega_p^2}{N(\mathbf{k},\omega)}\tilde{\rho}_{ext}(\mathbf{k},\omega)\,(\mathbf{k}\cdot\mathbf{v})\, e^{\imath\mathbf{k}\cdot\mathbf{r}-\imath\omega t}\,. \tag{2.113}$$

Equation 2.111 brings the first order stopping force to,

$$S_1 = -\frac{\imath}{v}\int d^3\mathbf{r}\, \rho_{ext}(\mathbf{r},t) \int \frac{d^3\mathbf{k}}{(2\pi)^3}\frac{d\omega}{2\pi}\frac{4\pi}{k^2}\frac{\omega_p^2}{N(\mathbf{k},\omega)}2\pi\delta(\omega-\mathbf{k}\cdot\mathbf{v})\tilde{\rho}_{proj}(\mathbf{k})\,(\mathbf{k}\cdot\mathbf{v})\, e^{\imath\mathbf{k}\cdot\mathbf{r}-\imath\omega t}\,. \tag{2.114}$$

Now, the external charge density, $\rho_{ext}(\mathbf{r},t)$ is just the projectile charge density, which we've already described as $\rho_{proj}(\mathbf{r}-\mathbf{v}t)$ in the projectile's frame of reference. Thus,

$$S_1 = -\frac{\imath}{v}\int d^3\mathbf{r}\, \rho_{proj}(\mathbf{r}-\mathbf{v}t) \int \frac{d^3\mathbf{k}}{(2\pi)^3}\frac{d\omega}{2\pi}\frac{4\pi}{k^2}\frac{\omega_p^2}{N(\mathbf{k},\omega)}2\pi\delta(\omega-\mathbf{k}\cdot\mathbf{v})\tilde{\rho}_{proj}(\mathbf{k})\,(\mathbf{k}\cdot\mathbf{v})\, e^{\imath\mathbf{k}\cdot\mathbf{r}-\imath\omega t}\,. \tag{2.115}$$

Taking the integration over ω consumes the delta,

$$S_1 = -\frac{\imath}{v}\int d^3\mathbf{r}\,\rho_{proj}(\mathbf{r}-\mathbf{v}t)\int \frac{d^3\mathbf{k}}{(2\pi)^3}\frac{d\omega}{2\pi}\frac{4\pi}{k^2}\frac{\omega_p^2}{N(\mathbf{k},\omega)}2\pi\tilde{\rho}_{proj}(\mathbf{k})\,(\mathbf{k}\cdot\mathbf{v})\,e^{\imath\mathbf{k}\cdot(\mathbf{r}-\mathbf{v}t)}\,. \quad (2.116)$$

Recognizing that,

$$\int d^3\mathbf{r}\,\rho_{proj}(\mathbf{r}-\mathbf{v}t)e^{\imath\mathbf{k}\cdot(\mathbf{r}-\mathbf{v}t)} = \tilde{\rho}_{proj}(-\mathbf{k}) = \tilde{\rho}^*_{proj}(\mathbf{k})\,, \quad (2.117)$$

we can pull all the constant terms outside of the integral and write the first order stopping force as,

$$S_1 = -\frac{\imath\omega_p^2}{2\pi^2 v}\int \frac{d^3\mathbf{k}}{k^2}(\mathbf{k}\cdot\mathbf{v})\frac{\tilde{\rho}_{proj}(\mathbf{k})\tilde{\rho}_{proj}(-\mathbf{k})}{N(\mathbf{k},\mathbf{k}\cdot\mathbf{v})}\,, \quad (2.118)$$

It is worthwhile to notice that all the information about the structure of the projectile is completely contained in the $\tilde{\rho}_{proj}(\mathbf{k})\tilde{\rho}_{proj}(-\mathbf{k})$ term. Should we change the type of projectile, the overall expression remains intact. The part of the expression which would change is the densities. For this reason it is convenient to define the first order *structure factor*, F_2,

$$F_2(\mathbf{k}) = \tilde{\rho}_{proj}(\mathbf{k})\tilde{\rho}_{proj}(-\mathbf{k}) = |\rho_{proj}(\mathbf{k})|^2\,, \quad (2.119)$$

and thus,

$$S_1 = -\frac{\imath\omega_p^2}{2\pi^2 v}\int \frac{d^3\mathbf{k}}{k^2}(\mathbf{k}\cdot\mathbf{v})\frac{F_2(\mathbf{k})}{N(\mathbf{k},\mathbf{k}\cdot\mathbf{v})}\,. \quad (2.120)$$

First Order Structure Factor: Ion

For an ion, the structure factor is given by,

$$F_2(\mathbf{k}) = \tilde{\rho}_{ion}(\mathbf{k})\tilde{\rho}_{ion}(-\mathbf{k})\,. \quad (2.121)$$

The charge density for an ion,

$$\rho_{ion}(\mathbf{r}) = Q\delta(\mathbf{r})\,. \quad (2.122)$$

and thus,

$$\tilde{\rho}_{ion}(\mathbf{k}) = Q\,. \quad (2.123)$$

and,

$$F_2^{ion}(\mathbf{k}) = Q^2\,. \quad (2.124)$$

First Order Structure Factor: Colinear Dicluster

A dicluster is a cluster with two ions separated by distance d. We assume that the dicluster is aligned so that the displacement vector, $\mathbf{D}$ between the two ions is aligned in the direction of travel. For a colinear dicluster which is static in its frame of reference,

$$\rho_{colin}(\mathbf{r}) = Q_1\delta(\mathbf{r}-\mathbf{r}_1) + Q_2\delta(\mathbf{r}-\mathbf{r}_2)\,, \tag{2.125}$$

where Q_i is the charge on the ith ion, and $\mathbf{r}_i$ is its position with respect to the moving frame of the cluster. Thus, in Fourier space,

$$\begin{aligned}\tilde{\rho}_{colin}(\mathbf{k}) = &\int d^3\mathbf{r} Q_1\delta(\mathbf{r}-\mathbf{r}_1) + Q_2\delta(\mathbf{r}-\mathbf{r}_2)e^{-\imath\mathbf{k}\cdot\mathbf{r}}\,, &(2.126)\\ = &\quad Q_1e^{-\imath\mathbf{k}\cdot\mathbf{r}_1} + Q_2e^{-\imath\mathbf{k}\cdot\mathbf{r}_2}\,. &(2.127)\end{aligned}$$

Assuming that the cluster is homonuclear, $Q_1 = Q_2 = Q$ and thus,

$$\begin{aligned}\tilde{\rho}_{colin}(\mathbf{k}) = &\quad Qe^{-\imath\mathbf{k}\cdot\mathbf{r}_1} + Qe^{-\imath\mathbf{k}\cdot\mathbf{r}_2}\,, &(2.128)\\ = &\quad Q\left(e^{-\imath\mathbf{k}\cdot\mathbf{r}_1} + e^{-\imath\mathbf{k}\cdot\mathbf{r}_2}\right)\,. &(2.129)\end{aligned}$$

Using this in our expression for the general structure factor, 2.144, we obtain,

$$\begin{aligned}F_2^{colin} = &\quad Q^2\left(e^{-\imath\mathbf{k}\cdot\mathbf{r}_1} + e^{-\imath\mathbf{k}\cdot\mathbf{r}_2}\right)\left(e^{\imath\mathbf{k}\cdot\mathbf{r}_1} + e^{\imath\mathbf{k}\cdot\mathbf{r}_2}\right)\,, &(2.130)\\ = &\quad Q^2(2+2\cos(\mathbf{k}\cdot(\mathbf{r}_1-\mathbf{r}_2)))\,, &(2.131)\\ = &\quad Q^2(2+2\cos(\mathbf{k}\cdot\mathbf{D}))\,. &(2.132)\end{aligned}$$

First Order Structure Factor: Randomly Oriented Dicluster

In current experiments one can not resolve the effect of a single dicluster incident on a target. Instead, beams of diclusters would be used. In this case, the orientation of the projectiles is completely random. Considering this fact, it is useful to calculate the average stopping force of a beam of randomly oriented diclusters. To this end, we obtain an expression for the structure factor for a randomly oriented dicluster.

The average first order stopping force of a cluster is calculated by averaging the first order stopping force over all cluster orientations. Since, as previously mentioned, the only information which enters into the stopping force due to the structure of the cluster comes from the cluster

factor. Thus, in order to obtain the average stopping force one needs only to average the cluster factor over the possible orientations. Therefore,

$$\begin{aligned} F_2^{rand} &= \rho_{rand}(\mathbf{k})\rho_{rand}(-\mathbf{k})\,, && (2.133)\\ &= \langle Q^2(2+2\cos(\mathbf{k}\cdot\mathbf{D}))\rangle\ , && (2.134)\\ &= Q^2(2+2\langle\cos(\mathbf{k}\cdot\mathbf{D})\rangle)\,, && (2.135)\\ &= Q^2\left(2+2\tfrac{\sin(kD)}{kD}\right) && (2.136)\end{aligned}$$

General Second Order Structure Factor, F_3

In the previous sections we discussed the first order structure factor for various clusters. In this section we outline the second order structure factors. As before we start out with the expression for the stopping force, but in this case we will consider the second order expression.

The second order stopping force is given by,

$$S_2 = -\frac{\imath}{v}\int d^3\mathbf{r}\,\rho_{ext}(\mathbf{r},t)\int\frac{d^3\mathbf{k}}{(2\pi)^3}\frac{d\omega}{2\pi}\frac{4\pi}{k^2}\tilde{n}_2(\mathbf{k},\omega)\,(\mathbf{k}\cdot\mathbf{v})\,e^{\imath\mathbf{k}\cdot\mathbf{r}-\imath\omega t}\,. \tag{2.137}$$

From our expression for $\tilde{n}_2$, (2.106), then the second order stopping force becomes,

$$\begin{aligned} S_2 \;=\; & -\frac{\imath n_0}{v}\int d^3\mathbf{r}\,\rho_{ext}(\mathbf{r},t)\int\frac{d^3\mathbf{k}}{(2\pi)^3}\frac{d\omega}{2\pi}\frac{4\pi}{k^2}\int\frac{d^3\mathbf{k}'}{(2\pi)^3}\frac{d\omega'}{2\pi}\,d^3\mathbf{k}''\;d\omega''\;\delta(\mathbf{k}-\mathbf{k}'-\mathbf{k}'')\delta(\omega-\omega'-\omega'')\\ & \frac{\phi_{ext}(\mathbf{k}',\omega')\phi_{ext}(\mathbf{k}'',\omega'')A(\mathbf{k},\mathbf{k}',\mathbf{k}'',\omega,\omega',\omega'')}{N(\mathbf{k},\omega)N(\mathbf{k}',\omega')N(\mathbf{k}'',\omega'')}(\mathbf{k}\cdot\mathbf{v})\,e^{\imath\mathbf{k}\cdot\mathbf{r}-\imath\omega t}\,. \end{aligned} \tag{2.138}$$

From Poisson's equation, and the definition of the Fourier Transform, it may be shown that,

$$\tilde{\phi}_{ext}(\mathbf{k},\omega) = \frac{4\pi}{k^2}\tilde{\rho}_{ext}(\mathbf{k},\omega)\,, \tag{2.139}$$

and from 2.111 the external potential may be written,

$$\tilde{\phi}_{ext}(\mathbf{k},\omega) = \frac{4\pi}{k^2}\left[2\pi\delta(\omega-\mathbf{k}\cdot\mathbf{v})\tilde{\rho}_{proj}(\mathbf{k})\right]\,. \tag{2.140}$$

Using this in our expression for the second order stopping force, as well as recalling that

$$\begin{aligned} \int d^3\mathbf{r}\,\rho_{ext}(\mathbf{r},t)e^{\imath\mathbf{k}\cdot(\mathbf{r}-\mathbf{v}t)} &= \int d^3\mathbf{r}\,\rho_{proj}(\mathbf{r}-\mathbf{v}t)e^{\imath\mathbf{k}\cdot(\mathbf{r}-\mathbf{v}t)} && (2.141)\\ &= \tilde{\rho}_{proj}(-\mathbf{k})\,, && (2.142)\end{aligned}$$

we may bring 2.138 to,

$$\begin{aligned} S_2 &= -\frac{in_0}{v}\int\frac{d^3\mathbf{k}}{(2\pi)^3}\int\frac{d^3\mathbf{k}'}{(2\pi)^3}\int d^3\mathbf{k}''\,\frac{4\pi}{k^2}\frac{4\pi}{k'^2}\frac{4\pi}{k''^2}(\mathbf{k}\cdot\mathbf{v})\tilde{\rho}_{proj}(-\mathbf{k})\tilde{\rho}_{proj}(\mathbf{k}')\tilde{\rho}_{proj}(\mathbf{k}'') \\ &\quad \delta(\mathbf{k}-\mathbf{k}'-\mathbf{k}'')\int d\omega\int d\omega'\int d\omega''\delta(\omega-\omega'-\omega'')\frac{\delta(\omega-\mathbf{k}\cdot\mathbf{v})\delta(\omega'-\mathbf{k}'\cdot\mathbf{v})\delta(\omega''-\mathbf{k}''\cdot\mathbf{v})}{N(\mathbf{k},\omega)N(\mathbf{k}',\omega')N(\mathbf{k}'',\omega'')} \\ &\quad A(\mathbf{k},\mathbf{k}',\mathbf{k}'',\omega,\omega',\omega'')\,. \end{aligned} \tag{2.143}$$

Introducing the second order structure factor,

$$F_3(\mathbf{k},\mathbf{k}',\mathbf{k}'') = \tilde{\rho}_{proj}(-\mathbf{k})\tilde{\rho}_{proj}(\mathbf{k}')\tilde{\rho}_{proj}(\mathbf{k}'')\,, \tag{2.144}$$

we get,

$$\begin{aligned} S_2 &= -\frac{in_0}{v}\int\frac{d^3\mathbf{k}}{(2\pi)^3}\int\frac{d^3\mathbf{k}'}{(2\pi)^3}\int d^3\mathbf{k}''\,\frac{4\pi}{k^2}\frac{4\pi}{k'^2}\frac{4\pi}{k''^2}(\mathbf{k}\cdot\mathbf{v})F_3(\mathbf{k},\mathbf{k}',\mathbf{k}'')\delta(\mathbf{k}-\mathbf{k}'-\mathbf{k}'') \\ &\quad \int d\omega\int d\omega'\int d\omega''\delta(\omega-\omega'-\omega'')\frac{\delta(\omega-\mathbf{k}\cdot\mathbf{v})\delta(\omega'-\mathbf{k}'\cdot\mathbf{v})\delta(\omega''-\mathbf{k}''\cdot\mathbf{v})}{N(\mathbf{k},\omega)N(\mathbf{k}',\omega')N(\mathbf{k}'',\omega'')} \\ &\quad A(\mathbf{k},\mathbf{k}',\mathbf{k}'',\omega,\omega',\omega'')\,. \end{aligned} \tag{2.145}$$

Second Order Structure Factor: Ion

As above, for an ion,

$$F_3^{ion}(\mathbf{k},\mathbf{k}',\mathbf{k}'') = \tilde{\rho}_{ion}(-\mathbf{k})\tilde{\rho}_{ion}(\mathbf{k}')\tilde{\rho}_{ion}(\mathbf{k}''). \tag{2.146}$$

Since the charge density for an ion,

$$\rho_{ion}(\mathbf{r}) = Q\delta(\mathbf{r})\,. \tag{2.147}$$

and thus,

$$\tilde{\rho}_{ion}(\mathbf{k}) = Q\,. \tag{2.148}$$

and,

$$F_3^{ion}(\mathbf{k},\mathbf{k}',\mathbf{k}'') = Q^3\,. \tag{2.149}$$

Second Order Structure Factor: Colinear Dicluster

As discussed above, the charge density of a general dicluster is,

$$\rho_{colin}(\mathbf{r}) = Q_1\delta(\mathbf{r}-\mathbf{r}_1) + Q_2\delta(\mathbf{r},-\mathbf{r}_2)\,, \tag{2.150}$$

thus, in Fourier space,

$$\tilde{\rho}_{colin}(\mathbf{k}) = Q_1 e^{-\imath\mathbf{k}\cdot\mathbf{r}_1} + Q_2 e^{-\imath\mathbf{k}\cdot\mathbf{r}_2} \tag{2.151}$$

Again, if the cluster is homonuclear,

$$\tilde{\rho}_{colin}(\mathbf{k}) = Q\left(e^{-\imath\mathbf{k}\cdot\mathbf{r}_1} + e^{-\imath\mathbf{k}\cdot\mathbf{r}_2}\right) \tag{2.152}$$

Using this in our expression for the general structure factor, 2.144, we obtain,

$$\begin{aligned}
F_3^{colin} = & \quad Q^3\left(e^{-\imath\mathbf{k}\cdot\mathbf{r}_1} + e^{-\imath\mathbf{k}\cdot\mathbf{r}_2}\right)\left(e^{\imath\mathbf{k}'\cdot\mathbf{r}_1} + e^{\imath\mathbf{k}'\cdot\mathbf{r}_2}\right)\left(e^{\imath\mathbf{k}''\cdot\mathbf{r}_1} + e^{\imath\mathbf{k}''\cdot\mathbf{r}_2}\right) && (2.153)\\
= & \quad 2Q^3(1+\cos(\mathbf{k}\cdot(\mathbf{r}_1-\mathbf{r}_2)) + \cos(\mathbf{k}'\cdot(\mathbf{r}_1-\mathbf{r}_2)) + \cos(\mathbf{k}''\cdot(\mathbf{r}_1-\mathbf{r}_2)))\,, && (2.154)\\
= & \quad 2Q^3(1+\cos(\mathbf{k}\cdot\mathbf{D}) + \cos(\mathbf{k}'\cdot\mathbf{D}) + \cos(\mathbf{k}''\cdot\mathbf{D}))\,, && (2.155)
\end{aligned}$$

Second Order Structure Factor: Randomly Oriented Dicluster

$$\begin{aligned}
F_3^{rand} = & \quad \rho_{rand}(-\mathbf{k})\rho_{rand}(\mathbf{k}')\rho_{rand}(\mathbf{k}'')\,, && (2.156)\\
= & \quad \langle 2Q^3(1+\cos(\mathbf{k}\cdot\mathbf{D}) + \cos(\mathbf{k}'\cdot\mathbf{D}) + \cos(\mathbf{k}''\cdot\mathbf{D}))\rangle\,, && (2.157)\\
= & \quad Q^3(1+\langle\cos(\mathbf{k}\cdot\mathbf{D}) + \cos(\mathbf{k}'\cdot\mathbf{D}) + \cos(\mathbf{k}''\cdot\mathbf{D})\rangle)\,, && (2.158)\\
= & \quad 2Q^3\left(1+\tfrac{\sin(kD)}{kD} + \tfrac{\sin(k'D)}{k'D} + \tfrac{\sin(k''D)}{k''D}\right) && (2.159)
\end{aligned}$$

2.3.3 First Order Stopping Force

We now use our first order cluster factors, F_2 in our final expression for the first order stopping force, 2.120 to obtain an formula for the calculation of the first order stopping force of the various projectiles under consideration.

First Order Stopping Force: Ion

Using 2.124 in 2.120 we obtain,

$$S_1 = -\frac{\imath\omega_p^2 Q^2}{2\pi^2 v}\int \frac{d^3\mathbf{k}}{k^2}(\mathbf{k}\cdot\mathbf{v})\frac{1}{N(\mathbf{k},\mathbf{k}\cdot\mathbf{v})}\,. \tag{2.160}$$

First Order Stopping Force: Colinear Dicluster

In the case of the colinear dicluster, we use 2.132 in 2.120 to arrive at,

$$S_1 = -\frac{\imath Q^2\omega_p^2}{\pi^2 v}\int \frac{d^3\mathbf{k}}{k^2}(\mathbf{k}\cdot\mathbf{v})\frac{1+\cos(\mathbf{k}\cdot\mathbf{D})}{N(\mathbf{k},\mathbf{k}\cdot\mathbf{v})}\,. \tag{2.161}$$

First Order Stopping Force: Randomly Oriented Dicluster

Finally, for the case of a randomly oriented dicluster we insert 2.136 into 2.120 to yield the first order stopping force for the randomly oriented dicluster,

$$S_1 = -\frac{\imath Q^2\omega_p^2}{\pi^2 v}\int \frac{d^3\mathbf{k}}{k^2}(\mathbf{k}\cdot\mathbf{v})\frac{\left(1+\frac{\sin(kD)}{kD}\right)}{N(\mathbf{k},\mathbf{k}\cdot\mathbf{v})}\,. \tag{2.162}$$

2.3.4 Second Order Stopping Force

As in the above subsections, we can use our expressions for the second order structure factors of our various projectiles, coupled with the second order stopping force formula to obtain the second order stopping force for an ion, colinear dicluster and randomly oriented dicluster.

Second Order Stopping Force: Ion

From 2.149 we see that,

$$F_3^{ion}(\mathbf{k},\mathbf{k}',\mathbf{k}'') = Q^3\,, \tag{2.163}$$

and, when this is used in 2.145 we get,

$$\begin{aligned} S_2 \;=\; & -\frac{\imath n_0 Q^3}{v}\int\frac{d^3\mathbf{k}}{(2\pi)^3}\int\frac{d^3\mathbf{k}'}{(2\pi)^3}\int d^3\mathbf{k}''\,\frac{4\pi}{k^2}\frac{4\pi}{k'^2}\frac{4\pi}{k''^2}(\mathbf{k}\cdot\mathbf{v})\delta(\mathbf{k}-\mathbf{k}'-\mathbf{k}'') \\ & \int d\omega\int d\omega'\int d\omega''\delta(\omega-\omega'-\omega'')\frac{\delta(\omega-\mathbf{k}\cdot\mathbf{v})\delta(\omega'-\mathbf{k}'\cdot\mathbf{v})\delta(\omega''-\mathbf{k}''\cdot\mathbf{v})}{N(\mathbf{k},\omega)N(\mathbf{k}',\omega')N(\mathbf{k}'',\omega'')} \\ & A(\mathbf{k},\mathbf{k}',\mathbf{k}'',\omega,\omega',\omega'')\,. \end{aligned} \tag{2.164}$$

Second Order Stopping Force: Colinear Dicluster

For the case of a colinear dicluster we use the structure factor given by 2.155 in 2.145, giving,

$$\begin{aligned} S_2 &= -\frac{\imath n_0 Q^3}{v}\int\frac{d^3\mathbf{k}}{(2\pi)^3}\int\frac{d^3\mathbf{k}'}{(2\pi)^3}\int d^3\mathbf{k}''\,\frac{4\pi}{k^2}\frac{4\pi}{k'^2}\frac{4\pi}{k''^2}(\mathbf{k}\cdot\mathbf{v})\left[1+\cos(\mathbf{k}\cdot\mathbf{D})+\cos(\mathbf{k}'\cdot\mathbf{D})+\cos(\mathbf{k}''\cdot\mathbf{D})\right] \\ &\quad \delta(\mathbf{k}-\mathbf{k}'-\mathbf{k}'')\int d\omega\int d\omega'\int d\omega''\delta(\omega-\omega'-\omega'')\frac{\delta(\omega-\mathbf{k}\cdot\mathbf{v})\delta(\omega'-\mathbf{k}'\cdot\mathbf{v})\delta(\omega''-\mathbf{k}''\cdot\mathbf{v})}{N(\mathbf{k},\omega)N(\mathbf{k}',\omega')N(\mathbf{k}'',\omega'')} \\ &\quad A(\mathbf{k},\mathbf{k}',\mathbf{k}'',\omega,\omega',\omega'')\,. \end{aligned} \tag{2.165}$$

Second Order Stopping Force: Randomly Oriented Dicluster

We conclude this section by inserting the randomly oriented dicluster structure factor, 2.159 into 2.145 to obtain the second order stopping force for a randomly oriented dicluster,

$$\begin{aligned} S_2 &= -\frac{\imath n_0 Q^3}{v}\int\frac{d^3\mathbf{k}}{(2\pi)^3}\int\frac{d^3\mathbf{k}'}{(2\pi)^3}\int d^3\mathbf{k}''\,\frac{4\pi}{k^2}\frac{4\pi}{k'^2}\frac{4\pi}{k''^2}(\mathbf{k}\cdot\mathbf{v})\left[1+\frac{\sin(kD)}{kD}+\frac{\sin(k'D)}{k'D}+\frac{\sin(k''D)}{k''D}\right] \\ &\quad \delta(\mathbf{k}-\mathbf{k}'-\mathbf{k}'')\int d\omega\int d\omega'\int d\omega''\delta(\omega-\omega'-\omega'')\frac{\delta(\omega-\mathbf{k}\cdot\mathbf{v})\delta(\omega'-\mathbf{k}'\cdot\mathbf{v})\delta(\omega''-\mathbf{k}''\cdot\mathbf{v})}{N(\mathbf{k},\omega)N(\mathbf{k}',\omega')N(\mathbf{k}'',\omega'')} \\ &\quad A(\mathbf{k},\mathbf{k}',\mathbf{k}'',\omega,\omega',\omega'')\,. \end{aligned} \tag{2.166}$$

Chapter 3

Calculation of Stopping Force

As outlined in the introduction and motivation, it is our intention to calculate the second order stopping force of an ion, colinear dicluster and randomly oriented dicluster traversing a metal. The preceding chapter described the development of the formulas for the first and second order stopping force in all three cases. This chapter outlines how the calculations were carried out. We employ two separate strategies, one for each of the first and second order calculations. As we shall see, the second order calculation is *much* more complex and will need some clever considerations and techniques.

Unless otherwise noted, from this point on we are considering the ions in the cluster to be protons, so that $Q = 1$.

3.1 General Strategy

In this section we describe the general strategies that were carried out for each of the first and second order calculations of the stopping force. We begin with the strategy for the first order stopping force.

3.1.1 First Order Strategy

To get a feel for the type of calculation we shall be carrying out, we recall the formula for the first order stopping force in the case of a single ion projectile given by 2.160,

$$S_1^{ion} = -\frac{\imath\omega_p^2}{2\pi^2 v}\int \frac{d^3\mathbf{k}}{k^2}(\mathbf{k}\cdot\mathbf{v})\frac{1}{N(\mathbf{k},\mathbf{k}\cdot\mathbf{v})}\,. \tag{3.1}$$

To simplify the manipulation of the integral, we introduce the scalar variable $\omega = \mathbf{k}\cdot\mathbf{v}$ which may be included explicitly by using the Dirac delta. Thus,

$$S_1^{ion} = -\frac{\imath\omega_p^2}{2\pi^2 v}\int \frac{d^3\mathbf{k}}{k^2}\int_{-\infty}^{\infty} d\omega\,\delta(\omega-\mathbf{k}\cdot\mathbf{v})\,\omega\frac{1}{N(\mathbf{k},\omega)}\,. \tag{3.2}$$

To exploit the spherical symmetry of the setup we carry out the integration over spherical coordinates, $\mathbf{k} = [k,\varphi,\theta]$ which has the added benefit of removing the k^2 singularity in the denominator. This is also convenient since one can see from 2.83 that N depends only on the magnitude of the vector $\mathbf{k}$. Choosing the z-axis in the direction of travel,

$$S_1^{ion} = -\frac{\imath\omega_p^2}{2\pi^2 v}\int_0^{\infty} dk\int_{-\infty}^{\infty} d\omega\,\omega\frac{1}{N(k,\omega)}\int_0^{2\pi} d\varphi\int_0^{\pi} d\theta\sin\theta\,\delta(\omega-kv\cos\theta)\,. \tag{3.3}$$

We now change to a more convenient variable, $\tau = \cos\theta$,

$$S_1^{ion} = -\frac{\imath\omega_p^2}{\pi v}\int_0^{\infty} dk\int_{-\infty}^{\infty} d\omega\,\omega\frac{1}{N(k,\omega)}\int_{-1}^{1} d\tau\,\frac{1}{kv}\delta(\frac{\omega}{kv}-\tau)\,. \tag{3.4}$$

From the properties of the Dirac delta the final integral over τ is in fact nothing more than a Heaviside function,

$$\int_{-1}^{1} d\tau\,\delta(\frac{\omega}{kv}-\tau) = H(k^2v^2-\omega^2)\,, \tag{3.5}$$

which has the effect of restricting the ω inetegral to values between $-kv$ and kv. This follows since only values of ω in this range will give a positive argument to the Heaviside function. Therefore, our simplified formula is,

$$S_1^{ion} = -\frac{\imath\omega_p^2}{\pi v^2}\int_0^{\infty}\frac{dk}{k}\int_{-kv}^{kv} d\omega\,\frac{\omega}{N(k,\omega)}\,. \tag{3.6}$$

The crucial step now comes from the realization that the stopping force must be real. Since $\Re[N(\omega)]$ is an even function of ω and $\Im[N(\omega)]$, the contribution to the integral which comes from the real part vanishes. Thus, the stopping force is indeed real. This also will provide a valuable check when performing out computations. We can thus replace $\frac{1}{N}$ by $\Im\left[\frac{1}{N}\right]$,

$$S_1^{ion} = \frac{\omega_p^2}{\pi v^2} \int_0^\infty \frac{dk}{k} \int_{-kv}^{kv} d\omega\, \omega\, \Im\left[\frac{1}{N(k,\omega)}\right] . \tag{3.7}$$

One sees that,

$$\Im\left[\frac{1}{N(k,-\omega)}\right] = -\Im\left[\frac{1}{N(k,\omega)}\right] , \tag{3.8}$$

which, when coupled with the odd symmetry of the single ω term, gives an overall even symmetry to the integrand, and thus,

$$S_1^{ion} = \frac{2\omega_p^2}{\pi v^2} \int_0^\infty \frac{dk}{k} \int_0^{kv} d\omega\, \omega\, \Im\left[\frac{1}{N(k,\omega)}\right] . \tag{3.9}$$

Now, from our expression for N (2.83) we find that,

$$\Im\left[\frac{1}{N(k,\omega)}\right] = \frac{\omega\eta}{(\beta k^4 + \alpha k^2 - \omega^2 + \omega_p)^2 + \omega^2\eta^2} , \tag{3.10}$$

Letting $\Gamma = |\omega|\eta$, $\omega_k^2 = \beta k^4 + \alpha k^2 + \omega_p^2$ and $x = \omega^2 - \omega_k^2$ then we can write,

$$\Im\left[\frac{1}{N(k,\omega)}\right] = \pi \frac{\frac{\Gamma}{\pi}}{x^2 + \Gamma^2} . \tag{3.11}$$

The benefit of doing this is that we now take the frictionless limit. Assuming that the friction goes to zero, then $\eta \to 0$ and thus $\Gamma \to 0$. From the definition of the Dirac delta,

$$\lim_{\Gamma\to 0} \frac{\frac{\Gamma}{\pi}}{x^2 + \Gamma^2} = \delta(x) . \tag{3.12}$$

Thus, taking the limit allows us to write,

$$\Im\left[\frac{1}{N(k,\omega)}\right] = \pi\, \text{sign}(\omega)\delta(\omega^2 - \omega_k^2) , \tag{3.13}$$

$$= \pi\, \text{sign}(\omega) \left[\frac{\delta(\omega - \omega_k)}{2\omega_k} + \frac{\delta(\omega + \omega_k)}{2\omega_k}\right] . \tag{3.14}$$

Since ω_k is strictly positive and the integration is only over a positive range of ω values, this expression simplifies to,

$$\Im\left[\frac{1}{N(k,\omega)}\right] = \frac{\pi}{2\omega_k}\delta(\omega-\omega_k)\,. \tag{3.15}$$

We note that this constitutes the so-called *plasmon-pole approximation* describing projectile energy loss due to excitation of the collective plasma oscillations in the electron gas with the dispersion relation,

$$\omega = \omega_k = \sqrt{\omega_p^2 + \alpha k^2 + \beta k^4}\,. \tag{3.16}$$

Using this expression in 3.9 gives,

$$S_1^{ion} = \frac{2\omega_p^2}{\pi v^2}\int_0^\infty \frac{dk}{k}\int_0^{kv} d\omega\,\omega_k\,\frac{\pi}{2\omega_k}\delta(\omega-\omega_k)\,, \tag{3.17}$$

$$= \frac{\omega_p^2}{v^2}\int_0^\infty \frac{dk}{k}\int_0^{kv} d\omega\,\delta(\omega-\omega_k)\,. \tag{3.18}$$

Now, from the definition of the Dirac delta,

$$\int_0^{kv} d\omega\,\delta(\omega-\omega_k) = \begin{cases} 1, & \text{if } \omega_k < kv \\ 0, & \text{if } \omega_k > kv \end{cases}\,. \tag{3.19}$$

This integral then puts a restriction on the values that k can take. Only values of k that satisfy $\omega_k < kv$ contribute to the k integral. Thus, the k integral is bounded by k_1 and k_2 which are the solutions of,

$$\beta k^4 - (v^2-\alpha)k^2 + \omega_p^2 = 0\,. \tag{3.20}$$

Treating this as a quadratic equation in k^2 the solution is given by,

$$k_{1,2}^2 = \frac{1}{2\beta}\left[v^2-\alpha \pm \sqrt{(v^2-\alpha)^2 - 4\beta\omega_p^2}\right]\,. \tag{3.21}$$

This brings our stopping formula to,

$$S_1^{ion} = \frac{\omega_p^2}{v^2}\int_{k_1}^{k_2}\frac{dk}{k}\,, \tag{3.22}$$

which, after carrying out the integration, gives,

$$S_1^{ion} = \frac{\omega_p^2}{v^2}\ln\frac{k_2}{k_1}\,, \tag{3.23}$$

where k_i is defined from 3.21.

We can now find the find the stopping force of an ion, given v, ω_p, β and α, by numerically solving for $k_{1,2}$ and using them in 3.23.

We use the above approach for the ion case, and generalize it to the case of clusters. W recall that the only change in the expressions for the different projectiles is brought about by the modification of the cluster factor, F_2. If we assume that the structure factor depends only on the magnitude of k then we may start from 2.120 and follow the exact same procedure as in the ion case, arriving at the general formula,

$$S_1 = \frac{\omega_p^2}{v^2} \int_{k_1}^{k_2} \frac{dk}{k} F_2(k) \,, \tag{3.24}$$

with $k_{1,2}$ given by 3.21.

Thus, for the case of the randomly oriented dicluster (which is spherically symmetric) we conclude that,

$$\begin{aligned} S_1 &= 2\frac{\omega_p^2}{v^2} \int_{k_1}^{k_2} \frac{dk}{k} \left(1 + \frac{\sin(kD)}{kD}\right) . \\ &= 2\frac{\omega_p^2}{v^2} \left[\ln\left(\frac{k_2}{k_1}\right) + \mathrm{Ci}(k_2 D) - \frac{\sin(k_2 D)}{k_2 D} - \mathrm{Ci}(k_1 D) + \frac{\sin(k_1 D)}{k_1 D}\right] , \end{aligned} \tag{3.25}$$

where Ci is the cosine integral, $\mathrm{Ci}(x) = \int dx \frac{\cos(x)}{x}$.

For the case of the colinear dicluster we recall 2.162,

$$S_1 = -\frac{\imath\omega_p^2}{\pi^2 v} \int \frac{d^3\mathbf{k}}{k^2} (\mathbf{k}\cdot\mathbf{v}) \frac{1 + \cos(\mathbf{k}\cdot\mathbf{D})}{N(\mathbf{k}, \mathbf{k}\cdot\mathbf{v})} \,. \tag{3.26}$$

Since $\mathbf{D}$ is colinear with $\mathbf{v}$ then we can write,

$$\mathbf{D} = \frac{D}{v}\mathbf{v} \,, \tag{3.27}$$

and hence,

$$\mathbf{k}\cdot\mathbf{D} = \frac{D}{v}\,\mathbf{k}\cdot\mathbf{v} \,, \tag{3.28}$$

Our first order stopping force for a colinear dicluster then becomes,

$$S_1 = -\frac{\imath\omega_p^2}{\pi^2 v} \int \frac{d^3\mathbf{k}}{k^2} (\mathbf{k}\cdot\mathbf{v}) \frac{1 + \cos(\frac{D}{v}\,\mathbf{k}\cdot\mathbf{v})}{N(\mathbf{k}, \mathbf{k}\cdot\mathbf{v})} \,. \tag{3.29}$$

Again, introducing ω as before, changing to spherical coordinates with the z-axis aligned with v, exploiting the low friction limit, we arrive at,

$$S_1 = 2\frac{\omega_p^2}{v^2}\int_{k_1}^{k_2}\frac{dk}{k}\left[1+\cos\left(\frac{D}{v}\omega_k\right)\right], \tag{3.30}$$

with $k_{1,2}$ given as before.

The strategy to compute the integral in 3.30 numerically is to do the following,

1. Specify a relative tolerance value and number of intervals, m
2. Provide an initial value for the integral, in this case, zero.
3. Discretize k from k_1 to k_2 into m intervals
4. Evaluate the integrand at each value of k
5. Use Simpson's Rule to sum the array of integrand values
6. Compare the relative difference between the current value and the previous value
7. While the relative difference is above the predefined value, double m and repeat steps 3-6

3.1.2 Second Order Integration Strategy

Owing to the increase in complexity of the second order electron density over its first order counterpart, the calculation of the second order stopping force is much more complicated than the first order calculation.

We recall the expression for the second order stopping force of a general projectile, 2.145,

$$\begin{aligned} S_2 \;=\; & -\frac{in_0}{v}\int\frac{d^3\mathbf{k}}{(2\pi)^3}\int\frac{d^3\mathbf{k}'}{(2\pi)^3}\int d^3\mathbf{k}''\,\frac{4\pi}{k^2}\frac{4\pi}{k'^2}\frac{4\pi}{k''^2}(\mathbf{k}\cdot\mathbf{v})F_3(\mathbf{k},\mathbf{k}',\mathbf{k}'')\delta(\mathbf{k}-\mathbf{k}'-\mathbf{k}'') \\ & \int d\omega\int d\omega'\int d\omega''\delta(\omega-\omega'-\omega'')\frac{\delta(\omega-\mathbf{k}\cdot\mathbf{v})\delta(\omega'-\mathbf{k}'\cdot\mathbf{v})\delta(\omega''-\mathbf{k}''\cdot\mathbf{v})}{N(\mathbf{k},\omega)N(\mathbf{k}',\omega')N(\mathbf{k}'',\omega'')} \\ & A(\mathbf{k},\mathbf{k}',\mathbf{k}'',\omega,\omega',\omega'')\,. \end{aligned} \tag{3.31}$$

In order to perform the calculation we must cast it in a form so that numerical integration may be carried out. To this end, we integrate out the Dirac delta's by integrating over every variable *except* $\mathbf{k}$ and $\mathbf{k}'$,

$$\begin{aligned} S_2 &= -\frac{\imath\omega_p^2}{4\pi^4 v}\int \frac{d^3\mathbf{k}}{k^2}\frac{(\mathbf{k}\cdot\mathbf{v})}{N(\mathbf{k},\mathbf{k}\cdot\mathbf{v})}\int \frac{d^3\mathbf{k}'}{k'^2(\mathbf{k}-\mathbf{k}')^2}F_3(\mathbf{k},\mathbf{k}',\mathbf{k}-\mathbf{k}') \\ &\quad \frac{A(\mathbf{k},\mathbf{k}',\mathbf{k}-\mathbf{k}',\mathbf{k}\cdot\mathbf{v},\mathbf{k}'\cdot\mathbf{v},(\mathbf{k}-\mathbf{k}')\cdot\mathbf{v})}{N(\mathbf{k}',\mathbf{k}'\cdot\mathbf{v})N(\mathbf{k}-\mathbf{k}',(\mathbf{k}-\mathbf{k}')\cdot\mathbf{v})}\,. \end{aligned} \tag{3.32}$$

To do the six dimensional integration we must use some clever tricks. The first is to divide the task into two separate integrations. We define,

$$F(\mathbf{k}) = \int \frac{d^3\mathbf{k}'}{k'^2(\mathbf{k}-\mathbf{k}')^2}F_3(\mathbf{k},\mathbf{k}',\mathbf{k}-\mathbf{k}')\frac{A(\mathbf{k},\mathbf{k}',\mathbf{k}-\mathbf{k}',\mathbf{k}\cdot\mathbf{v},\mathbf{k}'\cdot\mathbf{v},(\mathbf{k}-\mathbf{k}')\cdot\mathbf{v})}{N(\mathbf{k}',\mathbf{k}'\cdot\mathbf{v})N(\mathbf{k}-\mathbf{k}',(\mathbf{k}-\mathbf{k}')\cdot\mathbf{v})}\,, \tag{3.33}$$

which would then leave us only to do the integral,

$$S_2 = -\frac{\imath\omega_p^2}{4\pi^4 v}\int \frac{d^3\mathbf{k}}{k^2}\frac{(\mathbf{k}\cdot\mathbf{v})}{N(\mathbf{k},\mathbf{k}\cdot\mathbf{v})}F(\mathbf{k})\,. \tag{3.34}$$

Further simplifying the computation is the fact that one may show that $F(\mathbf{k})$ is indeed cylindrically symmetric, and thus may be written,

$$F(\mathbf{k}) = \tilde{F}(\varrho, z)\,, \tag{3.35}$$

where ϱ is the the magnitude of the radial vector from the z-axis. One may further show that in fact,

$$\tilde{F}(\varrho, z) = \tilde{F}(\varrho, -z)\,. \tag{3.36}$$

What's more, as shown in Appendix C, $\tilde{F}$ is real. This is a crucial development since it allows us to follow the simplification made for the first order stopping force calculation. Namely, that since the stopping force must be real, and since $\tilde{F}$ is also real, then the only way to ensure that the overall stopping force is real is that if the real part of $\frac{1}{N(\mathbf{k},\mathbf{k}\cdot\mathbf{v})}$ vanishes. Considering then the imaginary part of $\frac{1}{N(\mathbf{k},\mathbf{k}\cdot\mathbf{v})}$,

$$\Im\left[\frac{1}{N(k,\mathbf{k}\cdot\mathbf{v})}\right] = \frac{\pi}{2\omega_k}\left[\delta(\mathbf{k}\cdot\mathbf{v}-\omega_k)+\delta(\mathbf{k}\cdot\mathbf{v}+\omega_k)\right]\,, \tag{3.37}$$

with ω_k as given above.

If we use cylindrical coordinates, $\mathbf{k} = [\varrho, \theta, z]$ to carry out the integration over $\mathbf{k}$ with the z-axis chosen to coincide with the direction of motion, then $\mathbf{k} \cdot \mathbf{v} = vz$ and thus,

$$\Im\left[\frac{1}{N(k, \mathbf{k}\cdot\mathbf{v})}\right] = \frac{\pi}{2\omega_k}\left[\delta(vz-\omega_k) + \delta(vz+\omega_k)\right] . \tag{3.38}$$

With these manipulations our second order calculation becomes,

$$S_2 = \frac{2\pi\omega_p^2}{4\pi^4 v}\int_0^\infty d\varrho\varrho \int_{-\infty}^{\infty} \frac{dz}{\varrho^2+z^2}\frac{\pi v z}{2\omega_k}\left[\delta(vz-\omega_k) + \delta(vz+\omega_k)\right]\tilde{F}(\varrho, z) . \tag{3.39}$$

Since $\tilde{F}$ is even with respect to z then this simplifies to,

$$S_2 = \frac{\omega_p^2}{2\pi^2 v^2}\int_0^\infty d\varrho\varrho \int_0^{\infty} \frac{dz}{\varrho^2+z^2}\tilde{F}(\varrho, z)\,\delta(z - \frac{\omega_k}{v}) . \tag{3.40}$$

At this point we still have a two dimensional integration to do after, of course, doing the integration over $\mathbf{k}'$. However, the existence of the Dirac delta is of enormous use to us in simplifying the integration.

The first effect of the Dirac delta is to tie ϱ to z. In this way, for a given ϱ there exist only *two* values of z which satisfy the Dirac delta condition. Thus, the integration doesn't range over an infinite quarter plane, but rather over only a one dimensional slice of this space. Specifically, for a given ϱ, the only permissible values of z must satisfy,

$$z - \frac{\sqrt{\beta(\varrho^2+z^2)^2 + \alpha(\varrho^2+z^2) + \omega_p^2}}{v} = 0 . \tag{3.41}$$

What is more, the above equation also restricts the values of ϱ. Again, since the stopping force must be real, any solution to 3.41 must be real. Given a fixed value for the speed v, only a certain range of ϱ values yields a real solution. In fact, by rearranging 3.41,

$$\beta z^4 + (2\beta\varrho^2 + \alpha - v^2)z^2 + (\alpha\varrho^2 + \beta\varrho^4 + \omega_p^2) = 0 , \tag{3.42}$$

which gives the solution,

$$z^2 = \frac{-(2\beta\varrho^2 + \alpha - v^2) \pm \sqrt{(2\beta\varrho^2+\alpha-v^2)^2 - 4\beta(\alpha\varrho^2+\beta\varrho^4+\omega_p^2)}}{2\beta} . \tag{3.43}$$

For these solutions to be real we must have,

$$(2\beta\varrho^2 + \alpha - v^2)^2 - 4\beta(\alpha\varrho^2 + \beta\varrho^4 + \omega_p^2) \geq 0\,. \tag{3.44}$$

which restricts the range of ϱ. With these considerations we have that,

$$S_2 = \frac{\omega_p^2}{2\pi^2 v^2} \int_0^{\varrho_{max}(v)} d\varrho \left[\frac{\varrho}{\varrho^2 + z_1^2} \tilde{F}(\varrho, z_1) + \frac{\varrho}{\varrho^2 + z_2^2} \tilde{F}(\varrho, z_2) \right] . \tag{3.45}$$

This encourages the following calculation strategy:

1. Choose v
2. Discretize ϱ into m subintervals over the interval $[0, \varrho_{max}(v)]$
3. For each ϱ_i, $i \in [1, m]$ solve 3.43 for the two positive values of z_1 and z_2
4. Substitute ϱ_i, v, z_{ij}, $j \in [1, 2]$ into $\tilde{F}(\varrho, z)$
5. Integrate over $\mathbf{k}'$ to get $\tilde{F}(\varrho_i, z_{ij})$
6. Integrate over ϱ using Simpson's Rule.

The only step in the above strategy that requires development is step 5. To this point we have assumed only that the integration could *somehow* be carried out over $\mathbf{k}'$-space and called this result $F(\mathbf{k})$. The purpose of the next section is to explain how, given fixed values for ϱ and z (provided by steps 2 and 3) we can integrate to arrive at the numerical value for $\tilde{F}(\varrho, z)$.

3.2 Integration Scheme To Find $F(\mathbf{k})$

3.2.1 Integration Scheme

Having outlined the way in which we shall calculate the second order stopping force one task remains. Given a structure factor and values for ϱ and z we need to perform the integration,

$$F(\mathbf{k}) = \int \frac{d^3\mathbf{k}'}{k'^2(\mathbf{k} - \mathbf{k}')^2} F_3(\mathbf{k}, \mathbf{k}', \mathbf{k} - \mathbf{k}') \frac{A(\mathbf{k}, \mathbf{k}', \mathbf{k} - \mathbf{k}', \mathbf{k} \cdot \mathbf{v}, \mathbf{k}' \cdot \mathbf{v}, (\mathbf{k} - \mathbf{k}') \cdot \mathbf{v})}{N(\mathbf{k}', \mathbf{k}' \cdot \mathbf{v}) N(\mathbf{k} - \mathbf{k}', (\mathbf{k} - \mathbf{k}') \cdot \mathbf{v})} . \tag{3.46}$$

As mentioned the value for F is cylindrically symmetric, although the same cannot be said about the integrand. It seems that the most straightforward way to calculate this integral is by brute force numerical integration over cartesian coordinates. With this in mind we define,

$$\mathbf{k}' = [k'_x, k'_y, k'_z]\,, \tag{3.47}$$

$$\mathbf{v} = [0, 0, v]\,, \tag{3.48}$$

were we have chosen the k_z axis to coincide with the z axis of the cylindrical system for k and both axes colinear with the direction of travel.

Since the value of F is cylindrically symmetric in k-space, we can specify that in the integral 3.46,

$$\mathbf{k} = [\varrho, 0, z]\,, \tag{3.49}$$

with the zero simplifying the calculation considerably.

After making these assumptions, and specifying values for ϱ and z we are left with,

$$\tilde{F}(\varrho, 0, z) = \int \frac{dk'_x dk'_y dk'_z}{k'^2(\mathbf{k}-\mathbf{k}')^2} F_3(\mathbf{k}, \mathbf{k}', \mathbf{k}-\mathbf{k}') \frac{A(\mathbf{k}, \mathbf{k}', \mathbf{k}-\mathbf{k}', zv, k'_z v, (z-k'_z)v)}{N(\mathbf{k}', k'_z v) N(\mathbf{k}-\mathbf{k}', (z-k'_z)v)}\,. \tag{3.50}$$

From the structure of the integrand we see that there are points in which singularities may occur, namely when $\mathbf{k}' = 0$, when $\mathbf{k} = \mathbf{k}'$ and when either of the $N(\cdots)$ functions give zero. The later singularities may be avoided if we give η a small positive value, this prevents a singularity from occurring. Provided the value of η is small, we may remain confident that our use of the limiting assumption which yielded the Dirac delta functions in the above sections may still be used without losing very much accuracy. The first two singularities are not quite easily handled and we will need to be careful when performing out integration not to 'step' on these regions.

Obviously this integral must be performed numerically. What remains is to choose a numerical integrator. Matlab has a function which can perform triple integrals (triplequad), double integrals (dblquad) and single integrals (quad) numerically using adaptive quadrature. The obvious choice is to integrate using triplequad, but as we see in the following sections it will not be the ideal choice. In fact, none of the methods built into Matlab suffices and a novel approach is needed.

Since for each value of m we need to calculate the value of F twice (one for each z) thus for each given speed we need to perform the integration in 3.50 $2m$ times. Even for moderate values

of m (ie, 6) we need twelve calculations of 3.50. Thus, it would be ideal to have a relatively fast method to calculate F. Further, to numerically calculate this integral we cannot integrate over infinite space, so we need to truncate our upper and lower bounds for k'_x, k'_y and k'_z. Over the following four sections we evaluate 4 different methods to carry out the numerical integration in 3.50 as well as evaluate adequate bounds of integration and the times required to calculate them. We analyze the convergence of both the real part of the calculated value as well as the imaginary part. If we have the imaginary part converging to zero we shall gain confidence that our method is indeed converging to the correct numerical value.

For the following investigations we assume that $\varrho = 1$, $z = 3$, $v = 1$, $\omega_p = 0.5816$ (aluminum), $\alpha = 0$ (static gas case), $\eta = \frac{\omega_p}{10}$ and that the structure factor is that for an ion, $F_3 = 1$.

Triplequad

The first method we shall explore is the triple quad method built into Matlab. The most pressing issue for this method is that Matlab won't avoid the singularities mentioned above. Thus, in order to perform this calculation, we cannot hope to integrate the entire domain in one sweep. Rather, we must fracture the three dimensional domain into smaller domains, the bounds of which coming close to the singularities but making sure the singularities do not occur in any of subregions.

Figure 3.1(a) shows the convergence of real part of $F(1, 0, 3)$ as a function of the bounds of k'_x, k'_y and k'_z. We chose the bounds to be symmetric about zero and identical for each dimension. As we can see by 30 we are confident of convergence. Similarly figure 3.1(b) shows the convergence of the imaginary part of $F(1, 0, 3)$. Again, around a boundary value of 30 we see that the imaginary part is almost zero. This is what we expect, since the integral should be real. Despite the relatively good results obtained by this method, the problem is that it is extremely time consuming. As mentioned we may be performing this integration a dozen or more times for each speed. Figure 3.1(c) shows the computation time for each bound.

Clearly these calculations take too much time to be useful when triplequad is used. Not only that, it is not a very flexible method to avoid the singularities. For these two crucial reasons we seek a different method.

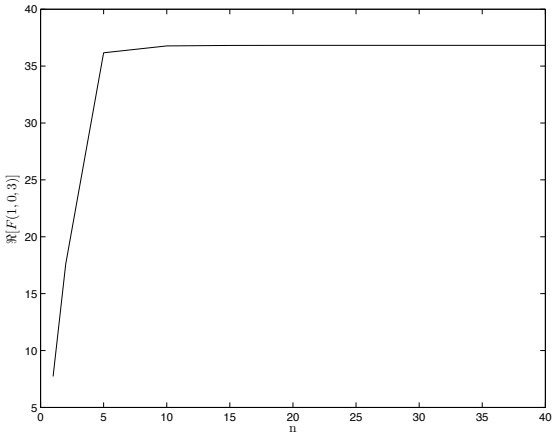

(a) Real part of $F(1,0,3)$ calculated using the triplequad method at various values for interval endpoints n, ie, calculated over the region $(-n,n)\times(-n,n)\times(-n,n)$

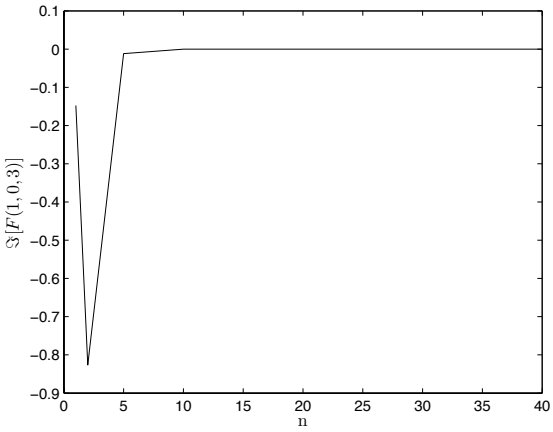

(b) Imaginary part of $F(1,0,3)$ calculated using the triplequad method at various values for interval endpoints n, ie, calculated over the region $(-n,n)\times(-n,n)\times(-n,n)$

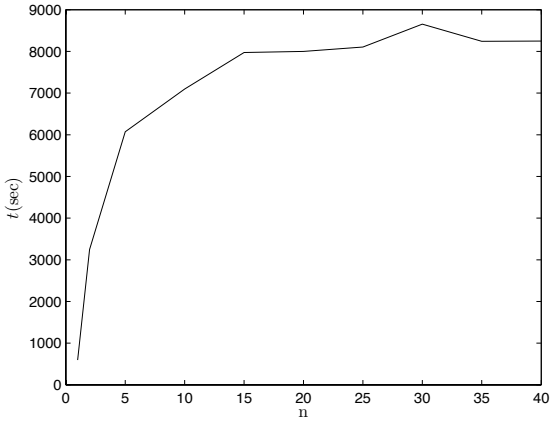

(c) Time required to calculate $F(1,0,3)$ using the triplequad method at various values for interval endpoints n, ie, calculated over the region $(-n,n)\times(-n,n)\times(-n,n)$

Figure 3.1: Convergence and runtime results for calculating F using the triplequad method

Double Quad, Single Trapezoidal

The above method relies on computing the three dimensional integral using the native triple-quad method which is too slow for our purposes. While numerically robust reliable, the quadrature method employed by matlab is what causes the calculation to slow down. There are faster methods available, such as straightforward integration using the trapezoidal rule. The next two methods described are a marriage of the built-in methods of matlab and the trapezoidal rule.

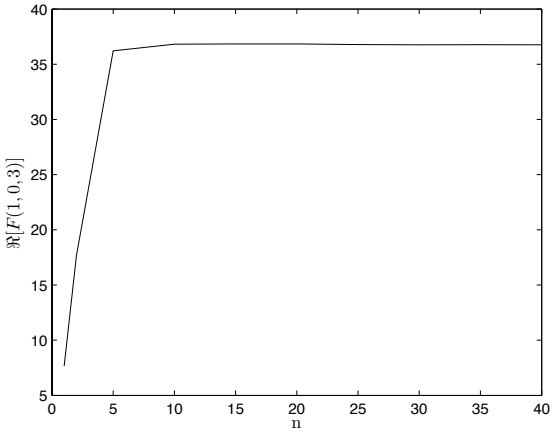

(a) Real part of $F(1,0,3)$ calculated using the doublequad-single trapezoidal method at various values for interval endpoints n, ie, calculated over the region $(-n,n)\times(-n,n)\times(-n,n)$

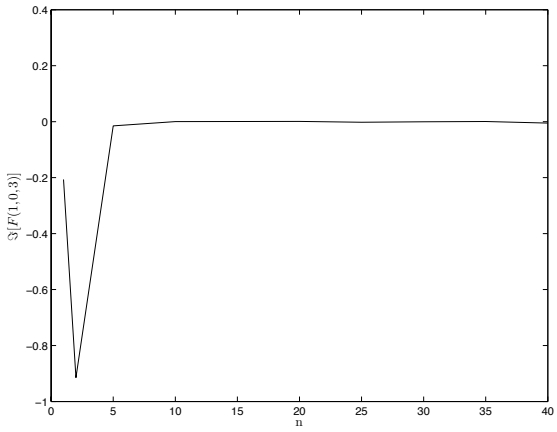

(b) Imaginary part of $F(1,0,3)$ calculated using the doublequad-single trapezoidal method at various values for interval endpoints n, ie, calculated over the region $(-n,n)\times(-n,n)\times(-n,n)$

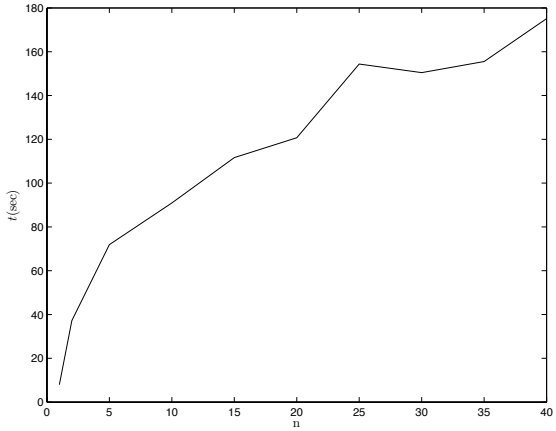

(c) Time required to calculate $F(1,0,3)$ using the doublequad-single trapezoidal method at various values for interval endpoints n, ie, calculated over the region $(-n,n)\times(-n,n)\times(-n,n)$

Figure 3.2: Convergence and runtime results for calculating F using the Doublequad-Single Trapezoidal Method

The first way to combine the two approaches is to discretize one of the dimensions and carry out numerical integration over that level slice using the matlab function dblquad. This produces an array of values which may then be integrated itself using the trapezoidal rule. This allows us to retain part of the robustness and accuracy of the built in quadrature method while speeding up the calculation.

This method does have another advantage, in that it can deal with the singularity issue much more transparently than the domain splitting that triplequad required. In this method we simply offset the discretized values by a very small amount, ensuring that the integrand is never evaluated at the origin. Further, if we choose the k'_y coordinate as the discretized one, the offset also ensures that the integrand is not evaluated at $\mathbf{k} = \mathbf{k}'$. The reason is that we set the second coordinate of $\mathbf{k}$ to zero to simplify the calculation. By offsetting the second coordinate of $\mathbf{k}$ we also ensure $\mathbf{k} \neq \mathbf{k}'$.

As with the above test, we analyze the convergence of the real part (Figure 3.2(a)) as well as the imaginary part (Figure 3.2(b)). From the two plots we see that by the time the endpoints reach 30, the real part is converging, as is the imaginary part.

We also plot the calculation time for each value of the endpoints (Figure 3.2(c)). Though it is faster than the triplequad method it is still clearly not fast enough. We next attempt to go one step further to speed up the process with the aforementioned considerations.

Single Quad, Double Trapezoidal

In this method we discretize two dimensions and perform a single quadrature integration along a line using matlab's quad method. After the single integration is finished at each point, we integrate over the two dimensional array, one dimension at a time, using the trapezoidal rule. This method again has the benefit of easily dealing with the singularities while also speeding up the computation.

As with the above methods the convergences of the real and imaginary parts are considered (Figure 3.3(a) and Figure 3.3(b) respectively). Again we see the convergence to zero for the imaginary plot and convergence in the real plot after 30. However, again the calculation time is far too long (Figure 3.3(c)). This prompts us to again consider another method.

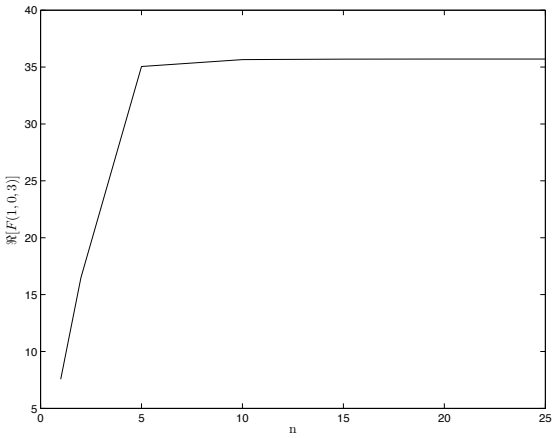

(a) Real part of $F(1,0,3)$ calculated using the singlequad-double trapezoidal method at various values for interval endpoints n, ie, calculated over the region $(-n,n)\times(-n,n)\times(-n,n)$

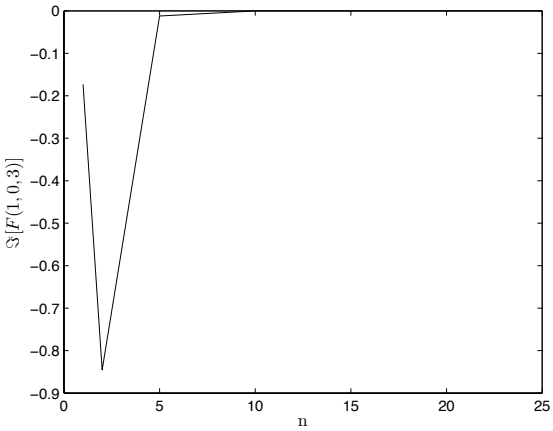

(b) Imaginary part of $F(1,0,3)$ calculated using the singlequad-double trapezoidal method at various values for interval endpoints n, ie, calculated over the region $(-n,n)\times(-n,n)\times(-n,n)$

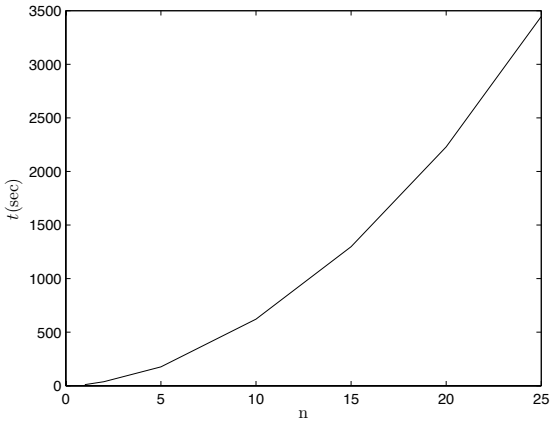

(c) Time required to calculate $F(1,0,3)$ using the singlequad-double trapezoidal method at various values for interval endpoints n, ie, calculated over the region $(-n,n)\times(-n,n)\times(-n,n)$

Figure 3.3: Convergence and runtime results for calculating F using the Single quad-Double Trapezoidal Method

Triple Trapezoidal

In this method we discretize the entire space and use the trapezoidal rule to integrate over each dimension one at a time. This obviously speeds up the process but at a price. From the above situations it became clear that setting the endpoints at 30 was sufficient to give adequate convergence. Thus, the entire space is a cube of $60^3 = 21600$ units. Even if we discretize with a fairly sparse grid (points every 0.25 units) then this requires over 17 million evaluations. Every attempt to make the grid denser requires exponentially more evaluations and memory. We quickly see (Figure 3.4(a) and Figure 3.4(b)) that we get poor convergence since we are limited by the density of our grid. The maximum density we could afford was about 350 points per dimension.

The upside was that this method was fairly fast as shown in Figure 3.4(c). This method also is able to handle the singularities without difficulty. This suggests trying to find a way to increase the density of the grid without increasing the demand on the memory. Thankfully, such a method is available by employing some clever tactics.

Holepunch Method

By plotting some level curves of $F(1, 0, 3)$ one discovers that the function has a quite helpful property. It turns out (not surprisingly) that the majority of contributions to the integral come within 2 or 3 units in each direction of the location of the singularities. This is useful indeed, since it allows us to vary the density of the grid in regions where not much 'action' is happening. The question to ask is 'how should we vary this grid spacing? '

Obviously the area around the singularities should receive the densest spacing. At first thought one However, again the calculation time is far too long (Figure 3.3(c)). This prompts us to again consider another method. wish to take the 350 points or so and focus a large deal of them around the singularities while distributing the rest in the less active regions. This is a reasonable approach but we are still limited by the 350 points. If we concentrate in one area we sacrifice the density in another area. There is an alternative however, called the *holepunch* method.

The holepunch method is based on the idea that we can divide the space into regions, perform integration over each region and sum the totals up. In this way it is not that unlike the original fracturing of the space that we required when using the triplequad method. However, this method is different in how it goes about the fracturing.

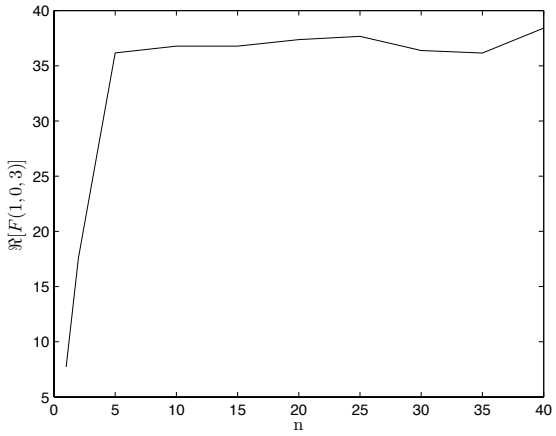

(a) Real part of $F(1,0,3)$ calculated using the triple trapezoidal method at various values for interval endpoints n, ie, calculated over the region $(-n,n) \times (-n,n) \times (-n,n)$

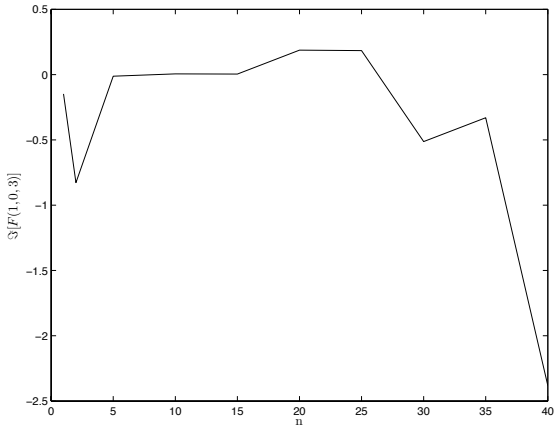

(b) Imaginary part of $F(1,0,3)$ calculated using the triple trapezoidal method at various values for interval endpoints n, ie, calculated over the region $(-n,n) \times (-n,n) \times (-n,n)$

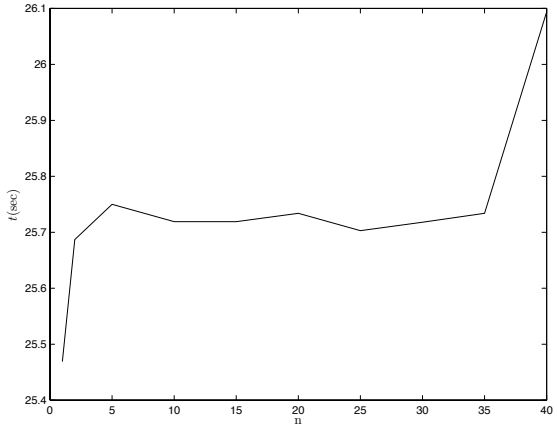

(c) Time required to calculate $F(1,0,3)$ using the triple trapezoidal method at various values for interval endpoints n, ie, calculated over the region $(-n,n) \times (-n,n) \times (-n,n)$

Figure 3.4: Convergence and runtime results for calculating F using the Triple Trapezoidal Method

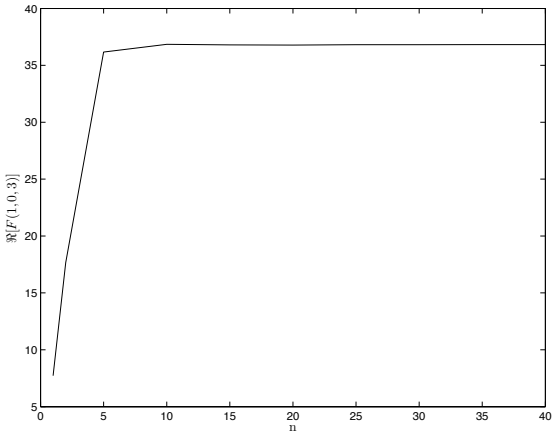

(a) Real part of $F(1,0,3)$ calculated using the holepunch method at various values for interval endpoints n, ie, calculated over the region $(-n,n) \times (-n,n) \times (-n,n)$

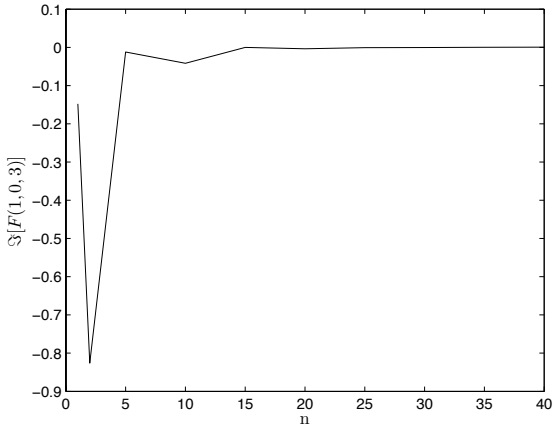

(b) Imaginary part of $F(1,0,3)$ calculated using the holepunch method at various values for interval endpoints n, ie, calculated over the region $(-n,n) \times (-n,n) \times (-n,n)$

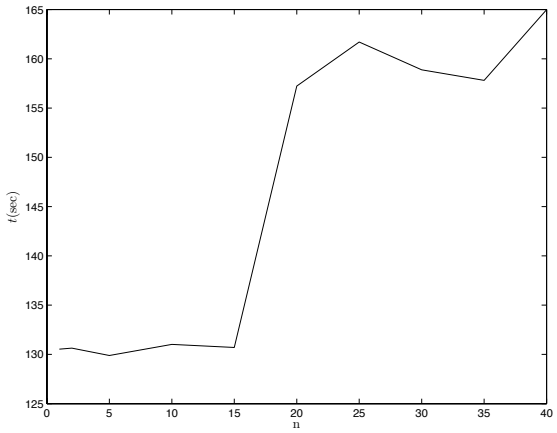

(c) Time required to calculate $F(1,0,3)$ using the holepunch method at various values for interval endpoints n, ie, calculated over the region $(-n,n) \times (-n,n) \times (-n,n)$

Figure 3.5: Convergence and runtime results for calculating F using the Holepunch Method

In the holepunch method regions are 'punched out' of the integration, and their function values set to zero. This means that the initial grid set-up doesn't have to adapt. One can maintain the original grid spacing over each region, greatly simplifying the actual integration. At areas of the grid where one wishes it to be denser, the function is set to zero. When the sparser integration is finished the 'punched out' region is revisited, this time with a full complement of 350 points, enabling one to get far greater accuracy in the region. Once all the regions have been integrated with the density and accuracy desired, the results are summed to give the value of the integral over the entire space.

The actual 'holepunching' is carried out by clever use of Heaviside functions. A one dimensional hole can be created from x_0 to x_1 by using,

$$h_x(x) = |H(x_0 - x) - H(x - x_1)|\,, \tag{3.51}$$

where H is the Heaviside function. Similar functions may be made for the the y and z dimensions,

$$h_y(y) = |H(y_0 - y) - H(y - y_1)|\,, \tag{3.52}$$

$$h_z(y) = |H(z_0 - z) - H(z - z_1)|\,. \tag{3.53}$$

These functions may be summarized as,

$$h_x(x) = \begin{cases} 0, & \text{if } x \in [x_0, x_1] \\ 1, & \text{otherwise} \end{cases}\,. \tag{3.54}$$

$$h_y(y) = \begin{cases} 0, & \text{if } y \in [y_0, y_1] \\ 1, & \text{otherwise} \end{cases}\,. \tag{3.55}$$

$$h_z(z) = \begin{cases} 0, & \text{if } z \in [z_0, z_1] \\ 1, & \text{otherwise} \end{cases}\,. \tag{3.56}$$

Now, the idea is that, should a grid point be inside a *box* created by these Heaviside functions, the function is set to zero. We could imagine a 'window function', $w(x, y, z)$, which would multiply the integrand by zero if the evaluation point is inside this box, and multiply it by one if the point lied outside the box. Our task is thus to find a proper formulation for this function $w(x, y, z)$. This is most easily understood by the use of Venn diagrams (Figure 3.6).

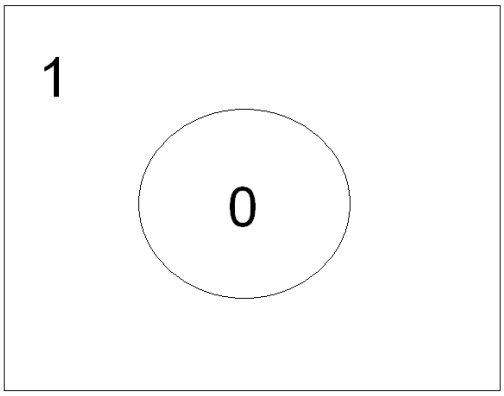

(a) Venn diagram representation of the one dimensional Holepunch method

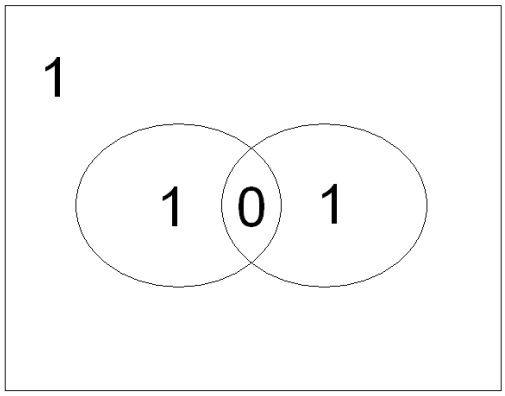

(b) Venn diagram representation of the two dimensional Holepunch method

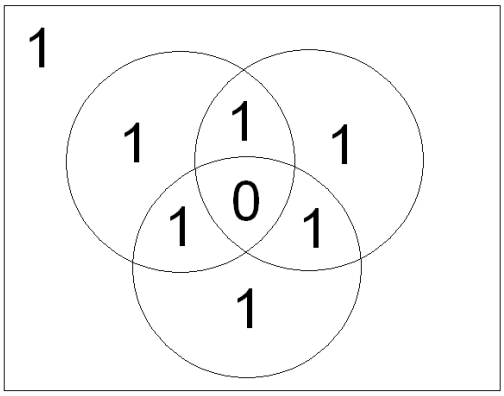

(c) Venn diagram representation of the three dimensional Holepunch method

Figure 3.6: Venn diagram representation of the Holepunch method

In one dimension we imagine the hole punched region as being described by the Venn diagram in Figure 3.6(a). In this case our holepunch function would simply be any of the above one dimensional adapted Heaviside functions ($w(x) = h_x(x)$ for example).

In two dimensions the situation is described in Figure 3.6(b). One may be tempted to try a

simple addition of two of these one dimensional modified Heaviside functions,

$$w(x, y) = h_x(x) + h_y(y) \,. \tag{3.57}$$

Certainly if a point were inside the region punched out by h_x and h_y then $w(x, y)$ would indeed be zero. However, if the evaluation point was to lie outside *both* regions then $w(x, y) = 2$. In effect, when the integral is calculated, points which were exterior to our 'hole' would *double* the value of the integrand, which is unacceptable. The solution to this dilemma is to subtract off the two functions multiplied together. Thus,

$$w(x, y) = h_x(x) + h_y(y) - h_x(x)h_y(y) \,. \tag{3.58}$$

One may easily convince oneself that this function indeed replicates the situation in Figure 3.6(b). The form of w should be familiar since it is similar to the counting formula in set theory. It is through this connection that we make the natural extension to the three dimensional case,

$$w(x, y, z) = h_x(x)+h_y(y)+h_z(z)-[h_x(x)h_y(y) + h_x(x)h_z(z) + h_z(z)h_y(y)]+h_x(x)h_y(y)h_z(z) \,. \tag{3.59}$$

Indeed this is precisely the formula which represents the situation depicted in Figure 3.6(c) and thus is the desired 'window' function.

To summarize, the idea is this. We wish to numerically integrate a function which we know is essentially featureless and slowly changing outside of two relatively small regions. Inside these regions our function of interest varies wildly and contributes the most to the value of the integral. We wish to use a version of the three dimensional trapezoid rule due to its speed to perform the integration. However, due to the 3 dimensional nature of the problem the memory required to perform such a calculation scales too rapidly with the number of grid points we use. To get a dense enough grid would require computational resources which are out of the domain of feasibility. On the other hand, if we use a sparser grid to cover our space we would have large inaccuracies. The solution is to punch two holes in the function, setting it to zero in the small, wildly changing, regions. We then use a sparse grid to integrate the large space and use a denser grid to calculate the integral over the smaller regions and then sum the three values.

Using two test functions we evaluate the accuracy and speed of this method. The results are in Table 3.1.

Method	$f_1(x)$		$f_2(x)$	
	Result	Time (sec)	Result	Time (sec)
Triplequad	11.1360	120.0630	5.2019	8002.6720
Doublequad-Single Trapz	11.0774	15.14	5.2089	425.6570
Singlequad-Double Trapz	11.1361	309.6720	5.1826	1678.0470
Triple Trapezoidal	11.1367	6.8280	5.1862	18.5630
Holepunch	11.1366	71.8750	5.2302	105.8750

Table 3.1: Comparison of calculated value and runtimes for the three dimensional integration of $f_1(x)$ and $f_2(x)$ for the triplequad, doublequad-single trapezoidal, singlequad-double trapezoidal, triple trapezoidal and holepunch methods.

Chapter 4

Verification of Method

In this chapter we present the results of the calculations of the stopping force for ions, colinear diclusters of protons and randomly oriented clusters of protons for in the low d limit. All calculations in this chapter, and following chapters, were carried out using the holepunch method explained in chapter 3.

4.1 Parameter Values

Further, in this and subsequent chapters we use the following values for our parameters.The plasma frequency was that of aluminum and calculated through the expression for the Wigner-Seitz radius, r_s,

$$r_s = (\frac{4\pi n_0 a_0^3}{3})^{-1/3}\,, \tag{4.1}$$

and thus,

$$r_s = (\frac{\omega_p^2 a_0^3}{3})^{-1/3}\,. \tag{4.2}$$

All calculations are done in atomic units and thus $a_0^3 = 1$ and hence,

$$\omega_p^2 = \frac{3}{r_s^3}\,. \tag{4.3}$$

The Wigner Seitz radius for aluminum is $r_s^{alum} = 2.07$ which gives a final value for the plasma frequency of $\omega_p = 0.5816$.

The units of distance were also in atomic units, but plots are expressed as multiples, d, of the equilibrium distance of protons in the H_2^+ molecule (which is $approx$ Å). Hence, in atomic units,

$$D \approx d\frac{1.06}{0.5219}\,. \tag{4.4}$$

We have also used $\alpha = 0$ which coincides with the case considered by previous authors for single ions [10, 11].

4.2 Low Limit d Verification

We begin the process of verification of our method by plotting the first order stopping force as well as the full (first and second order) stopping force in Figure 4.1.

We see that as the speed is increased we have the second order correction suppressed. In the high speed limit the full stopping force begins to coincide with the first order stopping force. This result agrees with the results given in [10] as well as in [11]. Having duplicated the established results for the ion case, we move to the case of diclusters.

One check we use is to plot the first order and full stopping forces against speed for distances of $d = 1,\, 0.5,\, 0.25$. For the first order case we also include the plot for $4S_1^{ion}$. For the full stopping force plots we include the value for $4S_1^{ion} + 8S_2^{ion}$. We do this because when we take the limit of our expressions of the cluster factors for both the colinear and randomly oriented case, we arrive at structure factors of 4 in the first order case and 8 in the second order case. Thus, as the distance between protons is reduced to zero we expect the first order stopping force to approach $4S_1^{ion}$ and the full stopping force to approach $4S_1^{ion} + 8S_2^{ion}$. The results for the colinear case are shown in Figure 4.2 and for the random case in Figure 4.3.

We clearly see that for the colinear case, as the distance is reduced the plots for the first order and full stopping forces approach their expected values. For the randomly oriented case we see similar behaviour.

Analogously, we plot the first and full stopping forces against d at set speeds of 2, 3, 4 and 5 for both the colinear and randomly oriented cases. As d approaches zero, we expect the first order stopping force to approach $4S_1^{ion}$ and the full stopping force to approach $4S_1^{ion} + 8S_2^{ion}$. Since, in the ion case, the stopping force does not depend on d, these limits will be represented by horizontal lines for each set speed. Our expectation is that, for each speed, the calculated

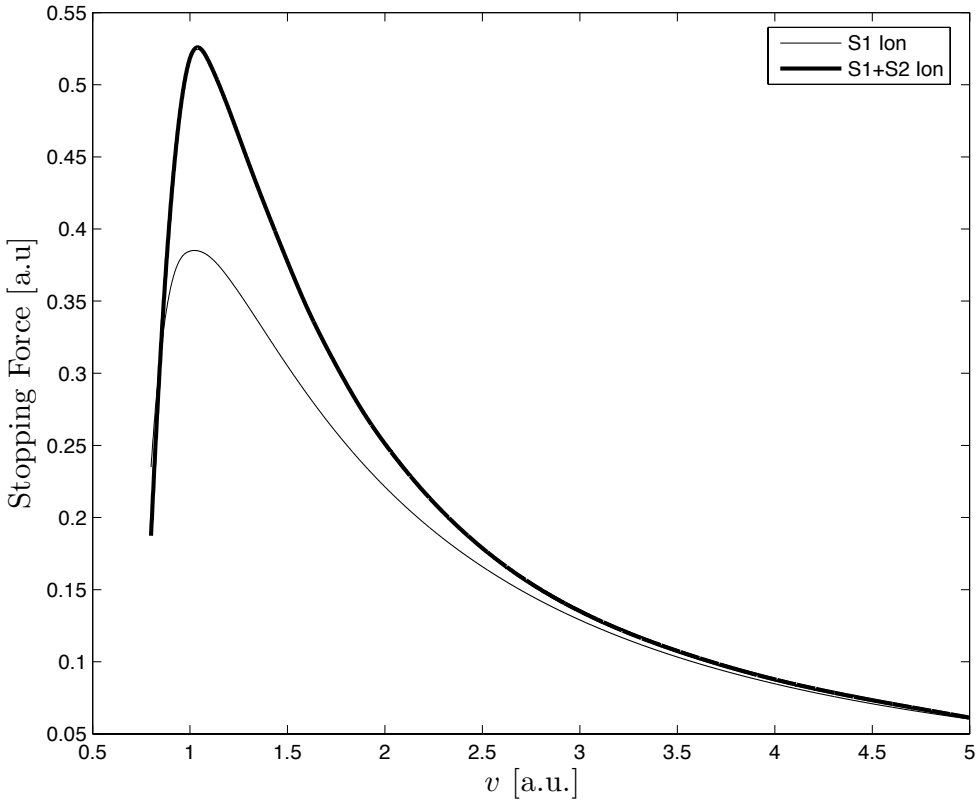

Figure 4.1: S_1 (thin line) and S_1+S_2 (thick line) for a single proton through a solid with $r_s = 2.07$ and $\eta = \omega_p/10$ vs speed

values will tend to the horizontal asymptotes as d goes go zero. The results are given in Figure 4.4 for the colinear case, and Figure 4.5 for the randomly oriented case.

Again, as above, we see that the first order and full stopping forces behave, smoothly, as expected in the low d limit for both the colinear and randomly oriented case.

Having established a good degree of confidence in our method, despite lack of experimental evidence, we turn our attention specifically to the results we sought initially.

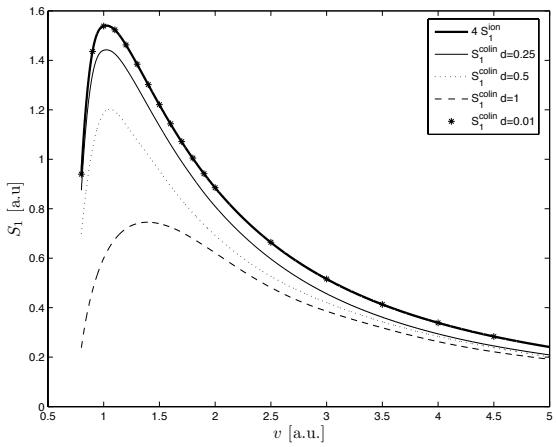

(a) S_1 for a colinear dicluster of protons of interproton distance $d = 0.25$ (—-), $d = 0.5$ ($\cdots$), $d = 1$ ($\cdots$), $d = 0.01$ (dots), traveling through a solid with $r_s = 2.07$, $\eta = \omega_p/10$ and $\alpha = 0$ plotted against the projectile speed

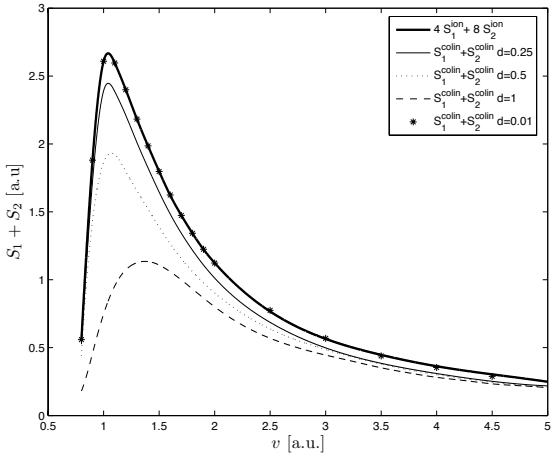

(b) $S_1 + S_2$ for a colinear dicluster of protons of interproton distance $d = 0.25$ (—-), $d = 0.5$ ($\cdots$), $d = 1$ ($\cdots$), $d = 0.01$ (dots), traveling through a solid with $r_s = 2.07$, $\eta = \omega_p/10$ and $\alpha = 0$ plotted against the projectile speed

Figure 4.2: Small d limit of the stopping force of a colinear dicluster of protons plotted against the projectile speed

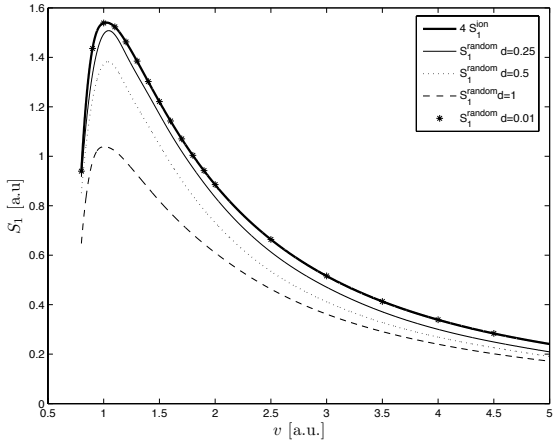

(a) S_1 for a randomly oriented dicluster of protons of interproton distance $d = 0.25$ (—), $d = 0.5$ ($\cdots$), $d = 1$ ($\cdots$),$d = 0.01$ (dots), traveling through a solid with $r_s = 2.07$, $\eta = \omega_p/10$ and $\alpha = 0$ plotted against the projectile speed

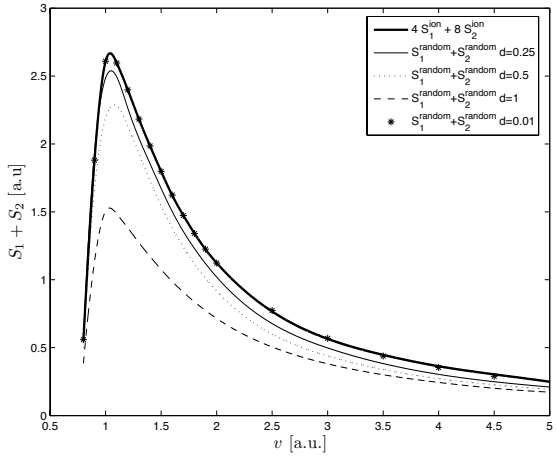

(b) $S_1 + S_2$ for a randomly oriented dicluster of protons of interproton distance $d = 0.25$ (—-), $d = 0.5$ ($\cdots$), $d = 1$ ($\cdots$),$d = 0.01$ (dots), traveling through a solid with $r_s = 2.07$, $\eta = \omega_p/10$ and $\alpha = 0$ plotted against the projectile speed

Figure 4.3: Small d limit stopping force for a randomly oriented dicluster of protons plotted against the projectile speed

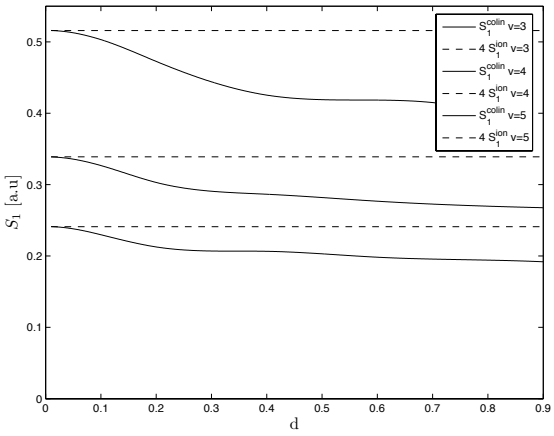

(a) S_1 for a colinear dicluster of protons of interproton distance $v = 3$ (top), $v = 4$ (middle), $v = 5$ (bottom) traveling through a solid with $r_s = 2.07$, $\eta = \omega_p/10$ and $\alpha = 0$ plotted against the interproton distance

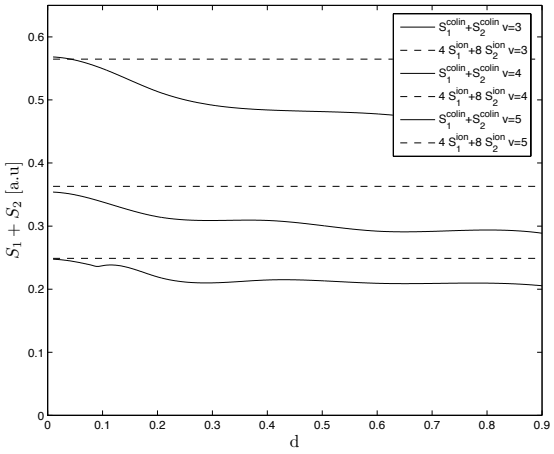

(b) S_1+S_2 for a colinear dicluster of protons of interproton distance $v = 3$ (top), $v = 4$ (middle), $v = 5$ (bottom) traveling through a solid with $r_s = 2.07$, $\eta = \omega_p/10$ and $\alpha = 0$ plotted against the interproton distance

Figure 4.4: Small d limit of the stopping force for a colinear dicluster of protons plotted against the interproton distance

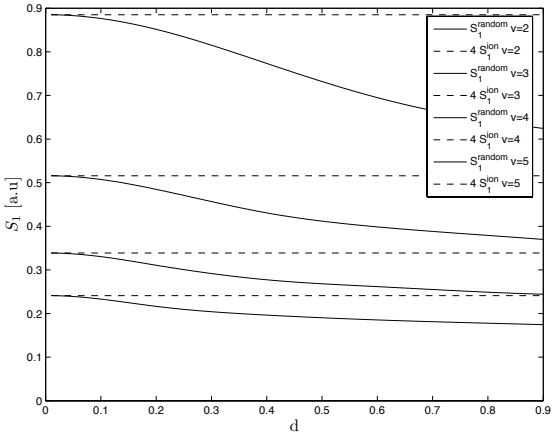

(a) S_1 for a randomly oriented dicluster of protons of interproton distance $v = 2$ (top), $v = 3$ (second from top), $v = 4$ (third from top), $v = 5$ (bottom) traveling through a solid with $r_s = 2.07$, $\eta = \omega_p/10$ and $\alpha = 0$ plotted against the interproton distance

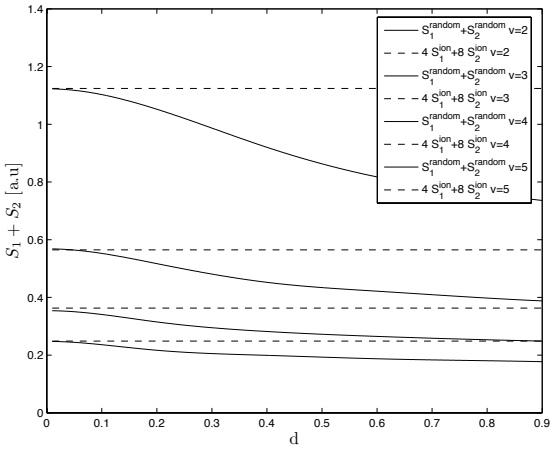

(b) $S_1 + S_2$ for a randomly oriented dicluster of protons of interproton distance $v = 2$ (top), $v = 3$ (second from top), $v = 4$ (third from top), $v = 5$ (bottom) traveling through a solid with $r_s = 2.07$, $\eta = \omega_p/10$ and $\alpha = 0$ plotted against the interproton distance

Figure 4.5: Small d limit of the stopping force for a randomly oriented dicluster of protons plotted against the interproton distance

Chapter 5

Results For Stopping Force On A Dicluster

In this chapter we present the results of carrying out the calculation of stopping force on a colinear dicluster as well as a randomly oriented dicluster. We perform the calculations as outlined above. It is worth mentioning again that results are in atomic units as well as Gauss' electromagnetic units. Distances are given in units of the equilibrium internuclear separation of H_2^+.

5.1 Results For A Colinear Dicluster

We begin by showing the first order stopping force for a colinear dicluster of protons for distances $d = 1, 2, 3$ which is shown in Figure 5.1. We have also plotted twice the stopping force of a single ion to show the difference between the total stopping force felt by two independent protons and a cluster. In this way we can see the contribution that interference plays. We immediately see that the curve which is most similar to the ion case is the $d = 1$ plot, which makes intuitive sense since the interference contribution increases with distance to a maximum before decreasing as the proton separation increases. We see the increased complexity coming from this interference as d increases to 2 and 3.

In Figure 5.2 we see the full stopping force on a colinear dicluster of protons for distances of 1, 2 and 3, with an even more pronounced effect of interference. For distances of 2 and 3 we see that the force the projectile 'feels' is less that for two independent protons for small speeds. As the speed is increased the effect of the interference is to increase the force that the projectile experiences.

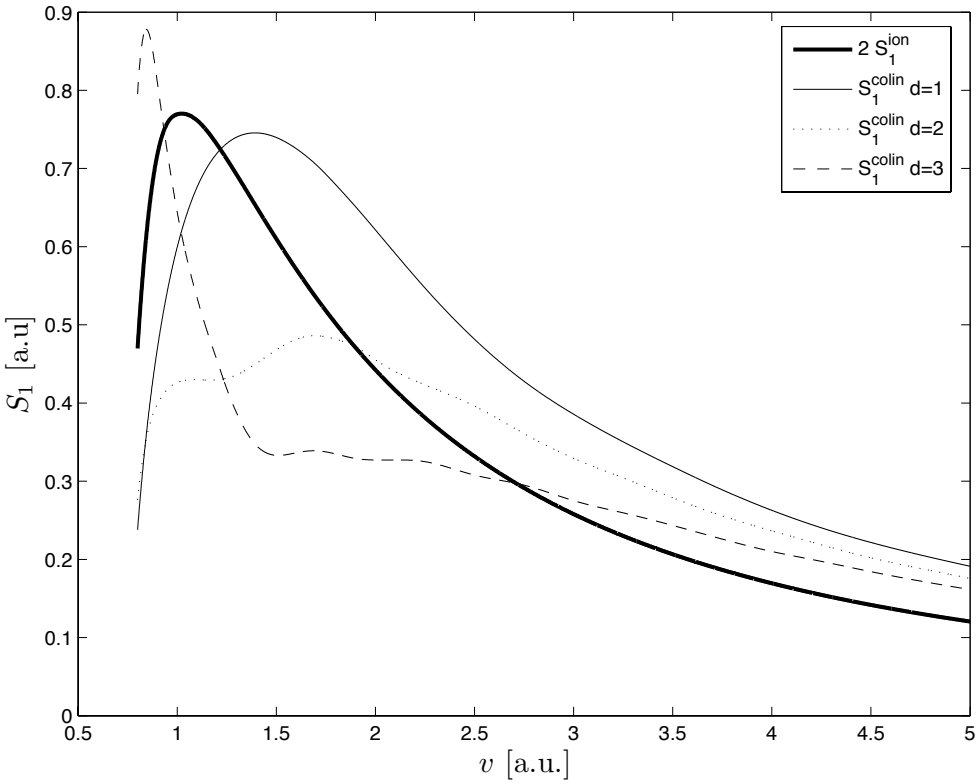

Figure 5.1: S_1 for a colinear dicluster of protons of interproton distance $d = 1$ (thin line), $d = 2$ ($\cdots$), $d = 3$ ($\cdots$) and two independent protons (thick line) traveling through a solid with $r_s = 2.07$, $\eta = \omega_p/10$ and $\alpha = 0$ plotted against the projectile speed

An effective way to visualize the effect of interference is to plot the following ratios,

$$R_1^{colin} = \frac{S_1^{colin}}{2S_1^{ion}}\,, \tag{5.1}$$

and

$$R_{12}^{colin} = \frac{S_1^{colin} + S_2^{colin}}{2(S_1^{ion} + S_2^{ion})}\,, \tag{5.2}$$

The more these ratios differ from unity, the more prominent the effect of interference is. These are shown in Figures 5.3 and 5.4, and show measures of the vicinage effect mentioned earlier.

From the plots we see that at high speeds, the effect on the first order stopping force due to interference decreases with interproton distance. However, at very low distances this analysis

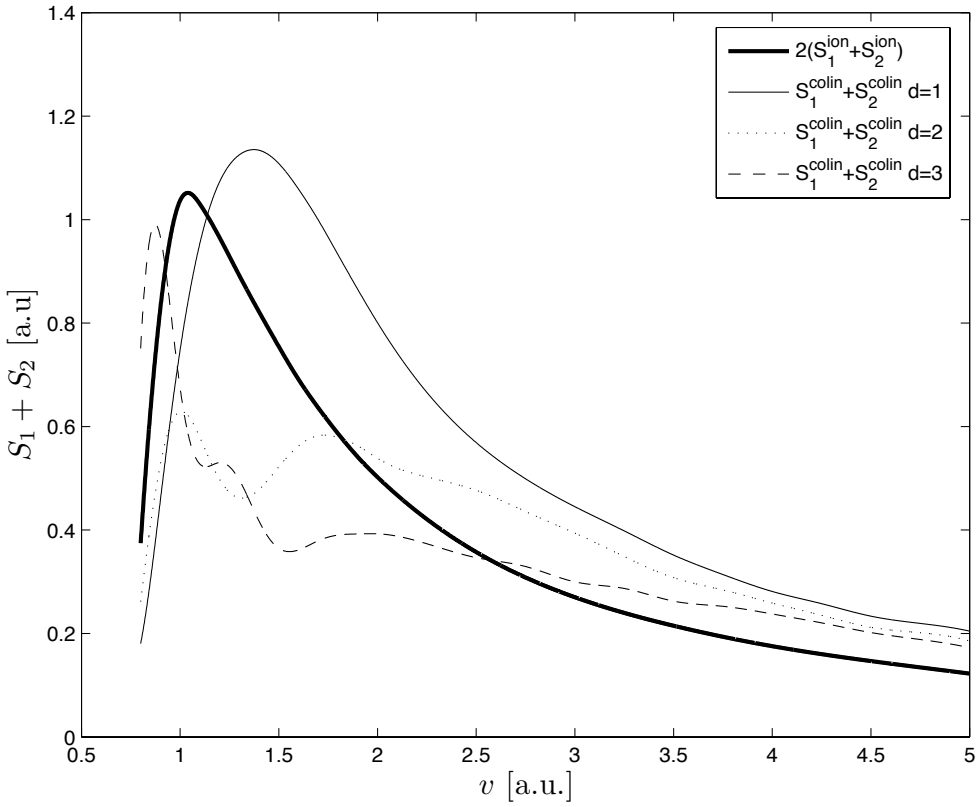

Figure 5.2: $S_1 + S_2$ for a colinear dicluster of protons of interproton distance $d = 1$ (thin line), $d = 2$ ($\cdots$), $d = 3$ ($\cdots$) and two independent protons (thick line) traveling through a solid with $r_s = 2.07$, $\eta = \omega_p/10$ and $\alpha = 0$ plotted against the projectile speed

breaks down.

The same general pattern is seen in the R case with even more instability in the low speed regime. Clearly this indicates an increase in complexity of interactions between the cluster and the electron gas. Similarly we may plot the same quantities against the interproton distance at fixed speeds, and thus examine the distance dependence of interference effects. These are given in Figures 5.5 and 5.6.

We see in these plots that in both the first order and full stopping force cases, at higher speeds the interproton distance plays less and less of a role. We also see that in all cases, as the distance increases, the stopping force experienced by the cluster decreases. As above, we may also plot

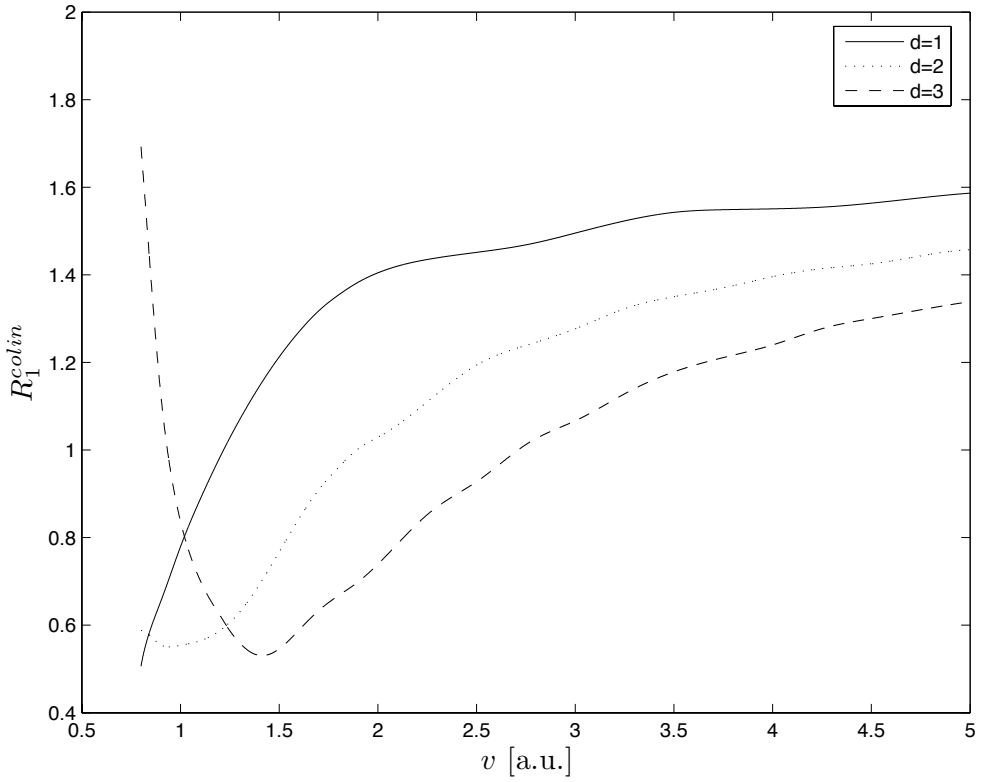

Figure 5.3: R_1 for a colinear dicluster of protons of interproton distance $d = 1$ (—), $d = 2$ ($\cdots$), $d = 3$ ($\cdots$) traveling through a solid with $r_s = 2.07$, $\eta = \omega_p/10$ and $\alpha = 0$ plotted against the projectile speed

the ratios, shown in Figure 5.7 and 5.8.

5.2 Results For A Randomly Oriented Dicluster

In this section we report the findings for the stopping force of a randomly oriented dicluster of protons at various projectile speeds and interproton distances. As above, we begin by considering the first order and full stopping forces of the cluster at fixed interproton distances verses the projectile speed. These are shown in Figures 5.9 and 5.10

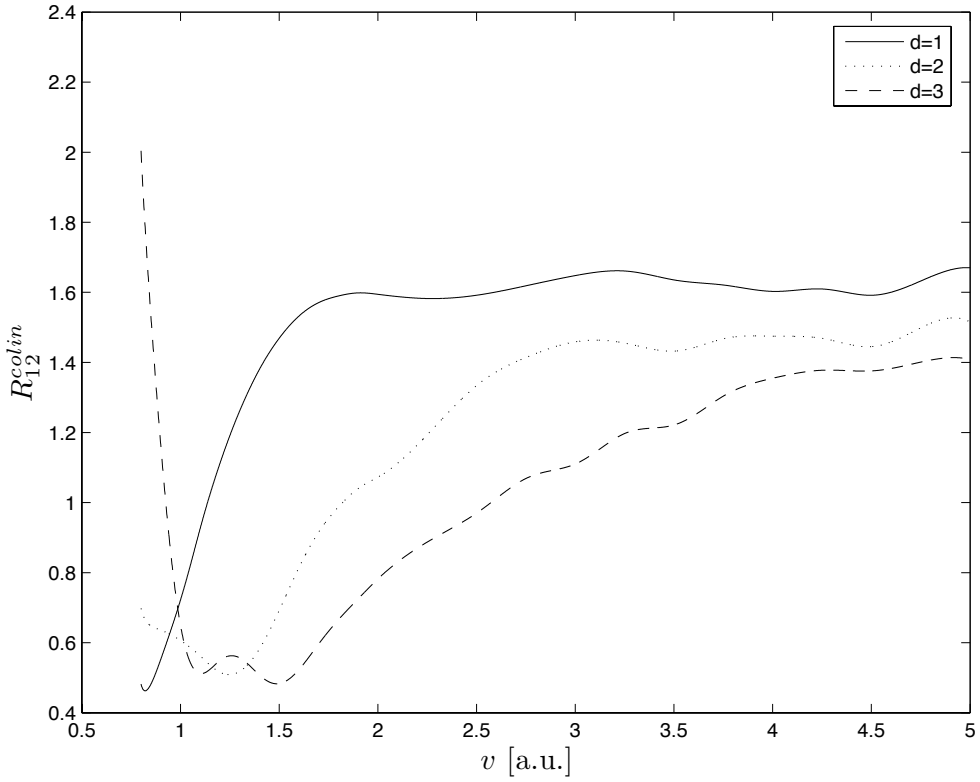

Figure 5.4: R_{12} for a colinear dicluster of protons of interproton distance $d = 1$ (—-), $d = 2$ ($\cdots$), $d = 3$ ($\cdots$) traveling through a solid with $r_s = 2.07$, $\eta = \omega_p/10$ and $\alpha = 0$ plotted against the projectile speed

We again define ratios,

$$R_1^{random} = \frac{S_1^{rand}}{2S_1^{ion}}\,, \tag{5.3}$$

and

$$R_{12}^{random} = \frac{S_1^{rand} + S_2^{rand}}{2(S_1^{ion} + S_2^{ion})}\,, \tag{5.4}$$

to help us articulate the effect on stopping force due to interference. These are plotted in Figures 5.11 and 5.12.

Finally, following the format of the above section we plot the dependence of the stopping force on the interproton distance for fixed speeds. These are shown in Figures 5.13 and 5.14.

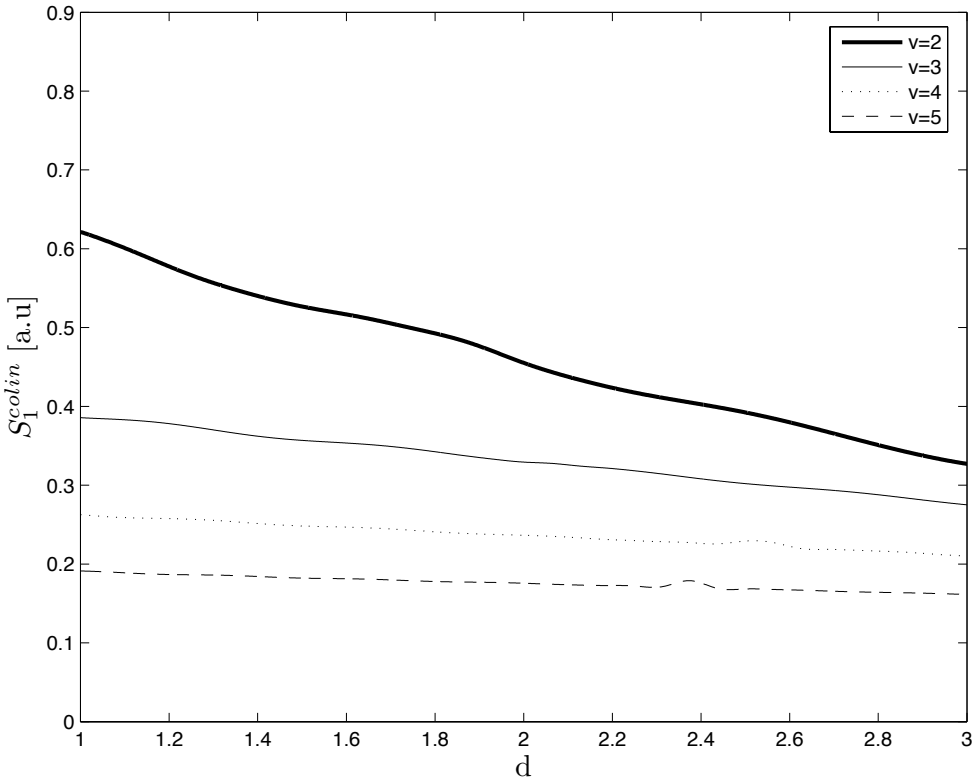

Figure 5.5: S_1 for a colinear dicluster of protons of speed $v = 2$ (thick line), $v = 3$ (thin line), $v = 4$ ($\cdots$), and $v = 5$ ($\cdots$) traveling through a solid with $r_s = 2.07$, $\eta = \omega_p/10$ and $\alpha = 0$ plotted against interproton distance

The ratio values for the randomly oriented proton dicluster versus interproton distance is given in Figures 5.15 and 5.16.

By comparing Figures 5.1 and 5.2 with Figures 5.9 and 5.10 we see that the most prominent difference is that the random case is much smoother. Both the colinear case and the random case exhibit a peak near $v = 1$ and decay with an increase in speed. What is also interesting to note, is that the peak for $d = 1$ is much higher in the randomly oriented case, than for the colinear case. In fact, from Figure 5.1 we notice that the highest stopping force comes from the $d = 3$ case, rather than the $d = 1$ case which is seen for randomly oriented clusters in Figure 5.9.

As one would expect, for the randomly oriented case, the peaks of the first order and full

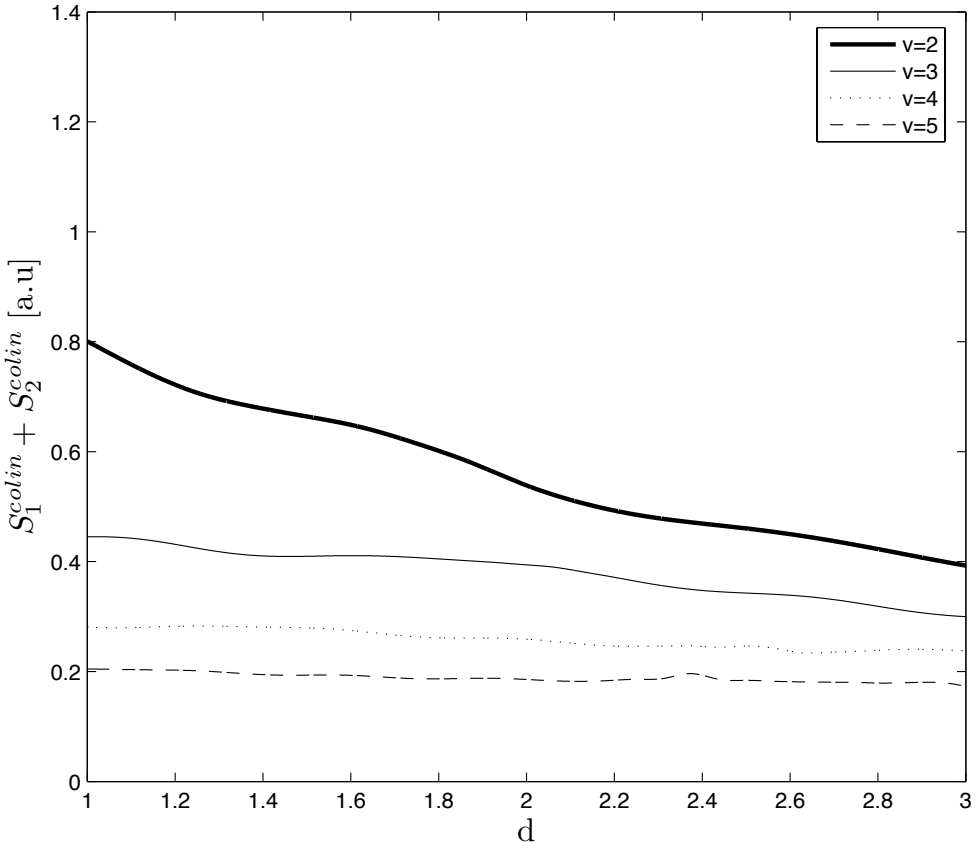

Figure 5.6: $S_1 + S_2$ for a colinear dicluster of protons of speed $v = 2$ (thick line), $v = 3$ (thin line), $v = 4$ ($\cdots$), and $v = 5$ ($\cdots$) traveling through a solid with $r_s = 2.07$, $\eta = \omega_p/10$ and $\alpha = 0$ plotted against interproton distance

stopping forces for higher d values (ie, $d = 2, 3$) begin to congregate around the value for two independent ions as shown in Figures 5.9 and 5.10. This is *not* true however for the colinear case where a more complex distribution for low speeds is shown (Figures 5.1 and 5.2).

Much like the plots for the stopping forces, the ratios R_1 and R_{12} are much smoother for the random case (Figures 5.11 and 5.12) than for the colinear case (Figures 5.3 and 5.4). However, many of the other aspects of the graphs are very similar. Notably in both cases the ratios R_1 and R_{12} are highest for $d = 1$, followed by $d = 2$ and finally by $d = 3$. Further, in both cases the ratios begin to plateau at higher speeds ($v > 3$) and all are above unity.

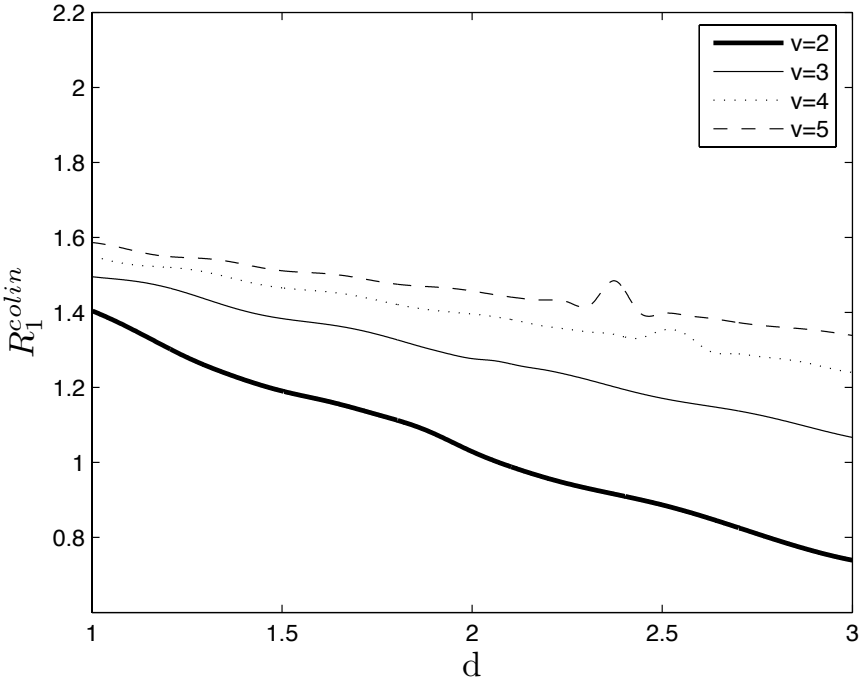

Figure 5.7: R_1 for a colinear dicluster of protons of speed $v = 2$ (thick line), $v = 3$ (thin line), $v = 4$ ($\cdots$), and $v = 5$ ($\cdots$) traveling through a solid with $r_s = 2.07$, $\eta = \omega_p/10$ and $\alpha = 0$ plotted against interproton distance

When comparing the distance dependence we notice that for the first order and full stopping force calculations, the same qualitative behaviour occurs for both the colinear (Figure 5.5) case and the randomly oriented case (Figure 5.13). However, the colinear case has a higher stopping force than the randomly oriented dicluster. This becomes more pronounced as the speed decreases, with the largest discrepancy occurring for the $v = 2$ case.

When one considers the ratios R_1 and R_{12} one notices that at large distances, the randomly oriented cluster experiences higher ratio values for higher speeds (Figures 5.15 and 5.16). This pattern also occurs for the colinear case as well (Figures 5.7 and 5.8). However, what is interesting to observe is that this pattern doesn't hold true as d approaches 1 in the case of R_{12}^{random} as shown in Figure 5.16. We can here that as d approaches 1, the R_{12} value for $v = 2$ crosses the other three and is in fact the largest at $d = 1$. This effect isn't seen for the colinear case

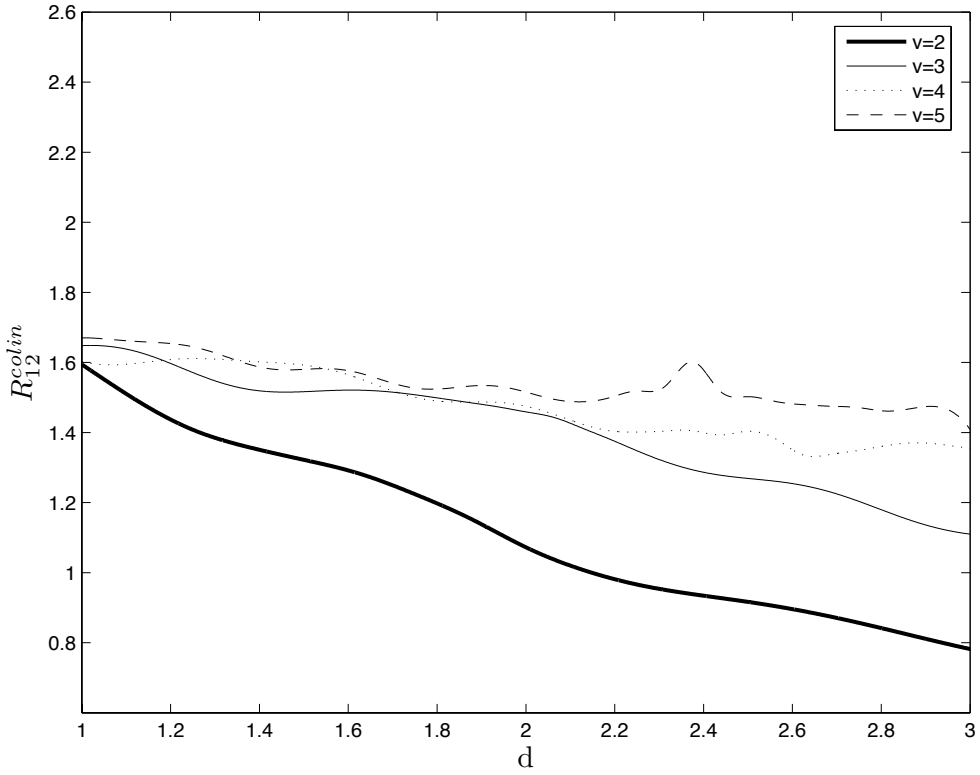

Figure 5.8: S_1 for a colinear dicluster of protons of speed $v = 2$ (thick line), $v = 3$ (thin line), $v = 4$ ($\cdots$), and $v = 5$ ($\cdots$) traveling through a solid with $r_s = 2.07$, $\eta = \omega_p/10$ and $\alpha = 0$ plotted against interproton distance

except in the regions where d is less than 1. Further, from Figure 5.15 we see that this 'layering' remains very much intact right up to $d = 1$. This means that the second order correction which is included in R_{12} begins to play a role in this case. What's more is that we see that for the randomly oriented cluster, the ratios R_1 and R_{12} appear to be shallowing before they reach unity as d increases. This is not found in the colinear case, as we see from Figures 5.7 and 5.8 that the $v = 2$ case crosses unity and even dips below 0.8.

The main results are seen conveniently in Figures 5.17, 5.18, 5.19 and 5.20, in which we can see clearly the non-linear effects on the stopping force.

In Figure 5.17 we notice that for a colinear dicluster at speeds in excess of around 2 atomic units, the non-linear effect on the stopping force is one which produces a higher ratio than if we

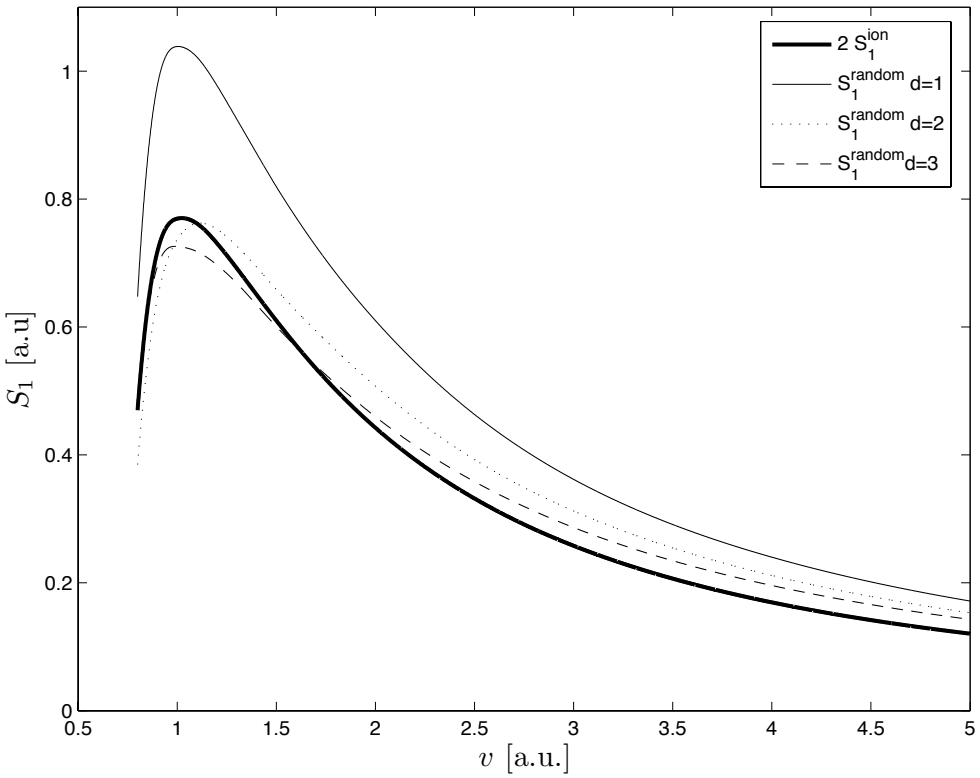

Figure 5.9: S_1 for a randomly oriented dicluster of protons of interproton distance $d = 1$ (thin line), $d = 2$ ($\cdots$), $d = 3$ ($\cdots$) and 2 independent protons (thick line) traveling through a solid with $r_s = 2.07$, $\eta = \omega_p/10$ and $\alpha = 0$ plotted against projectile speed

had just considered the linear ratio, R_1. This holds true for both the case of $d = 1$ and $d = 3$ with lower interproton distances yielding the higher ratio.

If we consider the interproton distance dependence in Figure 5.18 we notice that throughout the entire range of $d = 1$ to 3 the nonlinear terms again contributed positively to the ratio. As the interproton distance increased we notice a spreading of the ratio values for the three speeds considered with the lowest speed $v = 2$ having the smallest ratio, followed by $v = 3$ and finally $v = 5$ with the highest. We also see that as the distance was increased, both ratios decreased for all 3 speeds which agrees with the results from Figure 5.17.

For the randomly oriented case, we see that in Figure 5.19 that at around $v = 3$ both the $d = 1$ and $d = 3$ clusters undergo an inversion of highest ratio. Below $v = 3$ the nonlinear

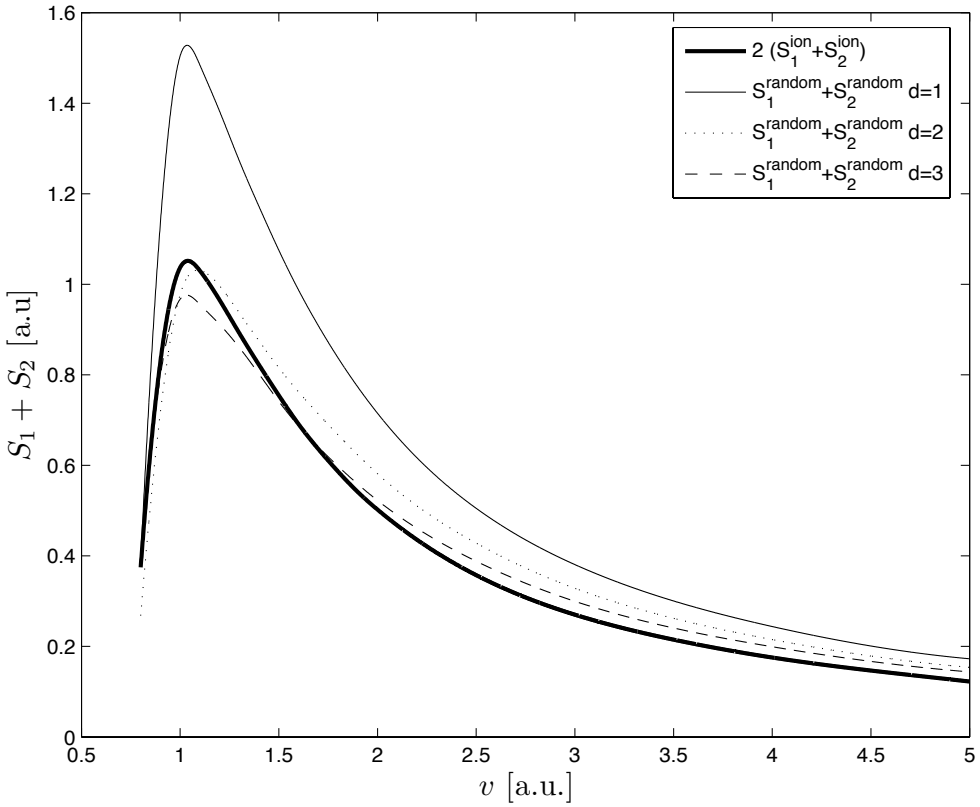

Figure 5.10: $S_1 + S_2$ for a randomly oriented dicluster of protons of interproton distance $d = 1$ (thin line), $d = 2$ ($\cdots$), $d = 3$ ($\cdots$) and 2 independent protons (thick line) traveling through a solid with $r_s = 2.07$, $\eta = \omega_p/10$ and $\alpha = 0$ plotted against projectile speed

effects cause an increase in ratio, where as after $v = 3$ we see that the nonlinear effect actually reduces the ratio. Further, the $d = 3$ case undergoes a steady increase in ratios whereas the $d = 1$ case has relatively flat behaviour with respect to the $d = 3$ case.

Finally when we look at Figure 5.20 we see that throughout the region $d = 1$ up to $d = 3$ the nonlinear effect increases the ratio for the clusters with $v = 2$ and 5. However, the effect is reversed for the $v = 5$ case where the nonlinear effect serves to decrease the ratio. This reflects our earlier result where we found an inversion after $v = 3$. Also, with respect to each other, as the distance is increased we see a general downwards slope of ratio which appears to be approaching unity. This is expected as each of the ratios should approach 1 as the distance between the protons

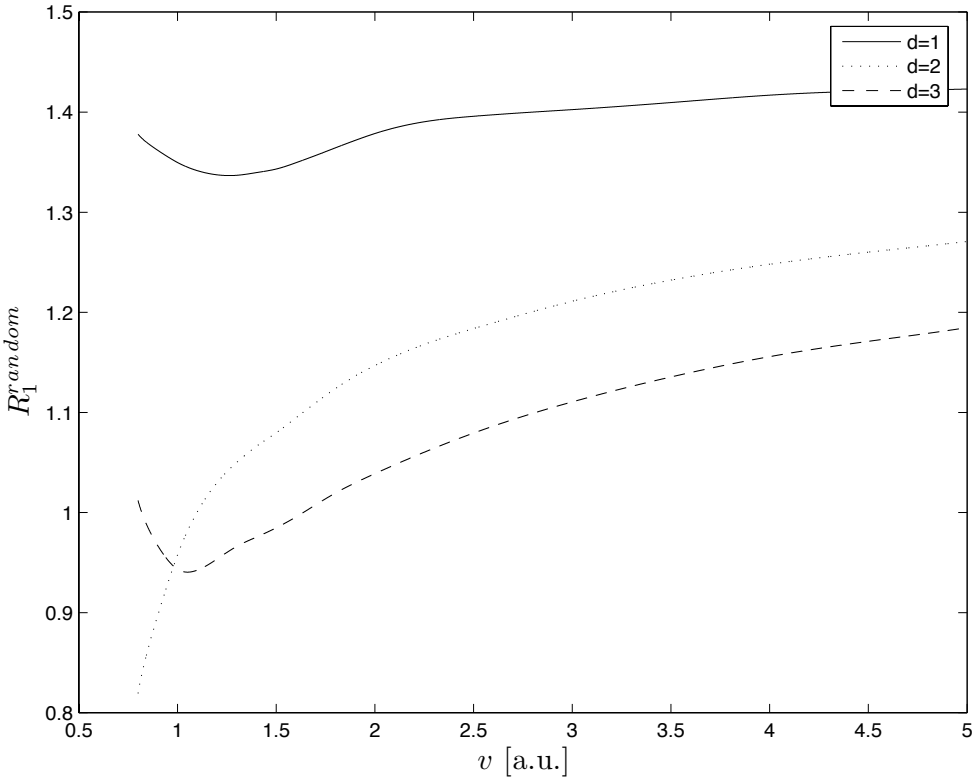

Figure 5.11: R_1 for a randomly oriented dicluster of protons of interproton distance $d = 1$ (—), $d = 2$ ($\cdots$), $d = 3$ ($\cdots$) traveling through a solid with $r_s = 2.07$, $\eta = \omega_p/10$ and $\alpha = 0$ plotted against projectile speed

is increased to infinity.

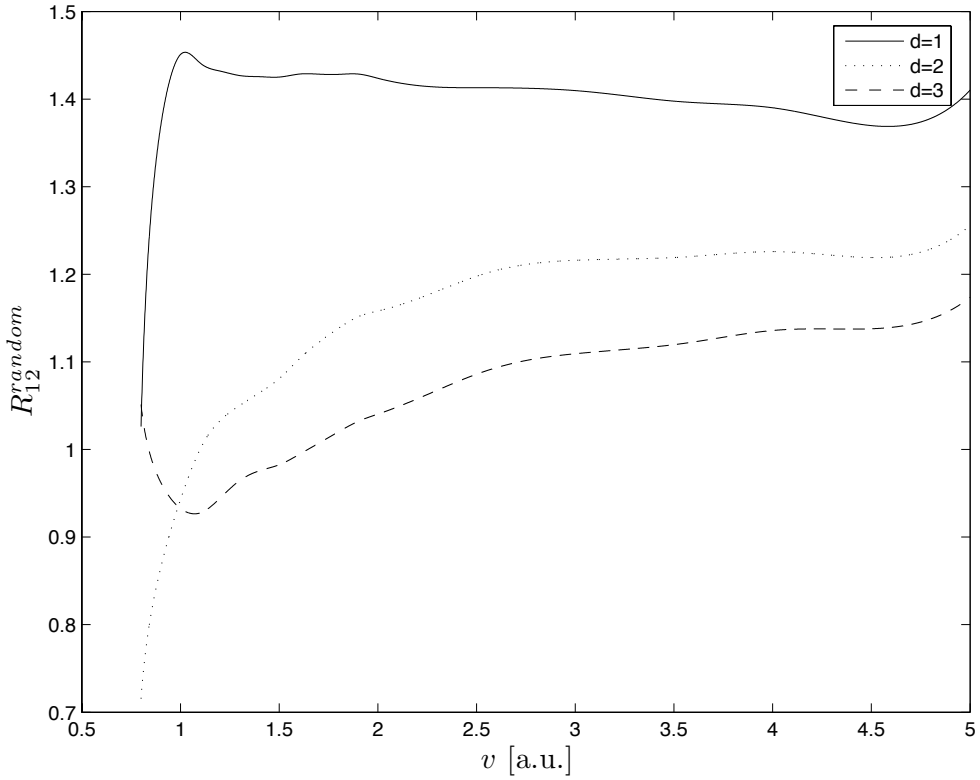

Figure 5.12: R_{12} for a randomly oriented dicluster of protons of interproton distance $d = 1$ (—), $d = 2$ ($\cdots$), $d = 3$ ($\cdots$) traveling through a solid with $r_s = 2.07$, $\eta = \omega_p/10$ and $\alpha = 0$ plotted against projectile speed

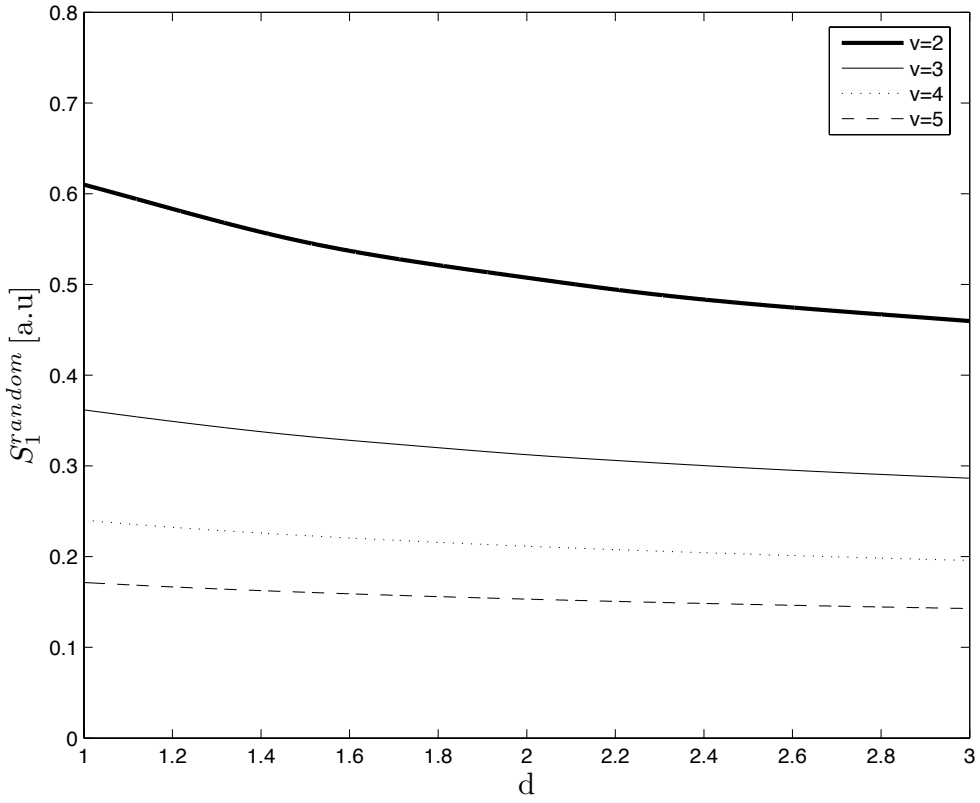

Figure 5.13: S_1 for a randomly oriented dicluster of protons of speed $v = 2$ (thick line), $v = 3$ (thin line), $v = 4$ ($\cdots$), and $v = 5$ ($\cdots$) traveling through a solid with $r_s = 2.07$, $\eta = \omega_p/10$ and $\alpha = 0$ plotted against interproton distance

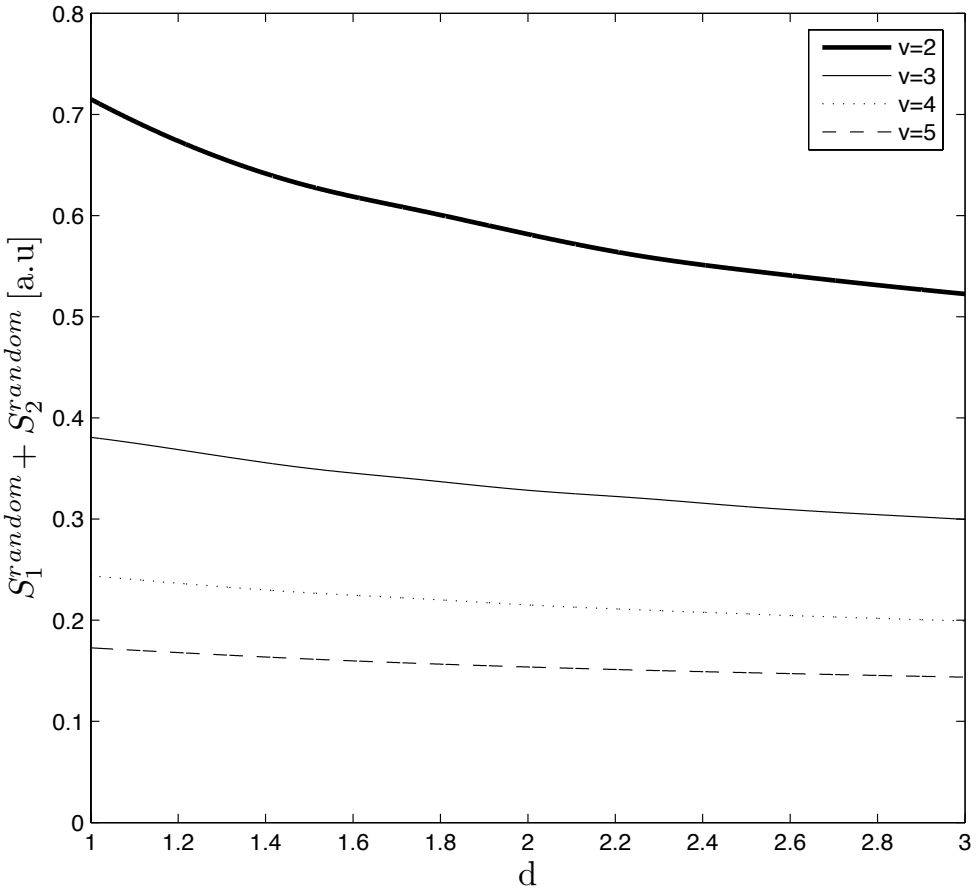

Figure 5.14: $S_1 + S_2$ for a randomly oriented dicluster of protons of speed $v = 2$ (thick line), $v = 3$ (thin line), $v = 4$ ($\cdots$), and $v = 5$ ($\cdots$) traveling through a solid with $r_s = 2.07$, $\eta = \omega_p/10$ and $\alpha = 0$ plotted against interproton distance

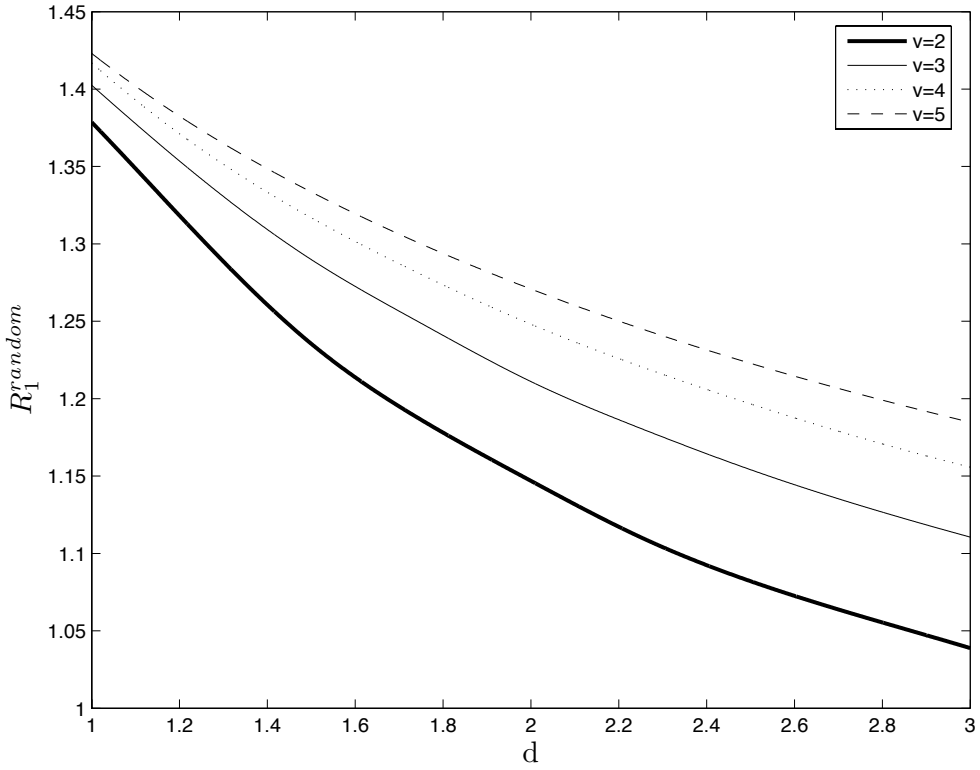

Figure 5.15: R_1 for a randomly oriented dicluster of protons of speed $v = 2$ (thick line), $v = 3$ (thin line), $v = 4$ ($\cdots$), and $v = 5$ ($\cdots$) traveling through a solid with $r_s = 2.07$, $\eta = \omega_p/10$ and $\alpha = 0$ plotted against interproton distance

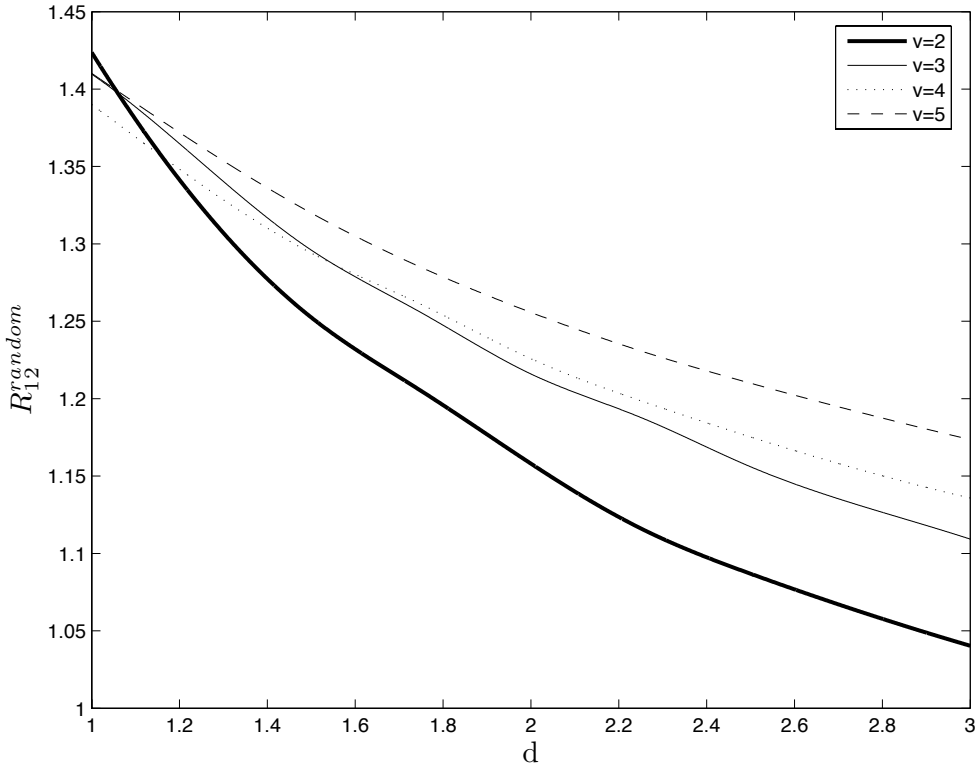

Figure 5.16: R_{12} for a randomly oriented dicluster of protons of speed $v = 2$ (thick line), $v = 3$ (thin line), $v = 4$ ($\cdots$), and $v = 5$ ($\cdots$) traveling through a solid with $r_s = 2.07$, $\eta = \omega_p/10$ and $\alpha = 0$ plotted against interproton distance

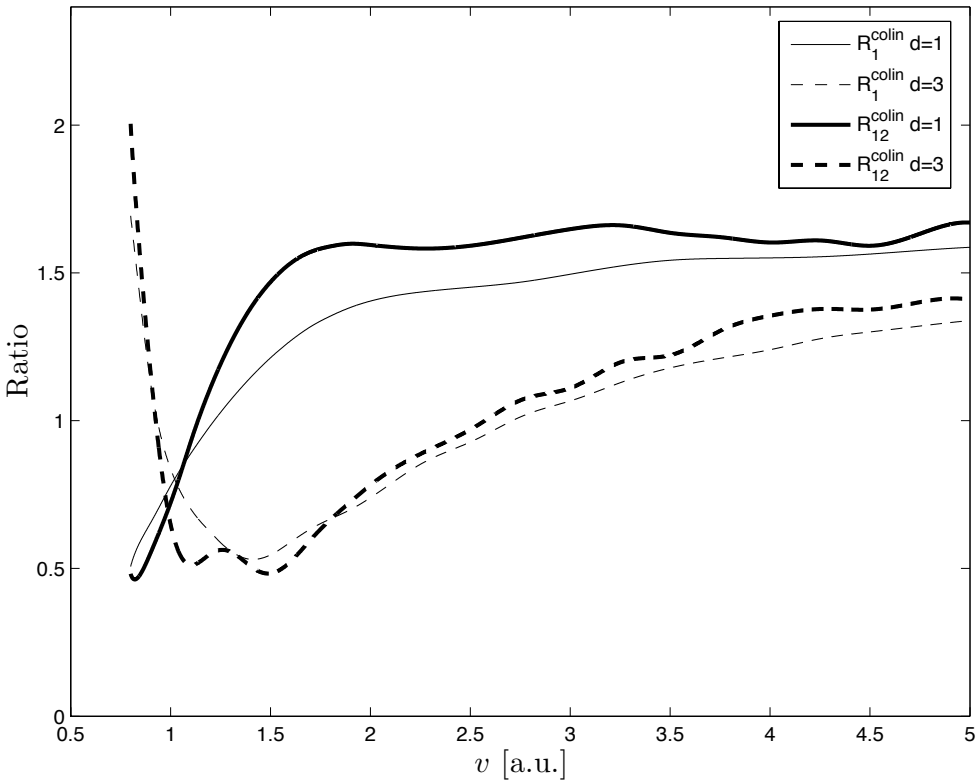

Figure 5.17: R_1 (thin line) compared with R_{12} (thick line) for a colinear dicluster of protons with interproton distance of $d = 1$ as well as R_1 (thin dashes) compared with R_{12} (thick dashes) for a colinear dicluster of protons with interproton distance of $d = 3$ vs projectile speed

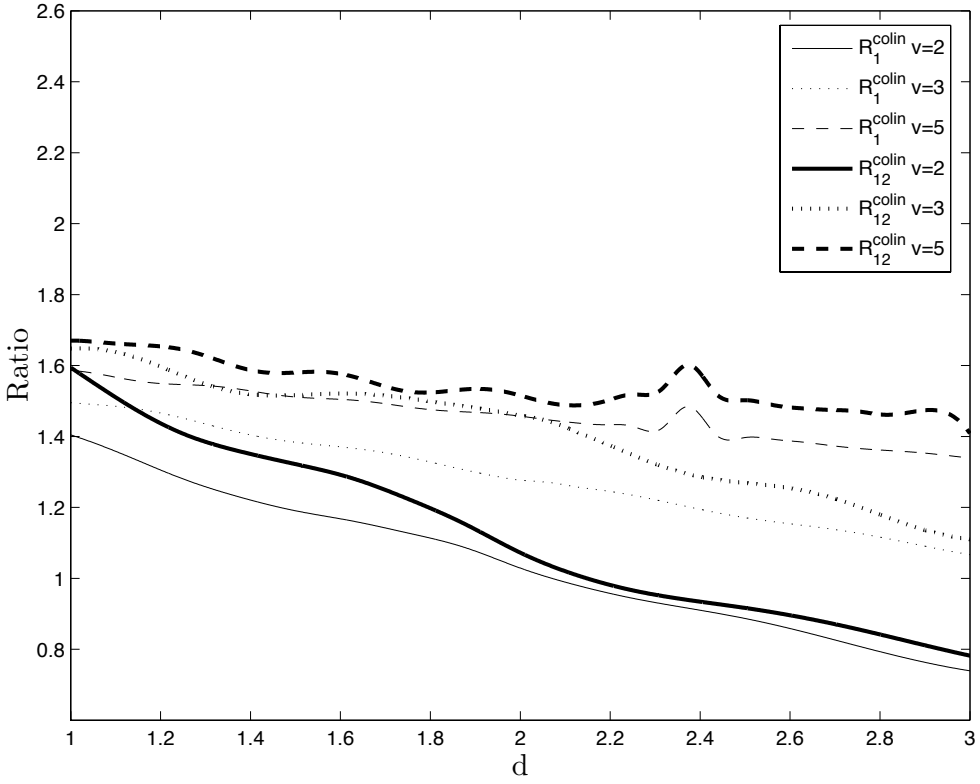

Figure 5.18: R_1 (thin line) compared with R_{12} (thick line) for a colinear dicluster of protons with veclocity of $v = 2$ as well as R_1 (thin dots) compared with R_{12} (thick dots) for a colinear dicluster of protons with veclocity of $v = 3$ and R_1 (thin dashes) compared with R_{12} (thick dashes) for a colinear dicluster of protons with speed of $v = 5$ vs interproton distance

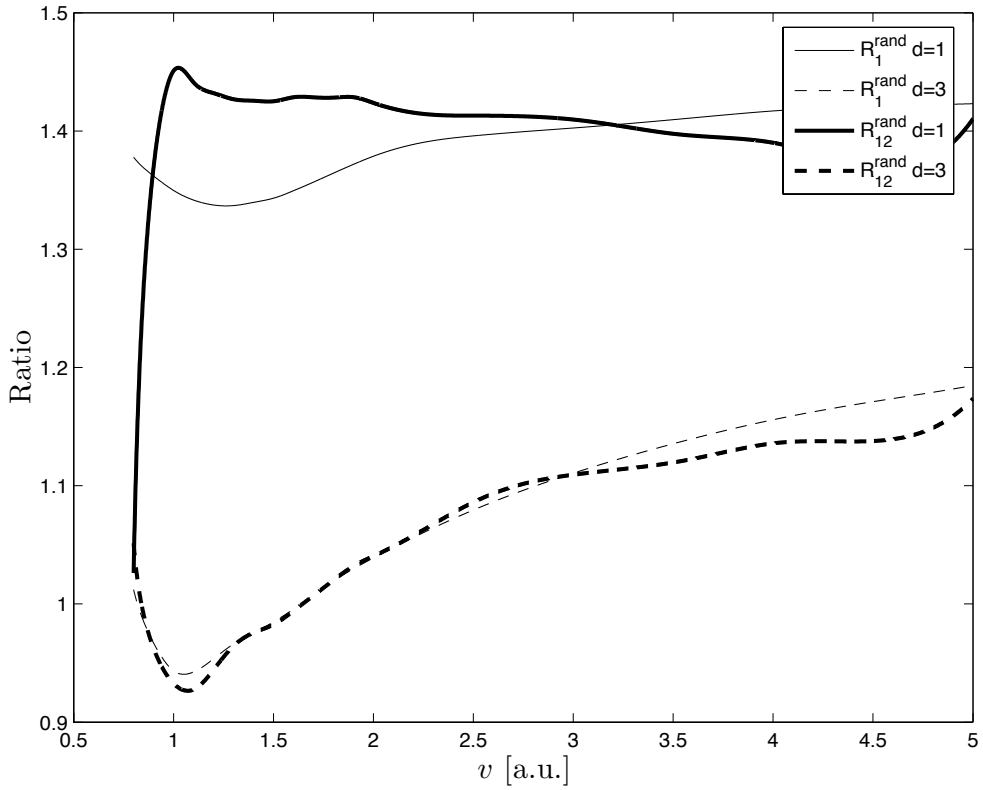

Figure 5.19: R_1 (thin line) compared with R_{12} (thick line) for a randomly oriented dicluster of protons with interproton distance of $d = 1$ as well as R_1 (thin dashes) compared with R_{12} (thick dashes) for a randomly oriented dicluster of protons with interproton distance of $d = 3$ vs projectile speed

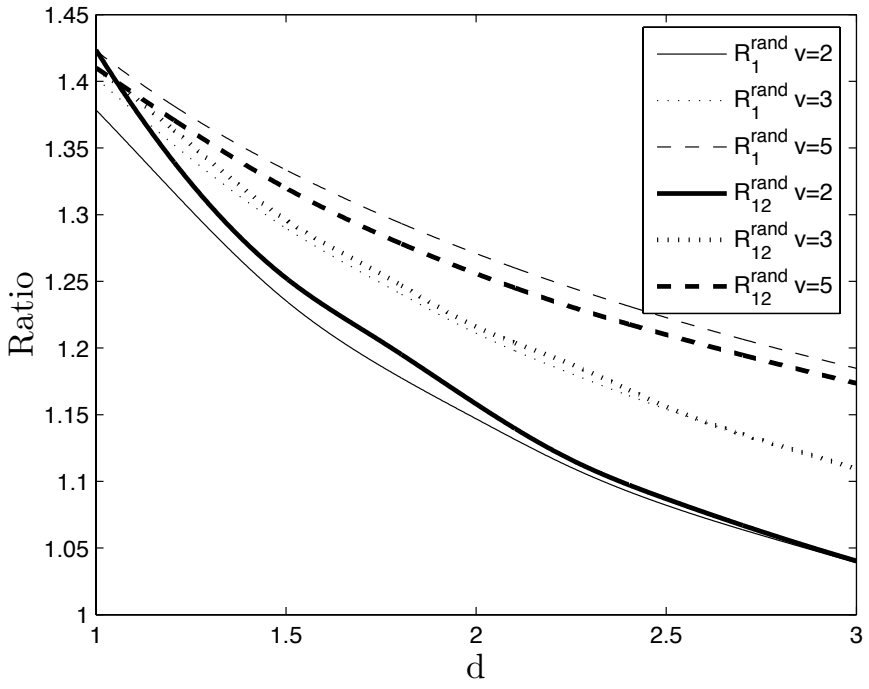

Figure 5.20: R_1 (thin line) compared with R_{12} (thick line) for a randomly oriented dicluster of protons with veclocity of $v = 2$ as well as R_1 (thin dots) compared with R_{12} (thick dots) for a randomly oriented dicluster of protons with veclocity of $v = 3$ and R_1 (thin dashes) compared with R_{12} (thick dashes) for a randomly oriented dicluster of protons with speed of $v = 5$ vs interproton distance

Chapter 6

Concluding Remarks

6.1 Summary

In this work we studied the stopping forces experienced by three types of projectiles incident on the electron gas of aluminum. Specifically we studied the non-linear (second order) stopping forces of a single ion projectile, a dicluster of protons with their interprotonic axis aligned in the direction of travel as well as a randomly oriented dicluster of protons. The colinear case and the randomly oriented case were chosen because they represent two extremes of configuration. It is expected that in the colinear case, the partner ion would experience the most effect due to the wake, since it travels directly behind the leading ion. On the other hand the randomly oriented case 'averaged out' the effects which would occur at different orientations.

In chapter 2 we outlined the development of the hydrodynamic model by constructing the Hamiltonian of the system and then appealing to variational calculus and the Euler-Lagrange equations to establish the equations of motion. These equations turned out to be the continuity and momentum balance equations of hydrodynamics. The quantum nature of the electron gas was introduced by using the Thomas-Fermi-Weizsäcker model of the internal energy of the electron gas. We then proceeded to expand the charge density and the velocity distribution of the system in a perturbation expansion and separated the resulting equations into first order (linear) and second order (non-linear) components. These first and second order expressions were solved to find the first and second order electron density distributions, which we used to obtain a formula for the first and second order stopping forces experienced by the projectile. The physical nature

of the projectile was introduced into the stopping force expressions by way of a first and second order structure factor.

In chapter 3 we described the integration strategy for both the first and second order stopping forces. The second order calculation was especially difficult since, even in the simplest case, as it involved integration over a six-dimensional space. To simplify the situation we took the zero viscosity limit allowing us to introduce delta functions, which consumed two of the integrations. Using cylindrical symmetry we were able to focus on a three dimensional integration, which was carried out numerically using a holepunch method to obtain the needed grid density and to avoid singularities. This method of integration was compared to four other methods and was shown to have the best combination of speed, scalability and accuracy to tackle the three dimensional integration.

In chapter 4 and 5 we presented the results obtained from these calculations. Due to the current lack of independent checks of the method, we presented limiting cases to check the robustness of the calculations. Having shown the accuracy of the method we proceeded to list the calculation results for the colinear and randomly oriented case and plot them against the projectile speed and also against the interproton distance.

6.2 Conclusions

In carrying out our initial investigation of calculation method we found that the most robust method of integration was completely unreasonable since it took nearly two and half hours per calculation which must be carried out at least twelve times per independent variable value (v or d). It became clear from the test of the other three standard methods that the only one which could perform in the time needed was the triple trapezoid method. However, this method was found to perform badly as the integration region was extended, due to memory limitations. After the test of the holepunch method on two trial functions as well as on a typical stopping force calculation it was found that the accuracy was very close to that of the most robust method and the time scale comparable to the triple trapezoid method. It would also be reasonable to conclude that this method would perform equally well on other functions, provided that they were slowly varying over most of their domains, with a finite number of more rapidly varying regions and/or non-essential singularities.

In the small d limit we can conclude that the first order and full stopping force of both the colinear and randomly oriented dicluster smoothly approached the case of a doubly charged ion at all explored speeds. What is more is that at these small distances, the speed dependence of stopping force for both types of projectiles produced a very smooth curve whereas at larger distances ($d = 1, 2, 3$) the plots became increasingly 'active'. This leads us to believe that as the distance between the protons shrinks, the interference becomes less and less noticeable. As d is increased the effect of the partner particle causes very non-linear behaviour. At higher speeds however, this effect gets 'washed' out by the v^{-2} nature of the stopping force.

We also find that in general, for both the first order and full stopping forces, the closer the protons were to each other, the stronger was the stopping force. This is especially true at high speeds.

Further, as the speed is increased the stopping force is decreased. This is true for all interproton distances and for both colinear and randomly oriented projectiles.

Thus, in the regime of this model ($v \approx 1 - 5$ a.u.), the most energy loss occurs for slower moving particles spaced closely together.

From the ratio plots, we see that as one increases the projectile speed, R_1 slowly increases for both the colinear and randomly oriented case. This indicates that, for first order, the effect of the partner (vicinage effect) increases with speed. On the other hand, the effect of the partner proton seems to plateau as the speed increases. This means that, although the overall stopping force is decreasing (as mentioned above), the effect of speed does not seem to change the effect of the partner proton. Hence, we conclude that, even at high speeds, this model predicts that stopping force in the presence of two protons in a cluster will be greater than that of two isolated protons. Of course (as mentioned above and as seen in the ratio plots) if the interproton distance is increased, this effect decreases. We clearly see this trend in the ratio plots against the interproton distance. As the distance is increased we see the ratio decreasing (for both types of clusters) towards unity. Thus, as the distance is increased to infinity, the stopping forces of the cluster (both first order and full) tend towards that of two isolated protons.

The main conclusions on the non-linear effect may be summarized from the Figures 5.17 - 5.20 where we concluded the following:

- The nonlinear effect tends to increase the vicinage effect on the stopping force as speed is increased except in the case of the randomly oriented cluster, which experiences an

'inversion' at around $v = 3$. That is, for randomly oriented clusters traveling at speeds higher that $v = 3$ the nonlinearity serves to *decrease* the vicinage effect.

- As distance is increased the effects of the non-linearity are reduced.
- The nonlinearity seems to have no preference in orientation as it seems to increase the stopping force in each configuration *except* in the case of high speeds and for randomly oriented clusters. In this case the nonlinearity *decreases* the stopping force.

6.3 Future Work

Obviously one could expand this model to include third order effects. While this might be a natural extension, it would be a rather difficult one in that the third order continuity and momentum equations would become that much more complex. The integrations that would be required may be beyond current computing capabilities. It is also uncertain if interesting physics would be uncovered as the contributions of higher order terms to the overall value of stopping force decrease with order. Simply put, the gains of exploring third order effects may come up very short of the efforts required to compute them.

On the other hand, within this framework one could (in principle) explore *any* cluster which satisfies cylindrical symmetry and is such that its presence induces only a small change of charge density in the electron gas. Some such clusters which may be of interest would include a colinear dipole, randomly oriented dipole or point dipole.

Further, these calculations were carried out for a static electron gas. One could extend this model to include non-static electron gases perhaps in the presence of an external electric field (possibly due to irradiation by a laser [28]).

Finally, within this framework, the plasma frequency used in this model belonged to aluminum. With the change of a single parameter, utilizing the existing framework and computational programs, one could extend this study to other metals such as gold, platinum and so on.

There are, however, several explorations which could be carried out that were not touched on in this work such as the self-energy of the projectile caused by its interaction with the target media as it passes. We also considered the case where the cluster passed through fast enough (or the

target was thin enough) so that the structure of the cluster was considered to be static. Certainly it would be worthwhile to consider the dynamical changes in structure (Coulomb explosion) that the projectile experiences. For that purpose one would need to evaluate the non-linear effects on the dynamically screened Coulomb force between the constituent ions [20]. Finally, for clusters or molecules made of heavier atoms (e.g. N_2, C_n, etc.) the well-documented vicinage effect on the ion charge states may be profoundly effected by the non-linearity in the polarization of the electron gas in the target [29].

Appendix A

Derivation of Hydrodynamic Equations From Boltzmann's Equation

A.1 The Boltzman Kinetic Equation

We begin by defining a function, $f(\mathbf{r}, \mathbf{v}, t)$, called the *distribution function*. The meaning of $f(\mathbf{r}, \mathbf{v}, t)$ is defined through,

$$f(\mathbf{r}, \mathbf{v}, t)\, dxdydzdv_x dv_y dv_z \tag{A.1}$$

as the number of particles at position $\mathbf{r}$, with velocity $\mathbf{v}$, at time t within a volume element (of phase space) of size $dxdydzdv_x dv_y dv_z$. Clearly then, by integrating over velocity space we obtain the number density of the particles,

$$n(\mathbf{r}, t) = \int_{\mathbf{v}} f(\mathbf{r}, \mathbf{v}, t) d\mathbf{v}\,, \tag{A.2}$$

We further demand that f is zero at positive and negative infinity, since it would be unphysical to allow parcels to approach infinite velocitites.

We define the change in f,

$$\frac{df}{dt} = I_{col}(f) \tag{A.3}$$

which is called the *kinetic equation*. The term on the right is called the *collison integral* which takes into account the variation of the distribution function due to pairwise particle interactions.

I_{col} describes the effect on f due to the collisions between two particles at a time. Collisions of more than two particles at a time are possible, but not considered here. Expanding the left hand side using the chain rule,

$$\begin{aligned}\frac{df}{dt} &= \frac{\partial f}{\partial t} + \frac{\partial f}{\partial x}\frac{\partial x}{\partial t} + \frac{\partial f}{\partial y}\frac{\partial y}{\partial t} + \frac{\partial f}{\partial z}\frac{\partial z}{\partial t} + \frac{\partial f}{\partial v_x}\frac{\partial v_x}{\partial t} + \frac{\partial f}{\partial v_y}\frac{\partial v_y}{\partial t} + \frac{\partial f}{\partial v_z}\frac{\partial v_z}{\partial t}\,, \\ &= \frac{\partial f}{\partial t} + \vec{\nabla} f \cdot \mathbf{v} + \vec{\nabla}_{\mathbf{v}} f \cdot \mathbf{a}\,, \\ &= \frac{\partial f}{\partial t} + (\mathbf{v}\cdot\vec{\nabla})f + \left(\mathbf{a}\cdot\vec{\nabla}_{\mathbf{v}}\right) f\,,\end{aligned}$$

where $\vec{\nabla}_{\mathbf{v}}$ is the velocity derivative.

Now, from Newtons law we know that $\mathbf{a} = \frac{\mathbf{F}}{m}$ where $\mathbf{F}$ is the external force, which depends only on space and time. We thus we have,

$$\frac{df}{dt} = \frac{\partial f}{\partial t} + (\mathbf{v}\cdot\vec{\nabla})f + \left(\frac{1}{m}\mathbf{F}\cdot\vec{\nabla}_{\mathbf{v}}\right) f\,.$$

Defining the *total derivative*,

$$\frac{D}{Dt} = \frac{\partial}{\partial t} + (\mathbf{v}\cdot\vec{\nabla}) + \frac{1}{m}\mathbf{F}\cdot\vec{\nabla}_v\,,$$

we may rewrite equation A.3 as,

$$\frac{Df}{Dt} = \frac{\partial f}{\partial t} + (\mathbf{v}\cdot\vec{\nabla})f + \left(\frac{1}{m}\mathbf{F}\cdot\vec{\nabla}_v\right) f = I_{col}(f)\,. \tag{A.4}$$

This is called the *Boltzmann Kinetic Equation* (BKE) which describes how the distribution function changes with time. Since f provides information about how the fluid parcels are distributed, the BKE tells us how physical properties of the fluid parcels evolve in time.

A.2 Moments of the Boltzmann Kinetic Equation

A.2.1 Moments

Ths distribution function generally contains more information than we need. We're most interested in how physical quantities such as the mass density, momentum and kinetic change over time.

The *nth veloctiy moment* of the BKE is found by multiplying the equation by the nth power of the velocity and then integrating over velocity space.

For example, the zeroth moment of the BKE is,

$$\int_{\mathbf{v}} \mathbf{v}^0 \frac{Df}{Dt} d\mathbf{v} = \int_{\mathbf{v}} \mathbf{v}^0 I_{col}(f) d\mathbf{v}\,,$$

or,

$$\int_{\mathbf{v}} \frac{\partial f}{\partial t} + (\mathbf{v}\cdot\vec{\nabla})f + \left(\mathbf{F}\cdot\vec{\nabla}_v f\right) d\mathbf{v} = \int_{\mathbf{v}} I_{col}(f) d\mathbf{v}\,.$$

Likewise, the first and second moments are,

$$\int_{\mathbf{v}} \mathbf{v}\cdot\left(\frac{\partial f}{\partial t} + (\mathbf{v}\cdot\vec{\nabla})f + \left(\mathbf{F}\cdot\vec{\nabla}_v f\right)\right) d\mathbf{v} = \int_{\mathbf{v}} \mathbf{v}\cdot I_{col}(f) d\mathbf{v}\,,$$
$$\int_{\mathbf{v}} v^2\cdot\left(\frac{\partial f}{\partial t} + (\mathbf{v}\cdot\vec{\nabla})f + \left(\mathbf{F}\cdot\vec{\nabla}_v f\right)\right) d\mathbf{v} = \int_{\mathbf{v}} v^2\cdot I_{col}(f) d\mathbf{v}\,,$$

respectively.

Higher moments may be calculated in an analogous manner. The important thing to note is that since f obeys the BKE then each moment equation gives a new dynamical equation for the system. However, only a few moments are of interest. Of particular interest are the moments associated with the mass density, momentum and kinetic energy. These are related to the zeroth, first and second moments respectively. We may see how these relationships come about by noting,

$$\rho = \int_{\mathbf{v}} m f d\mathbf{v}\,, \tag{A.5}$$

$$\rho\mathbf{u} = \int_{\mathbf{v}} m\mathbf{v} f d\mathbf{v}\,, \tag{A.6}$$

$$K = \frac{1}{2}\int_{\mathbf{v}} m v^2 f d\mathbf{v}\,, \tag{A.7}$$

where m is the mass of the fluid parcel.

Since ρ, $\rho\mathbf{u}$ and K are successive velocity moments of f, and since the BKE describes the evolution of f, we expect successive moments of the BKE to describe the evolution of ρ, $\rho\mathbf{u}$ and K. By writing these physical quantities in the above manner we see their close link with the moments of the BKE.

However, we limit our discussion to collisionless dynamics by taking $I_{col} = 0$. Thus, the final version of the Boltzmann Kinetic Equation we consider is,

$$\frac{Df}{Dt} = \frac{\partial f}{\partial t} + (\mathbf{v} \cdot \vec{\nabla}) f + \left(\frac{1}{m} \mathbf{F} \cdot \vec{\nabla}_{\mathbf{v}} \right) f = 0 \,. \tag{A.8}$$

A.2.2 Zeroth Moment: Conservation of Mass

We begin by looking at the zeroth moment of the Boltzmann Kinetic Equation. Here and in the following sections we assume that particles are moving with speeds much smaller than the speed of light (we may neglect relativistic effects and make use of Newton's law).

From A.8 we have,

$$\frac{Df}{Dt} = \frac{\partial f}{\partial t} + (\mathbf{v} \cdot \vec{\nabla}) f + \left(\frac{1}{m} \mathbf{F} \cdot \vec{\nabla}_{\mathbf{v}} \right) f = 0 \,.$$

To find the zeroth moment we multiply by $v^0 = 1$ and integrate over velocity space, yielding,

$$\int_{\mathbf{v}} \frac{\partial f}{\partial t} + (\mathbf{v} \cdot \vec{\nabla}) f + \left(\frac{1}{m} \mathbf{F} \cdot \vec{\nabla}_{v} f \right) d\mathbf{v} = 0 \,.$$

We may interchange the order of differentiation and integration in the first term since the integration is with respect to $\mathbf{v}$ and in phase space, $\mathbf{v}$ is independent of t. Therefore, the first term is,

$$\int_{\mathbf{v}} \frac{\partial f}{\partial t} d\mathbf{v} = \frac{\partial}{\partial t} \int_{\mathbf{v}} f d\mathbf{v} = \frac{\partial n}{\partial t} \,.$$

By noting that the integration does not depend on spatial variables (again, in phase space spatial variables and velocity are independent), we can pull the spatial gradient operator in the second term outside of the integral. So,

$$\begin{aligned} \int_{\mathbf{v}} \mathbf{v} \cdot \vec{\nabla} f d\mathbf{v} &= \int_{\mathbf{v}} \vec{\nabla} f \cdot \mathbf{v} d\mathbf{v} \,, & \text{(A.9)} \\ &= \vec{\nabla} \cdot \int_{\mathbf{v}} f \mathbf{v} d\mathbf{v} \,, & \text{(A.10)} \\ &= \left(n \vec{\nabla} \cdot \mathbf{u} \right) \,, \end{aligned}$$

where we've used $\mathbf{u} = \frac{1}{n} \int_{\mathbf{v}} f d\mathbf{v} \mathbf{V}$ to be the average velocity of the parcels (as noted earlier).

Since $\mathbf{F}$ does not explicitly depend on velocity, we can pull the force in the third term outside of the integration,

$$\frac{1}{m}\int_{\mathbf{v}} \mathbf{F}\cdot\vec{\nabla}_v f d\mathbf{v} = \frac{\mathbf{F}}{m}\cdot\int_{\mathbf{v}}\vec{\nabla}_{\mathbf{v}} f d\mathbf{v} = 0\,.$$

Now, since we demanded that the distribution function f be zero at positive and negative infinity, we see that the above integral vanishes, ie,

$$\frac{1}{m}\int_{\mathbf{v}} \mathbf{F}\cdot\vec{\nabla}_v f d\mathbf{v} = \frac{\mathbf{F}}{m}\cdot f|_{-\infty}^{\infty} = 0\,.$$

Thus, putting all together we obtain,

$$\frac{\partial n}{\partial t} + (n\vec{\nabla}\cdot\mathbf{u}) = 0\,. \tag{A.11}$$

If the flow is irrotational then we may write the velocity as the gradient of a velocity potential, ψ, and thus,

$$\frac{\partial n}{\partial t} + \vec{\nabla}\cdot(n\vec{\nabla}\psi) = 0\,. \tag{A.12}$$

which is the familiar conservation of mass equation first expressed in 2.24

A.2.3 1st Moment: Conservation of Momentum

We now turn our attention to the first moment of the Boltzmann Kinetic Equation by multiplying A.8 by v^1 and again integrating over velocity space. Thus,

$$\int_{\mathbf{v}} \mathbf{v}\cdot\left(\frac{\partial f}{\partial t} + (\mathbf{v}\cdot\vec{\nabla})f + \frac{1}{m}\mathbf{F}\cdot\vec{\nabla}_{\mathbf{v}} f\right) d\mathbf{v} = 0$$

The first term is easy to evaluate, namely,

$$\int_{\mathbf{v}} \mathbf{v}\frac{\partial f}{\partial t} d\mathbf{v} = \frac{\partial}{\partial t}\int_{\mathbf{v}} f\mathbf{v} d\mathbf{v}\,, \tag{A.13}$$

$$= n\frac{\partial \mathbf{u}}{\partial t}\,. \tag{A.14}$$

To simplify the second term we find it useful to note that,

$$\mathbf{v}\cdot\mathbf{v} = (\mathbf{v}-\mathbf{u})\cdot(\mathbf{v}-\mathbf{u}) + \mathbf{u}\cdot\mathbf{v} + \mathbf{v}\cdot\mathbf{u} - \mathbf{u}\cdot\mathbf{u}\,.$$

Thus,

$$\begin{aligned}
\int_{\mathbf{v}} \mathbf{v}\left(\mathbf{v}\cdot\vec{\nabla}f\right)d\mathbf{v} &= \vec{\nabla}\cdot\left(\int_{\mathbf{v}}\mathbf{v}\cdot\mathbf{v}f d\mathbf{v}\right), \\
&= \vec{\nabla}\cdot\left(\int_{\mathbf{v}}(\mathbf{v}-\mathbf{u})\cdot(\mathbf{v}-\mathbf{u})f d\mathbf{v} + 2\mathbf{u}\cdot\int_{\mathbf{v}}\mathbf{v}f d\mathbf{v} - \mathbf{u}\cdot\mathbf{u}\int_{\mathbf{v}} f d\mathbf{v}\right), \\
&= \vec{\nabla}\cdot\left(\int_{\mathbf{v}}(\mathbf{v}-\mathbf{u})\cdot(\mathbf{v}-\mathbf{u})f d\mathbf{v} + \mathbf{u}\cdot\mathbf{u}\int_{\mathbf{v}} f d\mathbf{v}\right), \qquad \text{(A.15)}
\end{aligned}$$

Defining the pressure tensor $\mathbf{P} = P_{ij}$ to be,

$$\mathbf{P} = \int_{\mathbf{v}} m(\mathbf{v}-\mathbf{u})\cdot(\mathbf{v}-\mathbf{u})f(\mathbf{r},\mathbf{v},t)\,d\mathbf{v}\,,$$

where P_{ij} is the average rate at which momentum is transferred in the ith direction across the jth surface with velocity $\mathbf{u}$. Thus, we may write A.15 as,

$$\int_{\mathbf{v}} \mathbf{v}\left(\mathbf{v}\cdot\vec{\nabla}f\right)d\mathbf{v} = \frac{1}{m}\vec{\nabla}\cdot\mathbf{P} + n\vec{\nabla}\cdot(\mathbf{u}\cdot\mathbf{u})\,.$$

For the third term,

$$\int_{\mathbf{v}} \mathbf{v}\left(\frac{1}{m}\mathbf{F}\cdot\vec{\nabla}_{\mathbf{v}}\right)f d\mathbf{v} = \frac{\mathbf{F}}{m}\cdot\int_{\mathbf{v}}\mathbf{v}\vec{\nabla}_{\mathbf{v}}f d\mathbf{v}\,.$$

Now, integrating by parts,

$$\begin{aligned}
\frac{\mathbf{F}}{m}\cdot\int_{\mathbf{v}}\mathbf{v}\cdot\vec{\nabla}_{\mathbf{v}}f d\mathbf{v} &= \frac{\mathbf{F}}{m}\left(\mathbf{v}f|_{-\infty}^{\infty} - \int_{\mathbf{v}} f d\mathbf{v}\right), \\
&= -n\frac{\mathbf{F}}{m}\,.
\end{aligned}$$

Thus, putting all three terms together we obtain,

$$\begin{aligned}
\int_{\mathbf{v}}\mathbf{v}\cdot\left(\frac{\partial f}{\partial t} + (\mathbf{v}\cdot\vec{\nabla})f + \frac{1}{m}\mathbf{F}\cdot\vec{\nabla}_{\mathbf{v}}f\right)d\mathbf{v} &= n\frac{\partial\mathbf{u}}{\partial t} + \frac{1}{m}\vec{\nabla}\cdot\mathbf{P} + n\vec{\nabla}\cdot(\mathbf{u}\cdot\mathbf{u}) - n\frac{\mathbf{F}}{m}\,, \\
&= 0\,. \qquad \text{(A.16)}
\end{aligned}$$

By using the definition of the material derivative, A.16 becomes,

$$n\frac{D\mathbf{u}}{Dt} = \frac{1}{m}\left(n\mathbf{F} - \vec{\nabla}\cdot\mathbf{P}\right) , \tag{A.17}$$

which, when multiplied by m on both sides becomes,

$$\frac{D\mathbf{p}}{Dt} = n\mathbf{F} - \vec{\nabla}\cdot\mathbf{P} , \tag{A.18}$$

which expresses conservation of momentum, as was to be expected. Comparing this expression to 2.45 and 2.46 one may write,

$$\mathbf{P} = \vec{\nabla}\left(\frac{\delta G}{\delta n}\right) , \tag{A.19}$$

and in this sense the internal energy of the electron gas may be thought of as a type of 'pressure' which acts on the fluid.

Appendix B

Thomas-Fermi-Wiezsäcker Model

In this section we describe the derivation of the internal energy of an electron gas using the Thomas-Fermi-Wiezsäcker model.

We consider a system of N electrons, with the ith electron being located at position $\mathbf{r}_i$. We may write this system's quantum mechanical state, Ψ, as,

$$\Psi = \Psi(\mathbf{r}_1, \sigma_1, \mathbf{r}_2, \sigma_2, \ldots, \mathbf{r}_N, \sigma_N)\,, \tag{B.1}$$

where σ_i is the spin of the ith electron. As it stands, the wave function describing our system is much too complicated so we appeal to the Hartree-Fock theory to simplify Ψ in terms of single electron orthonormal wave functions, Ψ_i. To this end we use the Slater Determinant so that,

$$\Psi_{HF} = \frac{1}{\sqrt{N}} \begin{vmatrix} \psi_1(\mathbf{r_1}, \sigma_1) & \psi_1(\mathbf{r_1}, \sigma_1) & \ldots & \psi_1(\mathbf{r_1}, \sigma_1) \\ \psi_2(\mathbf{r_2}, \sigma_2) & \psi_2(\mathbf{r_2}, \sigma_2) & \ldots & \psi_2(\mathbf{r_2}, \sigma_2) \\ \vdots & \vdots & \vdots & \vdots \\ \psi_N(\mathbf{r_N}, \sigma_N) & \psi_N(\mathbf{r_N}, \sigma_N) & \ldots & \psi_N(\mathbf{r_N}, \sigma_N) \end{vmatrix} \tag{B.2}$$

We also require that,

$$\int \psi_k^* \psi_l d^N\mathbf{r} = \delta_{kl}\,, \tag{B.3}$$

where δ_{kl} is the Kronecker delta.

Assuming a time-dependent Hamiltonian, the Schrödiner equation gives the dynamical equation of the system,

$$\hat{H}\Psi = E\Psi\,, \tag{B.4}$$

where $\hat{H}$ is the Hamiltonian operator and E is the energy eigenvalue.

The average energy, $\bar{E}$ of our system is given by the quantum mechanical expectation value,

$$\bar{E}[\Psi] = \int \Psi^* E \Psi d^N \mathbf{r} \,, \tag{B.5}$$

$$= \int \Psi^* \hat{H} \Psi d^N \mathbf{r} \,, \tag{B.6}$$

Thus, in the Hartree-Fock approximation,

$$\bar{E}_{HF} = \int \Psi^*_{HF} \hat{H} \Psi_{HF} d^N \mathbf{r} \,, \tag{B.7}$$

We make the further assumption that the Schrödinger equation is independent of spin in order that we may write,

$$\psi_i(\mathbf{r}_i, \sigma_i) = \phi_i(\mathbf{r}_i) \,. \tag{B.8}$$

Finally, we assume that each orbital is doubly occupied (closed shell).

We obtain the expression for the Thomas-Fermi kinetic energy before discussing the von Weizsäcker correction term.

B.1 Thomas-Fermi Kinetic Energy

The Thomas-Fermi kinetic energy comes from considering the kinetic energy term from the Hamiltonian, which term is given by,

$$KE_i = \frac{\|\mathbf{p}_i\|^2}{2m} \,, \tag{B.9}$$

which, in the position representation of quantum mechanics, becomes the operator,

$$\hat{KE}_i = -\frac{\hbar}{2m} \nabla_i^2 \,, \tag{B.10}$$

Thus, the Thomas-Fermi kinetic energy, T, may be written,

$$T_{HF} = \sum_{i=1}^{N} \int \phi_i^* \left(-\frac{\hbar}{2m} \nabla_i^2 \right) \phi_l d^3 \mathbf{r} \tag{B.11}$$

If we write the spinless two electron density function, $n(\mathbf{r}, \mathbf{r}')$, as,

$$n(\mathbf{r}, \mathbf{r}') = 2 \sum_{i=1}^{N/2} \phi_i^*(\mathbf{r}) \phi_i(\mathbf{r}') \tag{B.12}$$

we are lead naturally to the electron number density, $n(\mathbf{r})$,

$$n(\mathbf{r}) = n(\mathbf{r}, \mathbf{r}) = 2 \sum_{i=1}^{N/2} \phi_i^*(\mathbf{r}) \phi_i(\mathbf{r}) \,. \tag{B.13}$$

With these definitions we may write,

$$T_{HF}[n] = \int \left(-\frac{\hbar}{2m} \nabla^2 n(\mathbf{r}, \mathbf{r}') \right)_{\mathbf{r}'=\mathbf{r}} d^3\mathbf{r} \tag{B.14}$$

Assuming periodic boundary conditions,

$$\phi(x + L) = \phi(x) \tag{B.15}$$

we get,

$$\phi(n_x, n_y, n_z) = \frac{e^{\frac{2\pi\imath}{L}\mathbf{n}\cdot\mathbf{r}}}{L^{3/2}} \,, \tag{B.16}$$

where, n_x, n_y and n_z are integers.

With $\mathbf{k} = \frac{2\pi\mathbf{n}}{L}$, then

$$n(\mathbf{r}, \mathbf{r}') = \frac{2}{L^3} \sum_{\mathbf{k}} e^{i\mathbf{K}\cdot(\mathbf{r}-\mathbf{r};)} \tag{B.17}$$

Since we are dealing with an electron gas of many electrons, it is safe to make the assumption that $N >> 1$ and thus $\sum_{\mathbf{k}} \approx \int d\mathbf{k}$. Hence,

$$n(\mathbf{r}, \mathbf{r}') = \frac{2}{L^3} \int e^{i\mathbf{k}\cdot(\mathbf{r}-\mathbf{r};)} d\mathbf{n} \,. \tag{B.18}$$

Since,

$$d^3\mathbf{n} = dn_x \, dn_y \, dn_z \,, \tag{B.19}$$

$$= \frac{L^3}{(2\pi)^3} dk_x \, dk_y \, dk_z \,, \tag{B.20}$$

$$= \frac{V}{8\pi^3} d^3\mathbf{k} \,, \tag{B.21}$$

then we conclude,

$$n(\mathbf{r},\mathbf{r}') = \frac{1}{4\pi^3}\int e^{i\mathbf{k}\cdot(\mathbf{r}-\mathbf{r};)}d^3\mathbf{k}\,. \tag{B.22}$$

We now undertake the task of integrating this equation. Using spherical coordinates,

$$n(\mathbf{r},\mathbf{r}') = \frac{1}{4\pi^3}\int_0^{k_F} k^2dk\int_0^{2\pi}\int_0^{\pi} e^{i\mathbf{k}\cdot(\mathbf{r}-\mathbf{r};)}\sin\theta d\alpha d\theta\,. \tag{B.23}$$

If we consider the case $\mathbf{r}=\mathbf{r}'$ then,

$$\begin{aligned} n(\mathbf{r}) &= \frac{1}{4\pi^3}\int_0^{k_F} k^2dk\int_0^{2\pi}\int_0^{\pi}\sin\alpha d\alpha d\theta\,, &\text{(B.24)}\\ &= \frac{k_F^3}{3\pi^2}\,. &\text{(B.25)}\end{aligned}$$

Thus,

$$k_F = [3\pi^2 n(\mathbf{r})]^{1/3}\,. \tag{B.26}$$

Finishing the integration of B.23 we use let $\mathbf{k}\cdot(\mathbf{r}-\mathbf{r}') = ks\cos\alpha$ and thus B.23 becomes,

$$n(\mathbf{r},\mathbf{r}') = \frac{1}{4\pi^3}\int_0^{k_F} k^2dk\int_0^{2\pi} d\theta\int_0^{\pi} e^{iks\cos\alpha}\sin\alpha d\alpha\,. \tag{B.27}$$

Now, we change variable, $\tau=\cos\alpha$ and get,

$$\begin{aligned} n(\mathbf{r},\mathbf{r}') &= \frac{1}{2\pi^2}\int_0^{k_F} k^2dk\int_{-1}^{1} e^{\imath ks\tau}\sin\alpha d\tau\,, &\text{(B.28)}\\ &= \frac{1}{2\pi^2}\int_0^{k_F}\frac{k}{\imath s}\left(e^{\imath ks}-e^{-\imath ks}\right)dk\,, &\text{(B.29)}\\ &= 3n(\mathbf{r})\left[\frac{\sin(k_Fs)-\cos(k_Fs)k_Fs}{(k_Fs)^3}\right]\,. &\text{(B.30)}\end{aligned}$$

We let $\mathbf{R}=\frac{\mathbf{r}-\mathbf{r}'}{2}$ and $\mathbf{s}=\mathbf{r}_1-\mathbf{r}_2$ when $\nabla^2_{\mathbf{r}} = \frac{1}{4}\nabla^2_{\mathbf{R}}+\nabla^2_{\mathbf{s}}+\nabla_{\mathbf{R}}\nabla_{\mathbf{s}}$. Hence,

$$\begin{aligned} T_{HF}[n] &= \frac{-\hbar^2}{2m}\int\nabla^2_{\mathbf{r}}n(\mathbf{r},\mathbf{r}')d^3\mathbf{r}\,,\\ &= \frac{-\hbar^2}{2m}\int\left(\frac{1}{4}\nabla^2_{\mathbf{R}}+\nabla^2_{\mathbf{s}}+\nabla_{\mathbf{R}}\nabla_{\mathbf{s}}\right)3n(\mathbf{r})\left[\frac{\sin(k_Fs)-\cos(k_Fs)k_Fs}{(k_Fs)^3}\right]_{s=0}\\ &= \frac{-\hbar^2}{2m}\int\frac{1}{4}\nabla^2_{\mathbf{R}}n(\mathbf{R}) - 3^2\frac{n(\mathbf{R})k_F^2}{15}d^3\mathbf{R}\,, &\text{(B.31)}\end{aligned}$$

and if we assume that $\int \nabla^2_{\mathbf{R}} n(\mathbf{R}) d\mathbf{R} = 0$ then we arrive at the result required. Namely,

$$T_{HF}[n] = \frac{3}{10}\frac{\hbar}{m}\int (3\pi^2)^{2/3} n^{5/3}(\mathbf{r}) d^3\mathbf{r}\,. \tag{B.32}$$

This is the Thomas-Fermi kinetic energy of an electron gas. We now turn our attention to the 'gradient correction' term, ie, the von Weizsäcker correction.

B.2 von Weizsäcker Correction

It was quickly discovered that the Thomas-Fermi kinetic energy term did not provide an accurate enough description of the internal energy of an electron gas. A gradient correction term was suggested by von Weizsäcker in 1935. The derivation is carried out in Parr and Yang [30] and depends on considering modified plane waves, $\psi = (1 + \mathbf{a}\cdot\mathbf{r})e^{i\mathbf{k}\cdot\mathbf{r}}$. This ultimately leads to the correction,

$$T_w[n] = \frac{1}{8}\int d^3\mathbf{r}\frac{[\vec{\nabla} n(\mathbf{r})]^2}{n(\mathbf{r})}\,. \tag{B.33}$$

There is some discussion, however, about the value for λ when writing down the full Thomas-Fermi-Weizsäcker term,

$$G[n] = T + \lambda T_w[n]\,. \tag{B.34}$$

In this work (as was done originally by von Weizsäcker) we assume λ to be equal to unity. However, Parr and Yang obtain a value for λ of $\frac{1}{9}$. Other values have been suggested such as $\frac{1}{8}$ as well as empirically fitted values such as $\frac{1}{5}, 0.186$ and $\frac{1.4}{9}$.

Appendix C

Nature of $F(\mathbf{k})$

In this appendix we prove the stated symmetry properties of $F(\mathbf{k})$ .The proof relies on using the symmertic properties among $\mathbf{k}'$ and functions of it.

C.1 Preliminaries

Recall the expression for $F(\mathbf{k})$,

$$F(\mathbf{k}) = \int \frac{d^3\mathbf{k}'}{k'^2(\mathbf{k}-\mathbf{k}')^2} F_3(\mathbf{k},\mathbf{k}',\mathbf{k}-\mathbf{k}') \frac{A(\mathbf{k},\mathbf{k}',\mathbf{k}-\mathbf{k}',\mathbf{k}\cdot\mathbf{v},\mathbf{k}'\cdot\mathbf{v},(\mathbf{k}-\mathbf{k}')\cdot\mathbf{v})}{N(\mathbf{k}',\mathbf{k}'\cdot\mathbf{v})N(\mathbf{k}-\mathbf{k}',(\mathbf{k}-\mathbf{k}')\cdot\mathbf{v})}\,, \quad \text{(C.1)}$$

For notational ease, we make the following definitions,

$$\omega = \mathbf{k}\cdot\mathbf{v}\,, \quad \text{(C.2)}$$

$$\omega' = \mathbf{k}'\cdot\mathbf{v}\,, \quad \text{(C.3)}$$

$$\omega_k = \frac{k^2}{2}\,, \quad \text{(C.4)}$$

$$\text{(C.5)}$$

from which we see that,

$$\omega(-k) = -\omega\,, \quad \text{(C.6)}$$

$$\omega'(-k) = -\omega'\,, \quad \text{(C.7)}$$

$$\omega_k = \omega_{-k}\,. \quad \text{(C.8)}$$

We begin by considering the symmetry properties of $N(\mathbf{k},\omega)$. We recall,

$$N(\mathbf{k},\omega) = \beta k^4 + \alpha k^2 - \omega^2 + \omega_p^2 - \imath\omega\eta\,, \tag{C.9}$$

which we can write as,

$$N(\mathbf{k}) = \omega_k^2 + \omega_p^2 - (k\cdot v)^2 - \imath(\mathbf{k}\cdot\mathbf{v})\eta\,, \tag{C.10}$$

Thus, taking the conjugate,

$$\begin{aligned} N^*(\mathbf{k}) &= \omega_k^2 + \omega_p^2 - (k\cdot v)^2 + \imath(\mathbf{k}\cdot\mathbf{v})\eta\,, \\ &= \omega_k^2 + \omega_p^2 - (k\cdot v)^2 - \imath(-\mathbf{k}\cdot\mathbf{v})\eta\,, \\ &= \omega_k^2 + \omega_p^2 - (-k\cdot v)^2 - \imath(-\mathbf{k}\cdot\mathbf{v})\eta\,, \\ &= N(-\mathbf{k})\,. \end{aligned} \tag{C.11}$$

Further, we assume that,

$$F_3(\mathbf{k},\mathbf{k}'+\mathbf{k},-\mathbf{k}') = F_3(-\mathbf{k},\mathbf{k}',-\mathbf{k}-\mathbf{k}')\,, \tag{C.12}$$

which, for the clusters that are considered in this work, is a valid assumption. Now looking at the $A(\mathbf{k},\mathbf{k}',\mathbf{k}-\mathbf{k}',\omega,\omega',\omega-\omega')$ term, we have that,

$$A(\mathbf{k},\mathbf{k}',\mathbf{k}-\mathbf{k}',\omega,\omega',\omega-\omega') = Q(\mathbf{k},\mathbf{k}',\mathbf{k}-\mathbf{k}',\omega,\omega',\omega-\omega') + \frac{\alpha}{6}k^2k'^2(\mathbf{k}-\mathbf{k}')^2\,. \tag{C.13}$$

where,

$$\begin{aligned} Q(\mathbf{k},\mathbf{k}',\mathbf{k}-\mathbf{k}',\omega,\omega',\omega-\omega') &= \frac{1}{2}\big[-\omega(\omega-\omega')\mathbf{k}\cdot(\mathbf{k}-\mathbf{k}')k'^2 - \omega\omega'\mathbf{k}\cdot\mathbf{k}'(\mathbf{k}-\mathbf{k}')^2 \\ &\quad -\omega'(\omega-\omega')k^2\mathbf{k}'\cdot\mathbf{k}'' + \beta k^2k'^2(\mathbf{k}-\mathbf{k}')^2 \\ &\quad \big((\mathbf{k}-\mathbf{k}')^2 + k'^2 + \mathbf{k}'\cdot(\mathbf{k}-\mathbf{k}')\big)\big]\,. \end{aligned} \tag{C.14}$$

We may rewrite Q as $Q = a + b + c$ with,

$$\begin{aligned} a(\mathbf{k},\mathbf{k}',\mathbf{k}-\mathbf{k}',\omega,\omega',\omega-\omega') &= \omega\omega'\omega_{k-k'}^2 + \omega\omega''\omega_{k'}^2 - \omega'\omega''\omega_k^2 - \omega''^2\omega_k\omega_{k'} \\ &\quad -\omega'^2\omega_k\omega_{k-k'} - \omega^2\omega_{k'}\omega_{k-k'}\,, \end{aligned} \tag{C.15}$$

$$b(\mathbf{k},\mathbf{k}',\mathbf{k}-\mathbf{k}',\omega,\omega',\omega-\omega') = \omega_k\omega_{k'}\omega_{k-k'}\left(\omega_k+\omega_{k'}+\omega_{k-k'}\right)\,, \tag{C.16}$$

$$c(\mathbf{k},\mathbf{k}',\mathbf{k}-\mathbf{k}') = \frac{\alpha}{6}k^2k'^2(\mathbf{k}-\mathbf{k}')^2\,. \tag{C.17}$$

Now, we consider letting $\mathbf{k} \to -\mathbf{k}$. Then,

$$\begin{aligned} a(-\mathbf{k},\mathbf{k}',-\mathbf{k}-\mathbf{k}',-\omega,\omega',-\omega-\omega') &= -\omega\omega'\omega_{k+k'}^2+\omega(\omega+\omega')\omega_{k'}^2+\omega'(\omega+\omega')\omega_k^2\,, \\ &\quad -(\omega+\omega')^2\omega_k\omega_{k'}-\omega'^2\omega_k\omega_{k+k'}\,, \\ &\quad -\omega^2\omega_{k'}\omega_{k+k'}\,, \qquad \text{(C.18)} \\ b(-\mathbf{k},\mathbf{k}',-\mathbf{k}-\mathbf{k}',-\omega,\omega',-\omega-\omega') &= \omega_k\omega_{k'}\omega_{k+k'}\left(\omega_k+\omega_{k'}+\omega_{k+k'}\right)\,, \qquad \text{(C.19)} \\ c(-\mathbf{k},\mathbf{k}',-\mathbf{k}-\mathbf{k}') &= \frac{\alpha}{6}k^2k'^2(-\mathbf{k}-\mathbf{k}')^2\,. \qquad \text{(C.20)} \end{aligned}$$

Further, making the substitution, $\mathbf{k}' \to -\mathbf{k}'$

$$\begin{aligned} a(\mathbf{k},-\mathbf{k}',\mathbf{k}+\mathbf{k}',\omega,-\omega',\omega+\omega') &= -\omega\omega'\omega_{k+k'}^2+\omega(\omega+\omega')\omega_{k'}^2+\omega'(\omega+\omega')\omega_k^2\,, \\ &\quad -(\omega+\omega')^2\omega_k\omega_{k'}-\omega'^2\omega_k\omega_{k+k'}-\omega^2\omega_{k'}\omega_{k+k'}\,, \\ &= a(-\mathbf{k},\mathbf{k}',-\mathbf{k}-\mathbf{k}',-\omega,\omega',-\omega\omega')\,, \qquad \text{(C.21)} \\ b(\mathbf{k},-\mathbf{k}',\mathbf{k}+\mathbf{k}',\omega,\omega',\omega-\omega') &= \omega_k\omega_{k'}\omega_{k+k'}\left(\omega_k+\omega_{k'}+\omega_{k+k'}\right)\,, \\ &= b(-\mathbf{k},\mathbf{k}',-\mathbf{k}-\mathbf{k}',-\omega,\omega',-\omega-\omega')\,, \qquad \text{(C.22)} \\ c(\mathbf{k},-\mathbf{k}',\mathbf{k}+\mathbf{k}') &= \frac{\alpha}{6}k^2k'^2(\mathbf{k}+\mathbf{k}')^2\,. \qquad \text{(C.23)} \end{aligned}$$

To simplify expressions, we use the following notation,

$$\begin{aligned} a_+ &= a(\mathbf{k},\mathbf{k}',\mathbf{k}-\mathbf{k}',\omega,\omega',\omega-\omega')\,, \qquad \text{(C.24)} \\ a_- &= a(-\mathbf{k},\mathbf{k}',-\mathbf{k}-\mathbf{k}',-\omega,\omega',-\omega-\omega')\,, \qquad \text{(C.25)} \\ a'_- &= a(\mathbf{k},-\mathbf{k}',\mathbf{k}+\mathbf{k}',\omega,-\omega',\omega+\omega')\,, \qquad \text{(C.26)} \end{aligned}$$

and similarly for b and c.

The idea of the proof is to show that,

$$F^*(\mathbf{k}) = F(-\mathbf{k})\,, \qquad \text{(C.27)}$$

and that

$$F(\mathbf{k}) = F(-\mathbf{k})\,, \qquad \text{(C.28)}$$

from which we may conclude that,

$$F^*(\mathbf{k}) = F(\mathbf{k})\,. \qquad \text{(C.29)}$$

C.2 Proof of C.27

We take the conjugate of C.1:

$$F^*(\mathbf{k}) = \int_{k_0'}^{k_1'} d^3k'\, F_3(\mathbf{k}, \mathbf{k}', \mathbf{k}-\mathbf{k}') \frac{a+b+c}{k'^2(\mathbf{k}-\mathbf{k}')^2 N(-\mathbf{k}) N(\mathbf{k}-\mathbf{k}')}\,, \tag{C.30}$$

Now, we make the change of variables,

$$\mathbf{k}' = -\mathbf{k}'\,, \tag{C.31}$$

$$d\mathbf{k}' = -d\mathbf{k}'\,, \tag{C.32}$$

which brings C.30 to,

$$\begin{aligned} F^*(\mathbf{k}) &= -\int_{k_1'}^{k_0'} d^3k'\, F_3(-\mathbf{k}, \mathbf{k}', -\mathbf{k}-\mathbf{k}') \frac{a'_- + b'_- + c'_-}{k'^2(\mathbf{k}+\mathbf{k}')^2 N(\mathbf{k}') N(\mathbf{k}+\mathbf{k}')}\,, \\ &= \int_{k_0'}^{k_1'} d^3k'\, F_3(-\mathbf{k}, \mathbf{k}', -\mathbf{k}-\mathbf{k}') \frac{a_- + b_- + c_-}{k'^2(\mathbf{k}+\mathbf{k}')^2 N(\mathbf{k}') N(\mathbf{k}+\mathbf{k}')}\,, \\ &= F(-\mathbf{k})\,. \end{aligned} \tag{C.33}$$

Thus, C.27 is satisfied.

C.3 Proof of C.28

Again we begin with C.1,

$$F^(\mathbf{k}) = \int_{k_0'}^{k_1'} d^3k'\, F_3(\mathbf{k}, \mathbf{k}', \mathbf{k}-\mathbf{k}') \frac{a+b+c}{k'^2(\mathbf{k}-\mathbf{k}')^2 N(\mathbf{k}) N(\mathbf{k}-\mathbf{k}')}\,, \tag{C.34}$$

We consider the transformation: $\mathbf{k}' \to \mathbf{k}' + \mathbf{k}$

$$\begin{aligned} a(\mathbf{k}' \to \mathbf{k}' + \mathbf{k}) &= \omega(\omega' + \omega)\omega_{k'}^2 + \omega(-\omega')\omega_{k'+k}^2 - (\omega' + \omega)(-\omega')\omega_k^2 \\ &\quad -(\omega')^2\omega_k\omega_{k'+k} - (\omega' + \omega)^2\omega_k\omega_{k'} - \omega^2\omega_{k'+k}\omega_{k'} \,, \\ &= \omega(\omega' + \omega)\omega_{k'}^2 - \omega\omega'\omega_{k'+k}^2 + \omega'(\omega' + \omega)\omega_k^2 \\ &\quad -\omega'^2\omega_k\omega_{k'+k} - (\omega' + \omega)^2\omega_k\omega_{k'} - \omega^2\omega_{k'+k}\omega_{k'} \,, \\ &= a_- \,. \end{aligned} \tag{C.35}$$

$$\begin{aligned} b(\mathbf{k}' \to \mathbf{k}' + \mathbf{k}) &= \omega_k\omega_{k'}\omega_{k-k'}\left(\omega_k + \omega_{k'} + \omega_{k-k'}\right) \,, \\ &= \omega_k\omega_{k'+k}\omega_{k'}\left(\omega_k + \omega_{k'+k} + \omega_{k'}\right) \,, \\ &= b_- \,, \end{aligned} \tag{C.36}$$

$$\begin{aligned} c(\mathbf{k}' \to \mathbf{k}' + \mathbf{k}) &= \frac{\alpha}{6}k^2k'^2(\mathbf{k} + \mathbf{k}')^2 \,. \\ &= c_- \,. \end{aligned} \tag{C.37}$$

Therefore, making this transformation gives,

$$\begin{aligned} F(\mathbf{k}) &= \int d^3k' \, F_3(\mathbf{k}, \mathbf{k}' + \mathbf{k}, -\mathbf{k}') \frac{a(\mathbf{k}' \to \mathbf{k}' + \mathbf{k}) + b(\mathbf{k}' \to \mathbf{k}' + \mathbf{k}) + c(\mathbf{k}' \to \mathbf{k}' + \mathbf{k})}{(\mathbf{k}' + \mathbf{k})^2k'^2N(\mathbf{k}' + \mathbf{k})N(\mathbf{k}')} \,, \\ &= \int d^3k' \, F_3(-\mathbf{k}, \mathbf{k}', -\mathbf{k} - \mathbf{k}') \frac{a_- + b_- + c_-}{(\mathbf{k}' + \mathbf{k})^2k'^2N(\mathbf{k}' + \mathbf{k})N(\mathbf{k}')} \,, \\ &= F(-\mathbf{k}) \,. \end{aligned} \tag{C.38}$$

Thus, C.28 is satisfied. Hence we conclude that,

$$F^*(\mathbf{k}) = F(\mathbf{k}) \,, \tag{C.39}$$

as required.

Bibliography

[1] T. a. Mehlhorn, "A finite material temperature model for ion energy deposition in ion-driven inertial confinement fusion targets", *Journal of Applied Physics* **52**(11), 6522 (1981), URL http://link.aip.org/link/?JAP/52/6522/1.

[2] R. J. Beuhler, G. Friedlander, and L. Friedman, "Cluster-impact fusion", *Phys. Rev. Lett.* **63**(12), 1292 (Sep 1989), doi:10.1103/PhysRevLett.63.1292.

[3] C. Carraro, B. Q. Chen, S. Schramm, and S. E. Koonin, "Estimates of cluster-impact fusion yields", *Phys. Rev. A* **42**(3), 1379 (Aug 1990), doi:10.1103/PhysRevA.42.1379.

[4] R. L. Fleischer, *Nuclear Tracks in Solids* (Univeristy of California Press, 1975).

[5] J. Jensen, a. Dunlop, and S. Della-Negra, "Tracks in yig induced by mev c60 ions", *Nuclear Instruments and Methods in Physics Research Section B: Beam Interactions with Materials and Atoms* **135**, 295 (1998).

[6] S. Cruz, E. Gamaly, L. Chadderton, and D. Fink, "A simple model for latent track formation due to cluster ion stopping and fragmentation in solids", *Radiation Measurements* **36**, 145 (2003).

[7] W. Brandt, Ratkowsk.a, and R. H. Ritchie, "Energy-loss of swift proton clusters in solids", *Physical Review Letters* **33**(22), 1325 (1974).

[8] N. R. Arista, "Stopping of molecules and clusters", *Nuclear Instruments Methods in Physics Research Section B-Beam Interactions with Materials and Atoms* **164**, 108 (Apr 2000).

[9] Z. Vager and D. Gemmell, "Polarization induced in a solid by the passage of fast charged particles", *Phys. Rev. Lett.* **37**, 1352 (1976).

[10] H. Esbensen and P. Sigmund, "Barkas effect in a dense medium - stopping power and wake field", *Annals of Physics* **201**(1), 152 (Jul 1990).

[11] O. H. Crawford, J. J. Dorado, and F. Flores, "Nonlinear effects in interactions of swift ions with solids", *Nuclear Instruments and Methods in Physics Research Section B* **96**(3-4), 610 (May 1995).

[12] W. H. Barkas, W. Birnbaum, and F. M. Smith, "Mass-ratio method applied to the measurement of l-meson masses and the energy balance in pion decay", *Physical Review* **101**(2), 778 (1956).

[13] W. H. Barkas, "Correction", *Physical Review Letters* **11**(3), 138 (1963).

[14] F. M. Smith, W. Birnbaum, and W. H. Barkas, "Measurements of meson masses and related quantities", *Physical Review* **91**(3), 765 (1953).

[15] H. M. Urbassek, V. Droge, and R. M. Nieminen, "Orientation effects in the stopping of slow dimers in an electron-gas", *Journal of Physics-Condensed Matter* **5**(19), 3289 (May 1993).

[16] I. Nagy, a. Arnau, and P. M. Echenique, "Vicinage effect in slow-ion-dicluster stopping power", *Nuclear Instruments Methods in Physics Research Section B-Beam Interactions with Materials and Atoms* **48**(1-4), 54 (Mar 1990).

[17] R. D. Muino and a. Salin, "Energy and angular momentum transfer in the excitation of electron-hole pairs by slow dimers", *Physical Review B* **62**(8), 5207 (Aug 2000).

[18] P. Sigmund, I. S. Bitensky, and J. Jensen, "Molecule and cluster bombardment: Energy loss, trajectories, and collision cascades", *Nuclear Instruments Methods in Physics Research Section B-Beam Interactions with Materials and Atoms* **112**(1-4), 1 (May 1996).

[19] P. Sigmund, "Note on isotope sputtering", *Nuclear Instruments Methods in Physics Research Section B-Beam Interactions with Materials and Atoms* **82**(1), 192 (Jul 1993).

[20] Z. L. Miskovic, Y.-N. Wang, and Y.-H. Song, "Dynamics of fast molecular ions in solids and plasmas: A review of recent theoretical developments", *Nuclear Instruments Methods in Physics Research Section B-Beam Interactions with Materials and Atoms* **256**, 57 (2007).

[21] Z. L. Miskovic, S. G. Davison, F. O. Goodman, and W. K. Liu, "Stochastic treatment of charge states for ion stopping in solids", *Physical Review B* **60**(21), 14478 (Dec 1999).

[22] N. R. Arista and V. H. Ponce, "Energy-loss of correlated protons in channeling", *Journal of Physics C-Solid State Physics* **8**(9), L188 (1975).

[23] S. Lundqvist and N. March, *Theory of the Inhomogeneous Electron Gas* (Plenum Press, 1983).

[24] C. D. Hu and E. Zaremba, "Z3 correction to the stopping power of ions in an electron-gas", *Physical Review B* **37**(16), 9268 (Jun 1988).

[25] C. C. Sung and R. H. Ritchie, "Z13 dependence of the energy-loss of an ion passing through an electron-gas", *Physical Review A* **28**(2), 674 (1983).

[26] J. Pitarke, R. H. Ritchie, P. Enchenique, and Z. E., "The z(1)(3) correction to the blethe-bloch energy loss formula", *Europhys. Lett.* **24**, 613 (1993).

[27] M. J. Forray, *Variational Calculus in Science and Engineering* (McGraw-Hill, 1968).

[28] G. Q. Wang, Y. H. Song, Y. N. Wang, and Z. L. Miskovic, "Influence of a laser field on coulomb explosions and stopping power for swift molecular ions interacting with solids", *Physical Review A* **66**(4), 042901 (Oct 2002).

[29] Z. L. Miskovic, T. L. Wilson, and Y. N. Wang, "Feedback action of vicinage effect in cluster stopping via nonhomogeneous charge reduction", *Physical Review A* **67**(2), 022903 (Feb 2003).

[30] R. G. Parr and W. Yang, *Density-Functional Theory of Atoms and Molecules* (Oxford University Press, 1989).